

Trends in Renewable Energy

Volume 4, 2018

Special Issue on International Conference on Recent Innovations in Electrical, Electronics and Communication Systems (RIEECS 2017)



Editors
Dr. Afzal Sikander
Dr. Padmanabh Thakur

Trends in Renewable Energy

ISSN: 2376-2136 (Print) ISSN: 2376-2144 (Online)

<http://futureenergysp.com/>

Trends in Renewable Energy is an open accessed, peer-reviewed semi-annual journal publishing reviews and research papers in the field of renewable energy technology and science.

The aim of this journal is to provide a communication platform that is run exclusively by scientists working in the renewable energy field. Scope of the journal covers: Bioenergy, Biofuel, Biomass, Bioprocessing, Biorefinery, Biological waste treatment, Catalysis for energy generation, Energy conservation, Energy delivery, Energy resources, Energy storage, Energy transformation, Environmental impact, Feedstock utilization, Future energy development, Green chemistry, Green energy, Microbial products, Physico-chemical process for Biomass, Policy, Pollution, Renewable energy, Smart grid, Thermo-chemical processes for biomass, etc.

The Trends in Renewable Energy publishes the following article types: peer-reviewed reviews, mini-reviews, technical notes, short-form research papers, and original research papers.

The article processing charge (APC), also known as a publication fee, is fully waived for the Trends in Renewable Energy.

Editorial Team of Trends in Renewable Energy

EDITOR-IN-CHIEF

Dr. Bo Zhang

P.E., Prof. of Chemical Engineering, Editor, Trends in Renewable Energy, United States

HONORARY CHAIRMEN

Dr. Yong Wang

Voiland Distinguished Professor, The Gene and Linda Voiland School of Chemical Engineering and Bioengineering, Washington State University, United States

Dr. Mahendra Singh Sodha

Professor, Lucknow University; Former Vice Chancellor of Devi Ahilya University, Lucknow University, and Barkatulla University; Professor/Dean/HOD/Deputy Director at IIT Delhi; Padma Shri Award; India Professor of Industrial Chemistry, CEO of Eurochem Engineering srl, Italy

Dr. Elio Santacesaria

VICE CHAIRMEN

Dr. Mo Xian

Prof., Assistant Director, Qingdao Institute of BioEnergy and Bioprocess Technology, Chinese Academy of Sciences, China

Dr. Changyan Yang

Prof., School of Chemical Engineering & Pharmacy, Wuhan Institute of Technology, China

EDITORS

Dr. Yiu Fai Tsang,

Associate Prof., Department of Science and Environmental Studies, The Education University of Hong Kong

Dr. Melanie Sattler

Dr. Syed Qasim Endowed Professor, Dept. of Civil Engineering, University of Texas at Arlington, United States

Dr. Attila Bai

Associate Prof., University of Debrecen, Hungary

Prof. Christophe Pierre Ménézo

University of Savoy Mont-Blanc, France

Dr. Moinuddin Sarker

MCIC, FICER, MInstP, MRSC, FARSS., VP of R & D, Head of Science/Technology Team, Natural State Research, Inc., United States Associate Prof., Biomass Processing Laboratory, Centre for Biofuel and Biochemical Research, Green Technology Mission Oriented Research, Universiti Teknologi PETRONAS, Malaysia

Dr. Suzana Yusup

Global Technology Development, Monsanto Company, United States

Dr. Zewei Miao

Pfizer Inc., United States

Dr. Hui Wang

North Carolina Agricultural and Technical State University, United States

Dr. Shuangning Xiu

Associate Prof., Institute of Chemical Industry of Forest Products, China

Dr. Junming XU

Academy of Forest, China

Dr. Hui Yang

Prof., College of Materials Science and Engineering, Nanjing Tech University, China

Dr. Ying Zhang

Associate Prof., School of Chemistry and Materials Science, University of Science and Technology of China, China

Dr. Ming-Jun Zhu

Prof., Assistant Dean, School of Bioscience & Bioengineering, South China University of Technology, China

MANAGING EDITOR

Dr. Bo Zhang

P.E., Prof. of Chemical Engineering, Editor, Trends in Renewable Energy, United States

EDITORIAL BOARD

| | |
|---------------------------------|---|
| Dr. Risabh Dev Shukla | Dean and Associate Prof., Department of Electrical Engineering, Budge Budge Institute of Technology Kolkata, India |
| Dr. Neeraj Gupta | Indian Institute of Technology Roorkee, India |
| Dr. Elena Lucchi | Politecnico di Milano, Italy |
| Dr. Muhammad Mujtaba Asad | Faculty of Technical and Vocational Education, Universiti Tun Hussein Onn Malaysia, Malaysia |
| Dr. Afzal Sikander | Associate Prof., Department of Electrical Engineering, Graphic Era University, India |
| Dr. Padmanabh Thakur | Professor and Head, Department of Electrical Engineering, Graphic Era University, India |
| Dr. K. DHAYALINI | Professor, Department of Electrical and Electronics Engineering, K. Ramakrishnan College of Engineering, Tamilnadu, India |
| Shangxian Xie | Texas A&M University, United States |
| Dr. Tanmoy Dutta | Sandia National Laboratories, United States |
| Dr. Efstathios Stefanos | Pontifical Catholic University of Ecuador, Faculty of Exact and Natural Sciences, School of Physical Sciences and Mathematics, Ecuador |
| Dr. Xin Wang | Miami University, United States |
| Dr. Rami El-Emam | Assist. Prof., Faculty of Engineering, Mansoura University, Egypt |
| Dr. Rameshprabu Ramaraj | School of Renewable Energy, Maejo University, Thailand |
| Dr. ZAFER ÖMER ÖZDEMİR | Kirklareli University, Technology Faculty, Turkey |
| Dr. Vijay Yeul | Chandrapur Super Thermal Power Station, India |
| Dr. Mohanakrishna Gunda | VITO - Flemish Institute for Technological Research, Belgium |
| Dr. Shuai Tan | Georgia Institute of Technology, United States |
| Shahabaldin Rezania | Universiti Teknologi Malaysia (UTM), Malaysia |
| Dr. Madhu Sabnis | Contek Solutions LLC, Texas, United States |
| Dr. Qiang Yan | Mississippi State University, United States |
| Dr. Mustafa Tolga BALTA | Associate Prof., Department of Mechanical Engineering, Faculty of Engineering, Aksaray University, Turkey |
| Dr. María González Alriols | Associate Prof., Chemical and Environmental Engineering Department, University of the Basque Country, Spain |
| Dr. Nattaporn Chaiyat | Assist. Prof., School of Renewable Energy, Maejo University, Thailand |
| Dr. Nguyen Duc Luong | Institute of Environmental Science and Engineering, National University of Civil Engineering, Vietnam |
| Mohd Lias Bin Kamal | Faculty of Applied Science, Universiti Teknologi MARA, Malaysia |
| Dr. N.L. Panwar | Assistant Prof., Department of Renewable Energy Engineering, College of Technology and Engineering, Maharana Pratap University of Agriculture and Technology, India |
| Dr. Caio Fortes | BASF, Brazil |
| Dr. Flavio Pratico | Department of Methods and Models for Economics, Territory and Finance, Sapienza University of Rome, Italy |
| Dr. Wennan ZHANG | Docent (Associate Prof.) and Senior Lecturer in Energy Engineering, Mid Sweden University, Sweden |
| Dr. Ing. Stamatis S. Kalligeros | Assistant Prof., Hellenic Naval Academy, Greece |
| Carlos Rolz | Director of the Biochemical Engineering Center, Research Institute at Universidad del Valle, Guatemala |
| Ms. Liliash Makashini | Copperbelt University, Zambia |
| Dr. Ali Mostafaeipour | Assistant Prof., Industrial Engineering Department, Yazd University, Iran |
| Dr. Camila da Silva | Prof., Maringá State University, Brazil |
| Dr. Anna Skorek-Osikowska | Silesian University of Technology, Poland |
| Dr. Shek Atiqure Rahman | Sustainable and Renewable Energy Engineering, College of Engineering, University of Sharjah, Bangladesh |
| Dr. Emad J Elnajjar | Associate Prof., Department of Mechanical Engineering, United Arab Emirates University, United Arab Emirates |

| | |
|-----------------------------|---|
| Dr. Kenneth Okedu | Caledonian College of Engineering, Oman |
| Dr. Cheng Zhang | Sr. Materials Engineer, Medtronic, Inc., United States |
| Dr. Chandani Sharma | Assistant Prof., Department of Electrical Engineering, Graphic Era University, India |
| Dr. Kashif Irshad | Assistant Prof., Mechanical Engineering Department, King Khalid University, Saudi Arabia |
| Dr. Abhijit Bhagavatula | Principal Lead Engineer, Southern Company Services, United States |
| Dr. S. Sathish | Associate Prof., Department of Mechanical Engineering, Hindustan University, India |
| Mr. A. Avinash | Assistant Prof., KPR Institute of Engineering & Technology, India |
| Mr. Bindeshwar Singh | Assistant Prof., Kamla Nehru Institute of Technology, India |
| Dr. Yashar Hashemi | Tehran Regional Electric Company, Iran |
| Dr. Navanietha Krishnaraj R | South Dakota School of Mines and Technology, United States |
| Dr. SANDEEP GUPTA | JECRC University, India |
| Dr. Shwetank Avikal | Graphic Era Hill University, India |
| Dr. Xianglin Zhai | Poochon Scientific LLC, United States |
| Dr. Rui Li | North Carolina Agricultural and Technical State University, United States |
| Dr. Adam Elhag Ahmed | National Nutrition Policy Chair, Department of Community Services, College of Applied Medical Sciences, King Saud University, Saudi Arabia |
| Dr. Jingbo Li | Massachusetts Institute of Technology, United States |
| Dr. Srikanth Mutnuri | Associate Prof., Department of Biological Sciences, Associate Dean for International Programmes and Collaboration, Birla Institute of Technology & Science, India |
| Dr. Bashar Malkawi | S.J.D., Associate Prof., College of Law, University of Sharjah, United Arab Emirates |
| Dr. Simona Silvia Merola | Istituto Motori - National Research Council of Naples, Italy |
| Dr. Hakan Caliskan | Faculty of Engineering, Department of Mechanical Engineering, Usak University, Turkey |

Table of Contents

**Special Issue on International Conference on Recent Innovations in Electrical,
Electronics and Communication Systems (RIEECS 2017), Dehradun, India, 2017**

Editors: Dr. Afzal Sikander and Dr. Padmanabh Thakur

Preface

Dr. Afzal Sikander.....1-2

Conference Moments

.....3-7

Comparison of MPPT Systems in Error Optimization using PID, Fuzzy and Hybrid Fuzzy in Multivariable Environment

Chandani Sharma, Anamika Jain.....8-21

Application of Group Hunting Search Optimized Cascade PD-Fractional Order PID Controller in Interconnected Thermal Power System

Jyoti Ranjan Nayak, Binod Shaw.....22-33

Transient Analysis of Quasi Oppositional Based Lightning Search Algorithm Optimized PID Controller in Isolated Small Hydro Power Plant

Shashikant, Binod Shaw.....34-43

Design of Solar System by Implementing ALO Optimized PID Based MPPT Controller

Raj Kumar Sahu, Binod Shaw.....44-55

Heat Energy Recovery System

Ujjawal Kohli, Vaibhav Mishra, Sparsh Singh Kotwal.....56-63

Operation of Symmetrical and Asymmetrical Two-Phase Induction Motor by Using 3-Leg Voltage

Source Inverter

Sheetal Vishal Umredkar, Abhishek Junghare, M. M. Renge.....64-76

Low Cost Device for Charging Mobile Phone using Another Smartphone

Vaibhav Aggarwal, Vaibhav Gupta, Kiran Sharma, Neetu Sharma.....77-82

Analysis and Design of Solar Power System Interface Utility Using ZVS Converter

R. G. Deshbhratar, M. M. Renge.....83-101

Design and Implementation of Analog Controller Based Single Phase Full Bridge Inverter for

Photovoltaic Applications

Abhishek Ranjan, Sunil Jalutharia, Harsh Garg.....102-113

Establishing Contingency Analysis with FACTS Devices Using Power World Simulator

B. Monisha, K. Balamurugan.....114-131

Special Issue on International Conference on Recent Innovations in Electrical, Electronics and Communication Systems (RIEECS 2017), Dehradun, India, 2017

Afzal Sikander

Department of Instrumentation and Control Engineering,
Dr. B. R. Ambedkar National Institute of Technology Jalandhar, Punjab, India-144011

Recent years have witnessed a prolific growth in the fields of Electrical, Electronics and Communication Systems (RIEECS) that inspire us to organize an International Conference. In order to aware the researchers working worldwide about the latest development in these research fields; RIEECS 2017 was held on 28–29th October, 2017 at Graphic Era (Deemed to be University), Dehradun, India. Delegates for this conference were

- Prof. (Dr.) Nitish Patel, Department of Electrical and Computer Engineering, University of Auckland, New Zealand.
- Prof. (Dr.) S. N Singh, Vice Chancellor, Madan Mohan Malviya University of Technology Gorakhpur (UP) and IEEE R10 conference and technical seminar coordinator 2015 – 18
- Dr. Asheesh Kumar Singh, Associate Professor, EED, MNNIT Allahabad (UP) and Vice Chairman – IEEE UP Section.
- Mr. V. K Srivastava, General Manager (Technical Services), IOCL – Haldia (WB).
- Dr. Y. V. Hote, Associate Professor, EED, IIT Roorkee (Uttarakhand)
- Dr. Nagendra Prasad Pathak, Associate Professor, Department of Electronics and Communication Engineering, IIT Roorkee (Uttarakhand)
- Prof. (Dr.) Mak Sharma, Professor, Computer Science, Birmingham City University, United Kingdom.
- Prof. (Dr.) R. C Bansal, Professor, Electrical Electronics and Computer Engineering University of Pretoria, South Africa.

In this conference, total 98 research papers were received, among which 48 papers were finally selected for the presentation. The research contributions of various premier institutes, such as, IITs, NITs, BITs Meshra, Graphic Era Hill University, Rajiv Gandhi College of Engineering & Research, Nagpur, NIC New Delhi, Rajasthan Technical University, were presented in this conference. The speakers and authors identified key problems related to the fields of Electrical, Electronics, and Communication Systems. Based on the quality, research work and scope of the journal, out of 48 research papers, 12 research papers were selected by the conference committee. These selected papers were submitted as an extended version to the special issue on RIEECS2017 of Trends in Renewable Energy Journal.

On behalf of the organizing and program committee of the conference, I would like to thank the authority of Trends in Renewable Energy, to provide me an opportunity to work as an editor of this special issue. Also, thanks to all reviewers of the articles for their esteem effort and time to uphold the spirit of the special issue of the Trends in Renewable Energy. Finally, it is also observed that the published papers cover the research fields of electrical, electronics and communication systems and meeting the goals of this conference. I hope that the articles will be useful to the research community to put forward the progress in the respective and the allied research fields.

Conference Moments



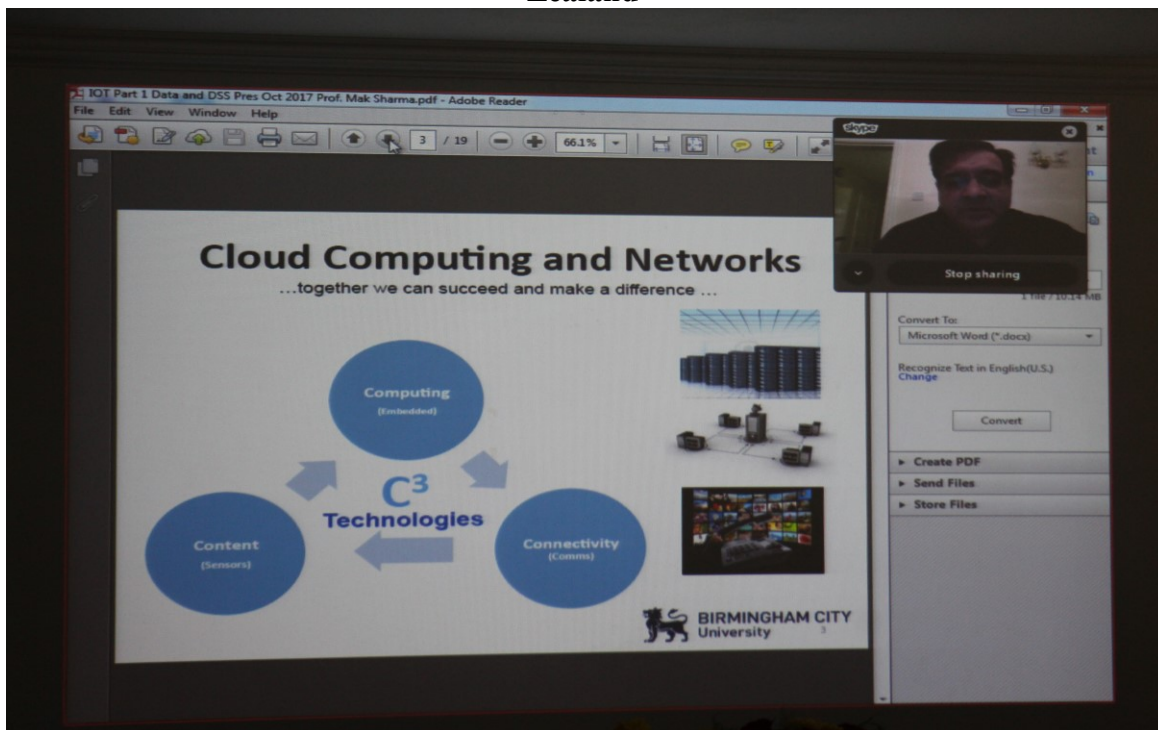
RIEECS2017-A Group Photograph



RIEECS2017-Few Organizing Committee Members



RIEECS2017-Keynote Speech by Dr. Nitish Patel, University of Auckland New Zealand



RIEECS2017-Lecture Delivered by Prof. (Dr.) Mak Sharma, Birmingham City University, United Kingdom through SKYPE



RIEECS2017-Paper Presentation by Participants



RIEECS2017-Panel of Judges During Technical Session



RIEECS2017- Dr. Afzal Sikander with Students



RIEECS2017- Professors (Drs.) and Students are Listening to a Speech



RIEECS2017-Vote of Thanks to Dr. Y. V. Hote, IIT Roorkee by Dr. Asheesh Kumar Singh, MNNIT Allahabad



RIEECS2017-Vote of Thanks to Prof. (Dr.) Nitish Patel by Prof. (Dr.) P. Thakur

Comparison of MPPT Systems in Error Optimization using PID, Fuzzy and Hybrid Fuzzy in Multivariable Environment

Chandani Sharma^{1*} and Anamika Jain²

1: Assistant Professor, Department of Electronics and Communication Engg., Graphic Era University, Dehradun, India

2: Professor, Department of Electronics and Communication Engg., Graphic Era University, Dehradun, India

Received January 4, 2018; Accepted March 15, 2018; Published April 23, 2018

Recent surveys conducted in the field of Power Control and Engineering show that photovoltaic (PV) systems are currently being discussed worldwide and research on the same is being carried globally. It is necessary to optimize the expanding use of photovoltaic systems through error detection in Maximum Power Point Tracking (MPPT) systems. Through this paper, an attempt is made to develop an efficient photovoltaic MPPT system using hybrid fuzzy technique to extract maximum power under a multivariable environment (changing temperature and irradiance). The MPPT system using Hybrid Controller (combining PID & FLC) has an increased efficiency and optimized output in comparison to the MPPT system using PID and Fuzzy individually. The system has explored a concept of computing academic performance indices with three MPPT models for future research based on global MPP calculation.

Keywords: PV; MPPT; Hybrid fuzzy; PID and Fuzzy; Global MPP; Academic performance indices

Introduction

The power output from photovoltaic (PV) systems is the largest when it is operated at the Maximum Power Point (MPP). Practically, under Standard Test Conditions (STC) it is obtained at temperature 25°C and irradiance 1000 W/m². A MPP Tracker is used to maintain this set point under a multivariable environment i.e. varying temperature and varying irradiance. Two different types of tracking systems are known: Passive and Active. Whereas a number of MPPT strategies are available based on single or multivariable approach designed using conventional or intelligent controllers [1-5].

Various types of MPPT systems are designed to meet voltage regulation, frequency regulation, power and harmonics control with quick response time, reduced error and increased gain. However, due to difference in real time system and results of digital simulated system it is sometimes not adaptable to obtain MPP in multivariable environment. Thus, there arises the need of error detection and optimization. The SPC (Statistical Process Control) management tool compiles an overall mathematical measure for multiple sets of simulation and determines performance index. The performance index

*Corresponding author: chandani19nov@gmail.com

estimates errors in the output. The appropriate response is calculated by detecting and reducing errors between measured and required set point.

The performance index approximates the process performance. It delivers an index for a process which measures how close a process is running to its desired specification limits, relative to the variability of the process. The larger the index, the lesser is the functional capability of system, *i.e.*, system does not operate at its full potential and the output is not within specified limits. Performance indices are classified as (a) Academic and (b) Practical indices. Academic indices are straight forward and computed along with simulation of the process or system being run at different instants of time. On the other hand, Practical indices are calculated for the final response obtained after the system has been simulated. It is found that academic performance indices are generally preferred over practical ones as the quantitative characterization is directly and quickly obtained when simulating with academic indices. Moreover, they are adaptive to changing environmental conditions. The other advantages include fast computation and reduced complexity of physical set up that raises the cost of the system when used with practical indices [6-22].

The approach used in the present work is to determine academic performance indices and thereby optimize MPPT system through attainment of suitable tuning and scaling gain constants. The tuning and scaling gain constants are evaluated on integral of error. The error is computed by difference of voltage obtained from PV and converter subsystem and desired set point at STC (21.07 V). The academic performance indices are computed and direct comparison between different MPPT systems using different sets of tuning parameters is obtained.

Design and Simulation of Three MPPT Systems

Three MPPT systems [1-3] are designed using conventional controller (PID), intelligent controller (FLC) and fusion of both, *i.e.*, hybrid controller (PD+I FLC) [4-6]. The commercially available Solarex MSX-60W panel is designed using mathematical Simulink modeling in MATLAB. Thereafter, Buck converter (Step Down) is connected across the output of panel to achieve STC [4-6]. The output of the converter is adjusted to the set point (21.07 V), and the controller is used to monitor set point under multivariable environment. The controller delivers a control function that acts as an input to make the converter output approach the set point. Different gain constants of controllers are tested and tuned to achieve optimized results for the converter output by minimizing error. Error is generated by difference in output obtained from converter to the desired *i.e.*, 21.07 V.

For PID, the tuning gains are three gain control parameters K_P (Proportional gain), K_I (Integral gain) and K_D (Derivative gain). For FLC, it is the fuzzy sets *i.e.*, the number and type of membership functions with crossover points and its respective range (*i.e.*, Universe of Discourse formulated with set of rules). For Hybrid PD+I FLC, in addition to FLC, four scaling gains *i.e.*, G_U (normalization gain), G_E (proportional gain), G_{CE} (derivative gain) and G_{IE} (integral gain) are added and the system is tuned to achieve appropriate results.

The academic performance metrics include: IAE (Integral of Absolute Error), ISE (Integral of Square Error), ITAE (Integral of Time multiplied by Absolute Error) and ITSE (Integral of Time multiplied by Square Error). The computed errors are minimized for integral of error $e(t)$. These are described below:

ISE (Integral of Squared Error): It is an analytical approach that uses linear quadratic weights for tracking set point based on cumulative sum of error. It is calculated using Parseval's theorem. The expression for ISE is:

$$ISE = \int_0^{\infty} \{e(t)\}^2 . dt \quad (1)$$

IAE (Integral of Absolute Error): It is a non-analytical form of error based on computing integral for a sum of areas below and above set point without adding any weights to track set point. The expression for IAE is:

$$IAE = \int_0^{\infty} |e(t)| . dt \quad (2)$$

ITSE (Integral of time multiplied by Squared Error): This criterion is used to check long duration errors, where an additional factor of time is multiplied with fast settling time. The expression for ITSE is:

$$ITSE = \int_0^{\infty} t. \{e(t)\}^2 . dt \quad (3)$$

ITAE (Integral of time multiplied by Absolute Error): This measure tunes system rapidly when compared to all other indices. It possesses various other features like easy applicability, optimal selectivity, and reliability. The least value of ITAE provides appropriate selectivity of the system performance. The expression for ITSE is:

$$ITAE = \int_0^{\infty} t. |e(t)| . dt \quad (4)$$

The three MPPT systems *i.e.*, conventional (PID), intelligent (FLC) and hybrid controller (PD+I FLC) are developed and simulated for obtaining ISE, IAE, ITSE and ITAE for multivariable conditions. Different temperatures in the range of 0°C to 45°C with varying Gaussian irradiance function are considered for same. The MPPT system performance is analyzed by using the converter voltage output and academic indices obtained. The system with least errors and the converter output close to set point yields optimized results, and thus are preferred for utility-based applications.

Firstly, the calculation of academic errors is done in MPPT system using Proportional Integral and Derivative controller. PID evaluates past error using proportional tuning factor K_P , present error using integral factor K_I and future predictive error using derivative of obtained error K_D due to difference in output obtained from converter to the desired *i.e.*, 21.07 V.

The tuning gains of the conventional controller were experimented for different values of three gain control parameters (K_P , K_I and K_D). However, the most appropriate results were obtained for K_P (Proportional gain) = 0.1, K_I (Integral gain) = 0.05 and K_D

(Derivative gain) = 0.1 and the same values are used in MPPT set up as shown in Figure 1.

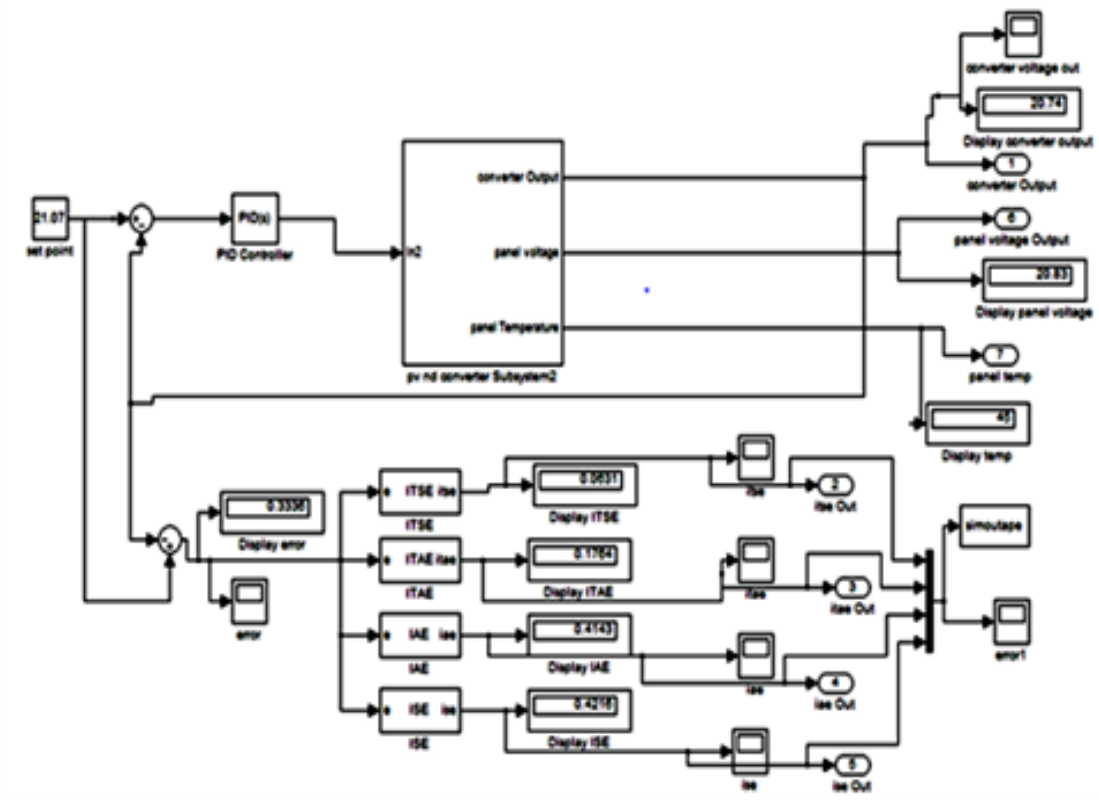


Figure 1. Block diagram of Implemented PID for error check

The output of PV and converter subsystem using PID appears 20.70 V. The developed MPPT on simulation for ISE, IAE, ITSE and ITAE delivers output responses as shown in Figure 2.

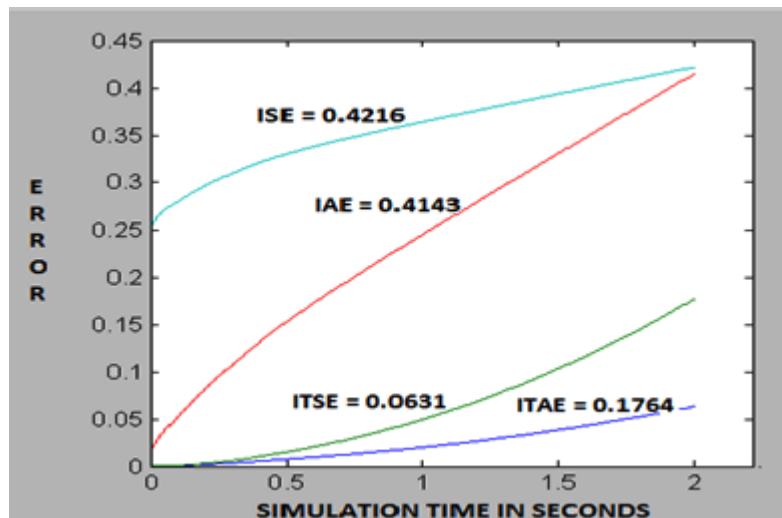


Figure 2. Simulated outputs using PID

Since the outputs and error indices are not appreciably good, simulation is then carried out using Fuzzy Logic controller. Fuzzy logic offers a promising solution to this

conceptual design of MPPT through fuzzy modeling by removing the dependence of tuning using a set of rules that automatically monitors system closer to set point.

In this context, Mamdani type FLC using two inputs (error $E(n)$ and change in error $\Delta E(n)$) with one output (duty cycle of converter) is designed. The effect of interaction between the two input parameters ($E(n)$ and $\Delta E(n)$) with output parameter duty cycle (DC) is tested for various types of membership functions using three and five subsets. From observations, three Gaussian functions are chosen for which crossover point 0.5 is selected. The universe of discourse for the input variable $E(n)$ is chosen to be $[-0.01, +0.15]$ and $\Delta E(n)$ is taken as $[-10, +10]$ while the output variable duty cycle is chosen to be as $[-0.4, 0]$ to monitor MPP for developed MPPT model.

The nine rules corresponding to same are written in rule editor of the Fuzzy Inference System and are fired when the input is given to the controller. Based on these rules, the system works, and the implication method is applied. The generalization or outputs obtained after the implication method are aggregated and the defuzzification is done to find the crisp output.

The MPPT system designed using a Fuzzy Logic Controller is given in Figure 3.

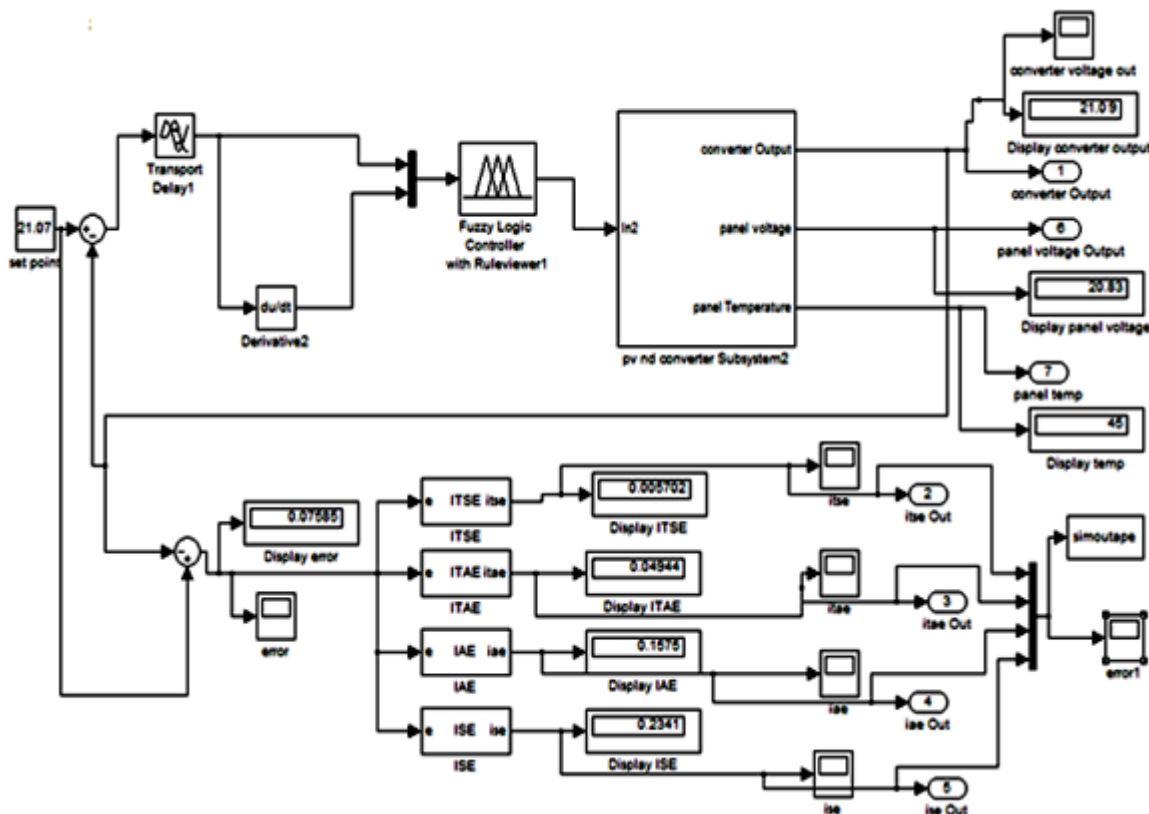


Figure 3. Block diagram of Implemented FLC for error check

The converter output obtained is improved and found to be 21.03 V at STC. The system results for academic indices simulation are shown in Figure 4.

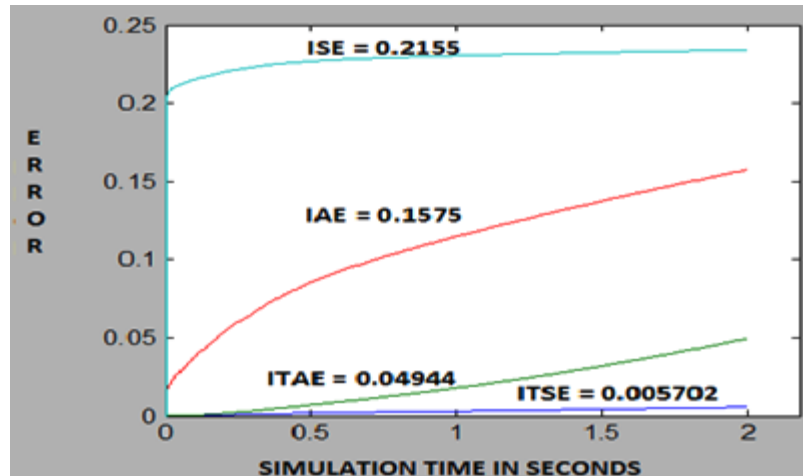


Figure 4. Simulated outputs using FLC

Despite the advantages and improved converter output with optimized indices of FLC over PID, there remain a number of drawbacks in its implementation. Fuzzy Controllers are characterized by a number of parameters such as input/output scales, center and width of membership function, selection of appropriate fuzzy control rules etc. The complexity of these parameters can be varied by simply developing a hybrid controller. The PID and FLC controllers are combined together and PD+I FLC MPPT system.

The MPPT system developed using hybrid fuzzy technique uses a Fuzzy logic controller with a rule viewer, two summing elements, two multiplexers, a differentiator, an input block, four gain elements representing the scaling gains (GU demoralization factor, GE proportional gain, GCE the derivative gain and GIE integral gain). The system developed is shown in Figure 5.

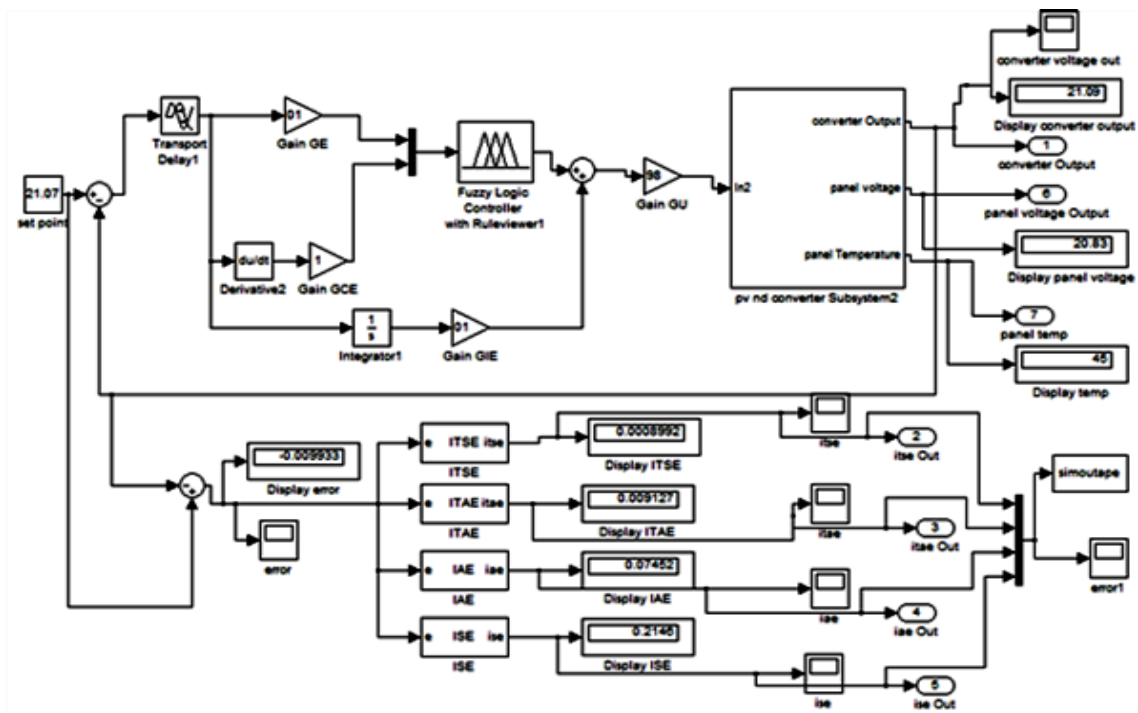


Figure 5. Block diagram of Implemented PD+I FLC for error check

The system is tuned for the optimum output with four scaling gains, which are achieved with $GE = 0.1$, $GCE = 1$, $GIE = 0.01$, $GU = 1.5$. The converter output obtained from hybrid controller is 21.04 V that was the closest to set point (21.07 V) as compared to PID (20.70V) and FLC (21.03V). The academic performance indices obtained by simulating the system is shown in Figure 6.

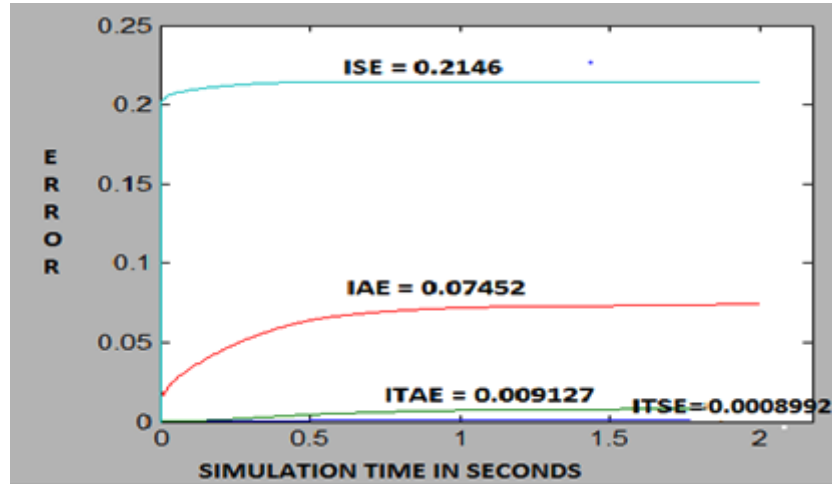


Figure 6. Simulated outputs using PD+I FLC

Comparison of Three MPPT Systems

A comparison is framed for academic performance indices calculated for three MPPT designed and simulated models. This is shown below in Tables 1 to 4 with graph outputs Figures 7 to 10. Firstly, the comparison is made for Integral of time multiplied by square error (ITSE). Table 1 shows observations for same followed by graphs in Figure 7.

Table 1. Observation for ITSE

| T °C | PID | FLC | PD+I FLC |
|-----------|---------------|-----------------|------------------|
| 5 | 0.0003 | 0.000006 | 0.0000132 |
| 10 | 0.0007 | 0.000142 | 0.0000525 |
| 15 | 0.0015 | 0.000328 | 0.0001056 |
| 20 | 0.0032 | 0.000724 | 0.0002569 |
| 25 | 0.0133 | 0.001610 | 0.0004247 |
| 30 | 0.0163 | 0.002259 | 0.0005944 |
| 35 | 0.0254 | 0.003257 | 0.0006172 |
| 40 | 0.0356 | 0.004897 | 0.0007985 |
| 45 | 0.0631 | 0.005702 | 0.0008992 |

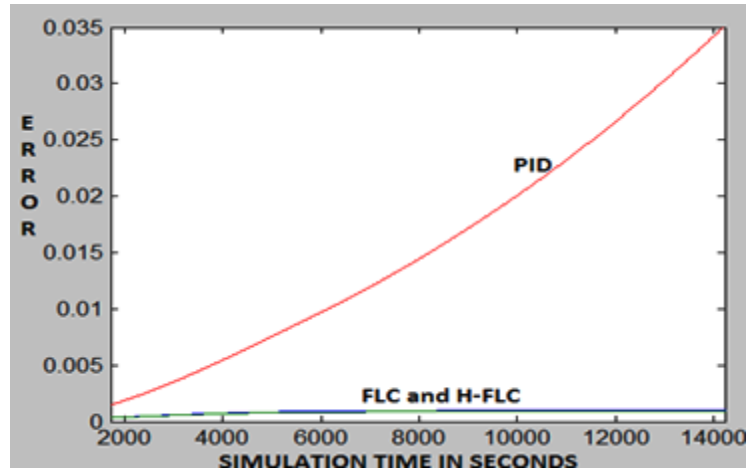


Figure 7. Graphical comparison of MPPT Systems for ITSE

It is observed that ITSE appears the minimum for the hybrid system when compared to intelligent and conventional systems. At the STC temperature of 25 °C, the respective values of errors appear 0.0133 (PID), 0.001610 (FLC) and 0.0004247(PD+I FLC) and on process completion appear 0.0631(PID), 0.005702(FLC) and 0.0008992(PD+I FLC). This proves the least error in PD+I FLC based MPPT system. Next, the comparison is made for Integral of time multiplied by absolute error (ITAE). Table 2 and Figure 8 show the same.

Table 2. Observation for ITAE

| T °C | PID | FLC | PD+I FLC |
|-----------|---------------|----------------|-----------------|
| 5 | 0.0001 | 0.00000 | 0.000000 |
| 10 | 0.0009 | 0.00004 | 0.000047 |
| 15 | 0.0018 | 0.00009 | 0.000098 |
| 20 | 0.0042 | 0.00024 | 0.000135 |
| 25 | 0.0168 | 0.00097 | 0.000478 |
| 30 | 0.0345 | 0.00465 | 0.000956 |
| 35 | 0.0987 | 0.00947 | 0.001180 |
| 40 | 0.1452 | 0.02535 | 0.004765 |
| 45 | 0.1764 | 0.04944 | 0.009127 |

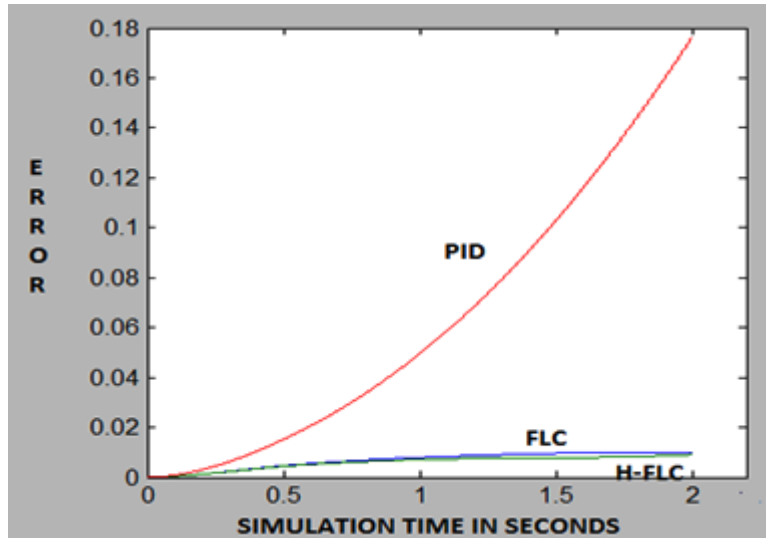


Figure 8. Graphical comparison of MPPT Systems for ITAE

From the results, it can be seen that ITAE appears the minimum for the hybrid system when compared to an intelligent and conventional system. At the STC temperature-25°C, the respective values of errors appear 0.0168 (PID), 0.00097(FLC) and 0.000478 (PD+I FLC) and on process completion appear 0.176 (PID), 0.04944 (FLC) and 0.009127 (PD+I FLC). This proves the least error in PD+I FLC-based MPPT system. Next, observations for Integral of absolute error (IAE) are carried out. This is shown in Table 3 followed by graphical outputs in Figure 9.

Table 3. Observation for IAE

| T °C | PID | FLC | PD+I FLC |
|-----------|---------------|---------------|----------------|
| 5 | 0.0041 | 0.0015 | 0.00030 |
| 10 | 0.0097 | 0.0021 | 0.00051 |
| 15 | 0.0214 | 0.0047 | 0.00097 |
| 20 | 0.0643 | 0.0078 | 0.00174 |
| 25 | 0.0987 | 0.0089 | 0.00389 |
| 30 | 0.1146 | 0.0587 | 0.00887 |
| 35 | 0.2156 | 0.0877 | 0.01421 |
| 40 | 0.3289 | 0.1214 | 0.04778 |
| 45 | 0.4143 | 0.1575 | 0.07452 |

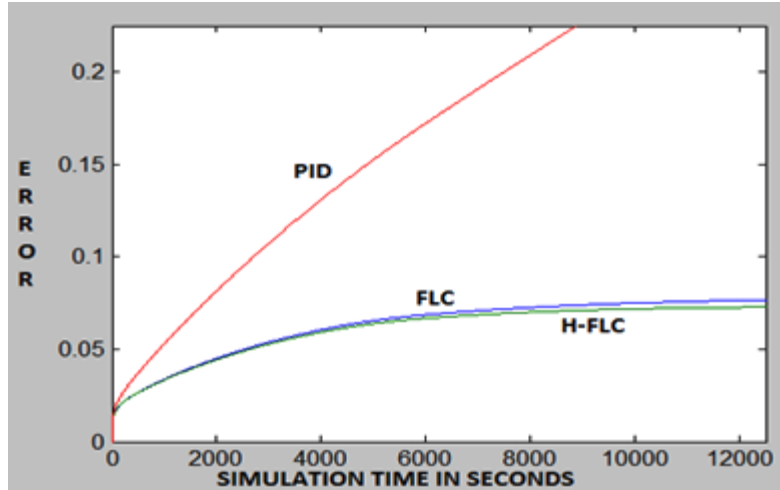


Figure 9. Graphical comparison of MPPT Systems for IAE

It is clear from above that, IAE appears to be the least for the hybrid system when compared to an intelligent and conventional system. At STC temperature 25 °C, the respective values of errors appear 0.0987 (PID), 0.0089 (FLC) and 0.00389 (PD+I FLC) and on process completion appear 0.4143 (PID), 0.1575(FLC) and 0.07452 (PD+I FLC). This proves the least error is obtained in PD+I FLC-based MPPT system. Now, test results are compared for Integral of Squared Error (ISE), observation for same is shown in Table 4 followed by Figure 10.

Table 4. Observations for ISE

| T °C | PID | FLC | PD+I FLC |
|------|--------|--------|----------|
| 5 | 0.2092 | 0.2007 | 0.2000 |
| 10 | 0.2131 | 0.2011 | 0.2009 |
| 15 | 0.3255 | 0.2017 | 0.2012 |
| 20 | 0.3487 | 0.2048 | 0.2037 |
| 25 | 0.3941 | 0.2098 | 0.2089 |
| 30 | 0.4003 | 0.2106 | 0.2101 |
| 35 | 0.4161 | 0.2115 | 0.2108 |
| 40 | 0.4198 | 0.2138 | 0.2125 |
| 45 | 0.4216 | 0.2155 | 0.2146 |

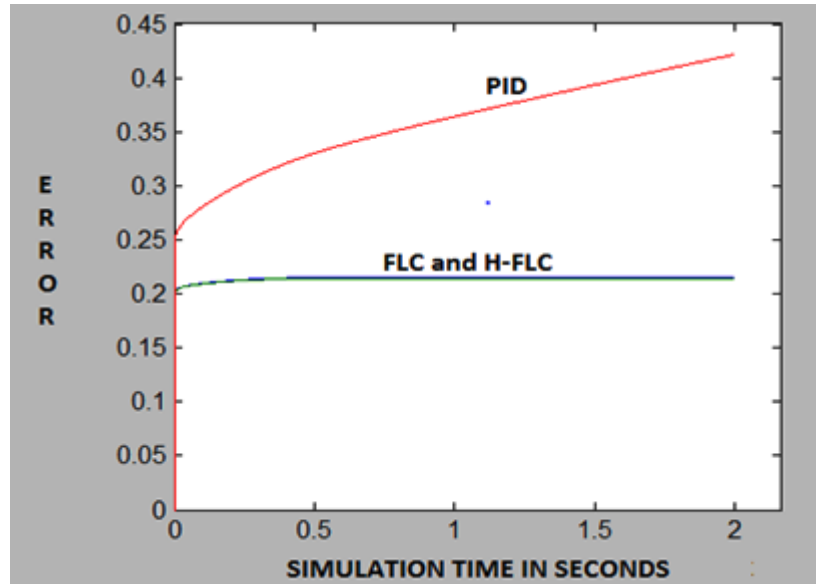


Figure 10. Graphical comparison of MPPT Systems for ISE

For ISE also, it is found that value appears the minimum for the hybrid system when compared to an intelligent and conventional system. At the STC temperature of 25 °C, the respective values of errors appear 0.3941 (PID), 0.2098 (FLC) and 0.2089 (PD+I FLC) and on process completion appear 0.4216 (PID), 0.2155 (FLC) and 0.2146 (PD+I FLC). This proves the least error in PD+I FLC based MPPT system.

Thus, it is clear from observations (Tables 1 to 4) and graphical displays (Fig. 7 to 10) that the PID controlled system gives very large errors in comparison to FLC and hybrid FLC controlled system. The academic indices are optimized appropriately in hybrid MPPT system when compared to intelligent MPPT system. Also, the converter output is the closest to set point and achieved throughout simulation in comparison to other two systems. This is shown in Figure 11.

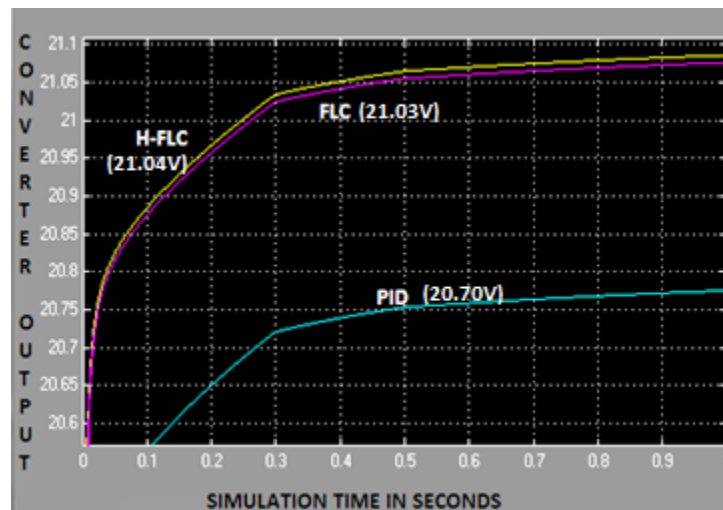


Figure 11. Converter outputs for PID, FLC, and Hybrid FLC designed MPPT Systems

CONCLUSIONS

The three MPPT systems developed are tested for Academic Performance Indices and its optimization. The converter outputs corresponding to three different controllers are obtained and optimized with the most appropriate results in the hybrid MPPT. It is found that by using suitable values of scaling gains the PD+I FLC system generates the most convenient outputs. It is clear from observations that the academic indices were least calculated for PD+I FLC system and the MPPT output obtained is very close to desired set point. The developed MPPT system can be further used for different application-based systems. The results obtained can serve as an advantage for future scholars and researchers working on MPPT systems.

ACKNOWLEDGMENTS

The research acknowledges direct and indirect contribution made by Organization and others.

CONFLICTS OF INTEREST

The authors declare that there is no conflict of interests regarding the publication of this paper.

REFERENCES

- [1] Chandani Sharma, Anamika Jain, "Solar Panel Mathematical Modelling using Simulink" International Journal of Engineering Research and Applications, vol. 4, no. 5, pp 67-72, May 2014.
- [2] Chandani Sharma, Anamika Jain, "Simulink based Multivariable Solar Panel Modelling" Telkominika Indonesian Journal of Electrical Engineering, vol. 12, no. 8, pp 5784-5792, August 2014.
- [3] Chandani Sharma, Anamika Jain, "Maximum Power Point Tracking Techniques-A Review" International Journal of Recent Research in Electrical and Electronics Engineering, vol. 1, no. 1, pp. 25-33, June 2014.
- [4] Chandani Sharma, Anamika Jain, "Performance Comparison of PID and Fuzzy Controllers in Distributed MPPT" International Journal of Power Electronics and Drive Systems, vol. 6, no. 3, pp. 625-635, September 2015.
- [5] Chandani Sharma, Anamika Jain, "Modeling of Buck Converter Models in MPPT using PID and FLC", TELKOMNIKA (Telecommunication Computing Electronics and Control), vol. 13, no. 4, pp. 1270-1280, December 2015.
- [6] Chandani Sharma, Anamika Jain, "Academic Performance Indices: Error Calculation in Distributed MPP Tracking using PID and FLC" Journal of Graphic Era University, vol. 4, no. 1, pp. 1-16, August 2016.
- [7] B. Subudhi, R. Pradhan, "Characteristics evaluation and parameter extraction of a solar array based on experimental analysis," in Proceedings of 9th IEEE Power

- Electronics and Drives Systems, Singapore, December 5–8, 2011. DOI: 10.1109/PEDS.2011.6147269
- [8] Tarak Salmi, Mounir Bouzguenda, Adel Gastli, Ahmed Masmoudi, “MATLAB/Simulink Based Modelling of Solar Photovoltaic Cell”, *International Journal of Renewable Energy Research*, vol. 2, no. 2, pp. 213-218, 2012.
- [9] J. Jantzen, “Tuning of Fuzzy PID Controllers”, Tech. report no 98-H 871 (fpid), Technical University of Denmark, Department of Automation, 30 Sep 1998. <https://pdfs.semanticscholar.org/7d0e/da80a8b206d4d29fe6df65597c8078a110b2.pdf> (accessed on 4/26/2018)
- [10] S. Z. He, S. Tan and F. L. Xu, “Fuzzy self-tuning of PID controllers”, *Fuzzy Sets and Systems*, vol. 56, pp. 37-46, 1993.
- [11] J. Surya Kumari, C. Saibabu, “Maximum Power Point Tracking Algorithms for Grid Connected Photovoltaic Energy Conversion System”, *International Journal of Power Electronics and Drive System*, vol. 3, no. 4, pp. 424-437, December 2014.
- [12] B. Subudhi, R. Pradhana, “A Comparative Study on Maximum Power Point Tracking Techniques for Photovoltaic Power Systems” *IEEE Transactions on Sustainable Energy*, vol. 4, no. 1, pp. 89 – 98, January 2013.
- [13] M. S. Ait Cheikh, C. Larbes, G. F. Tchoketch Kebir, A. Zerguerras “Maximum power point tracking using a fuzzy logic control scheme”, *Revue des Energies Renouvelables*, vol. 10 no. 3, pp. 387 – 395, 2007.
- [14] C. A. R. Paja, G. Spagnuolo, G. Petrone, M. Vitelli, J. D. Bastidas, “A multivariable MPPT algorithm for granular control of PV systems,” in *Proc. IEEE Int. Symp. Ind. Electron.*, pp. 3433–3437, 2010.
- [15] Rosa A. Mastromauro, Marco Liserre, Antonio Dell Aquila, “Control Issues in Single-Stage Photovoltaic Systems MPPT, Current and Voltage Control” *IEEE Transactions on Industrial Informatics*, vol. 8, no. 2, pp. 241-254, May 2012.
- [16] Huiying Zheng, Shuhui Li, Timothy A. Haskew, Yang Xiao, “Impact of uneven shading and bypass diodes on energy extraction characteristics of solar photovoltaic modules and arrays”, *International Journal of Sustainable Energy*, vol. 32, no. 5, pp. 351-365, October 2013.
- [17] Tow Leong Tiang, Dahaman Ishak, “Modeling and simulation of deadbeat-based PI controller in a single-phase H-bridge inverter for stand-alone applications”, *Turkish Journal of Electrical Engineering & Computer Sciences*, vol. 22, pp. 43-56, January 2014.
- [18] International Energy Agency, *Technology Roadmap: Solar Photovoltaic Energy*, 2014. https://www.iea.org/publications/freepublications/publication/TechnologyRoadmapSolarPhotovoltaicEnergy_2014edition.pdf (accessed on 4/26/2018)
- [19] D. Sera, L. Mathe, T. Kerekes, S.V. Spataru, R. Teodorescu, “On the Perturb-and-Observe and Incremental Conductance MPPT Methods for PV Systems” *IEEE Journal of Photovoltaics*, vol 3, no. 3, pp. 1070 – 1078, July 2013.
- [20] Essam Natsheh, A. Khalid Buragga, “Comparison between Conventional and Fuzzy Logic PID Controllers for Controlling DC Motors”, *International Journal of Computer Science Issues*, vol. 7, no. 5, pp. 128-134, September 2010.
- [21] P. Venugopal, A. Ganguly, P. Singh, “Design of Tuning Methods of PID Controller using Fuzzy Logic”, *International Journal of Emerging trends in Engineering and Development*, vol. 5, no. 3, pp. 239-248, September 2013.

- [22] Reseeds, “Control System Optimisation: Criteria and Analytical Methods”, 2003.
<http://www.reseeds.com/control%20system%20optimisation.pdf> (accessed on 4/26/2018)

Article copyright: © 2018 Chandani Sharma and Anamika Jain. This is an open access article distributed under the terms of the [Creative Commons Attribution 4.0 International License](https://creativecommons.org/licenses/by/4.0/), which permits unrestricted use and distribution provided the original author and source are credited.



Application of Group Hunting Search Optimized Cascade PD-Fractional Order PID Controller in Interconnected Thermal Power System

Jyoti Ranjan Nayak* and Binod Shaw

Department of Electrical Engineering, National Institute of Technology, Raipur, India

Received January 4, 2018; Accepted March 15, 2018; Published April 23, 2018

This paper is an endeavor to enhance the performance of the Automatic Generation Control (AGC) by adopting cascade PD-FOPID (Proportional Derivative - Fractional Order PID) controller in a two-area mutually connected thermal power plant with Generation Rate Constraint (GRC). The performance of the cascade PD-FOPID controller is validated by contrasting PID and FOPID controllers implemented in each area as AGC. The basic goal of the design of these controllers is to lessen the area control error (ACE) of corresponding area by conceding the frequency and tie-line power deviation. Group Hunting Search (GHS) algorithm is adopted to explore the gain parameters of the controllers to lessen the objective function (ITAE). A small step load transition of 0.01 p.u. is enforced in area-1 to investigate the controller performance. Cascade PD-FOPID controller optimized by GHS algorithm performs precisely better than PID and FOPID controller in the proposed system.

Keywords: Automatic Generation Control (AGC); Proportional-Integral-Derivative controller (PID); Fractional Order PID (FOPID); Group Hunting Search (GHS); Cascade PD-FOPID controller

Introduction

In the power system, the basic objective is to counterbalance the generated power and demand power comprising power loss. Interconnected power system is a significant advent to utilize the generating units and transmission lines intelligently to counterbalance the power. The rotating mass of the generators are the primary controllers to regulate the small deviations of frequency and power. Due to the huge deviation of load, the diversity of frequency and tie-line power extends over the different mutually connected areas. The secondary controller Automatic Generation Control (AGC) is a significant approach to handle the huge deviations of frequency and power. The capability to attain the stability is enhanced due to the fast response of the secondary controller [1, 2]. The fast response of AGC enhances the capability of the system to handle continuous deviation of load. The fundamental objectives of AGC are

- i. To contribute reliable, stable, economic and quality power.
- ii. To set the system frequency to the nominal frequency.
- iii. To lessen the undershoot (U_{sh}), overshoot (O_{sh}) and settling time (T_s) of the frequency and tie-line power deviation.

*Corresponding author: bapi.jyoti.2@gmail.com

Many concepts to enhance the ability of AGC have been proposed by many authors from last few decades. Conventional PID controller is validated over I and PI controllers optimized by Imperialist Competitive Algorithm (ICA) as illustrated in [3, 4]. The cascade combination of PI and PD controllers is adopted as inner and outer controller loop in multi-area power system. The cascade PI-PD controller is validated as a better controller over conventional PID controller and the parameters of the controller are tuned by Flower Pollination Algorithm (FPA) to enhance the performance of the controller in [5]. The degree of freedom (DOF) of the PID controller is increased in [6, 7] entitled as 2DOF PID controller to enhance the performance of the AGC in the multi-area power system optimized by Cuckoo Search Algorithm (CSA) and Teaching Learning Based Optimization (TLBO) algorithms respectively. The superiority of Fuzzy-PID controller optimized by various algorithms and hybrid algorithms over PID as AGC is validated in [8-12]. Xue and Chen [13] have portrayed a brief comparison between four different types of fractional order controller. Fractional order PID controller (FOPID), Tilted Integral Derivative controller (TID), and fuzzy-FOPID controller optimized by different algorithms are adopted as AGC in [14-24]. Application of some superior algorithms in the power system is beautifully expressed in [25-28].

The basic purpose of this paper is to design AGC for two-area power system. Each area subsists of a thermal power unit with Generation Rate Constraint (GRC) with saturation limit of ± 0.05 . PID, FOPID, and PD-FOPID controllers are adopted as the controller in the system to minimize the objective function by concerning frequency and power deviations. The design variables (controller gains) enormously influence the system performance. Group Hunting Search (GHS) technique is adopted to minimize the error of this single objective constraint problem by hunting the appropriate pair of controller gains.

System Investigated

The proposed system is a two-area coupled together by tie-line. Thermal power plants of same characteristics with GRC reside in each area of the interconnected system. The model of the system is portrayed in Fig. 1. Normally hydro and thermal power plants have a saturation limit of change of generated power. The generation power can swift at a particular maximum rate. Generation rate is considered for the proposed system with 5% (± 0.05) of saturation limit. The transfer function parameters are portrayed in appendix 1. A small load swift of 5% (0.05) in area-1 is implemented to analyze the transient response of the system. This load change in area-1 propagates error in both the areas entitled as Area Control Errors (ACE_1 and ACE_2). ACEs concerning deviations of frequency and tie-line power have to be minimized and may be defined as equations (1) and (2).

$$ACE_1 = B_1 \Delta f_1 + \Delta P_{tie} \quad (1)$$

$$ACE_2 = B_2 \Delta f_2 + \Delta P_{tie} \quad (2)$$

Where B_1 and B_2 are the bias factors. The deviations of frequency with respect to nominal values in the area-1 and area-2 are Δf_1 and Δf_2 , respectively. The deviation of power in tie-line is ΔP_{tie} and is characterized in equation (3).

$$\Delta P_{tie} = \frac{2\pi T_{12}}{s} (\Delta f_1 - \Delta f_2) \quad (3)$$

PID, FOPID and PDFOPID controllers are executed in both the areas individually to examine the controller potential to enhance the system performance. Intelligent PD-FOPID controller is observed as a superior controller over PID and FOPID controllers. ITAE (Integral Time Absolute Error) holds fine capability to handle long period transients of the signal than ISE, IAE, and ITSE indices as described in [23]. The sensitivity of deviations increases with respect to time, *i.e.*, small deviations from the nominal value after a long period are higher sensitive than large deviations earlier. ITAE is adopted as objective function by concerning errors (Δf_1 , Δf_2 , and ΔP_{tie}) and time as described in equation (4).

$$ITAE = \int_0^T t(\Delta f_1 + \Delta f_2 + \Delta P_{tie})$$

Subject to

$$0.001 \leq K_i \leq 2 \quad i = 1, 2, \lambda, n \quad (4)$$

Where n is the designed variable.

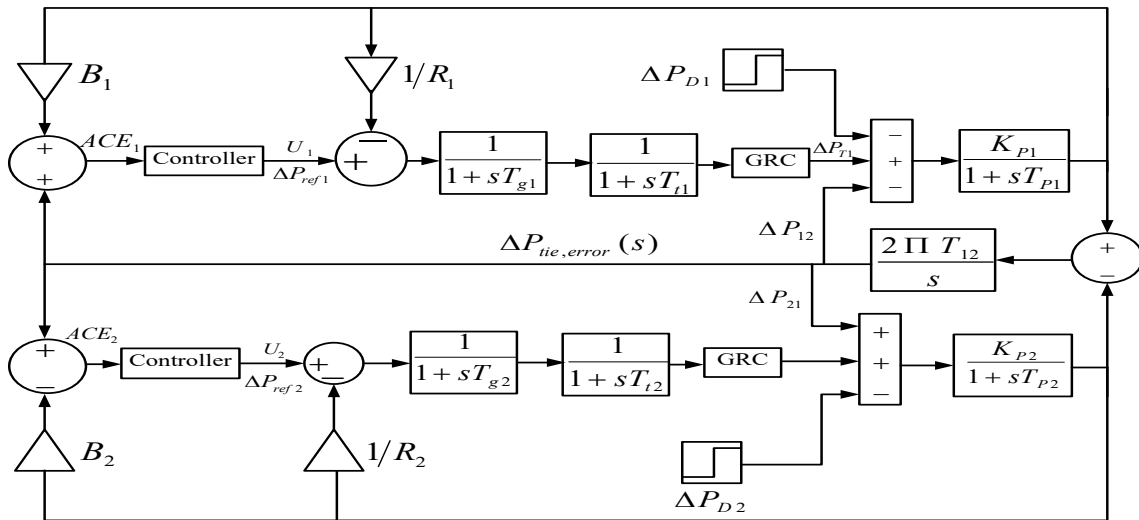


Figure 1. Power system model [24]

Controller Structure

The performance of the system mostly relies upon the controller design. Picking up the appropriate pair of gain parameters of controllers is also very significant factor.

FOPID Controller

Fractional order PID controller is a novel approach recommended from the fractional calculus. The orders of the integration and differentiation (λ and μ) are fractional values. λ and μ values may not be integer. The transfer function of the FOPID controller is characterized in equation (5).

$$G_C(s) = K_p + \frac{K_I}{s^\lambda} + s^\mu K_D \quad (5)$$

Due to fractional order, it has supremacy control over PID controller to maintain stability of the system. PID and FOPID controller structures are portrayed in Fig. 2(a) and 2(b) respectively.

Cascade PD-FOPID controller

The purposed controller comprises two loops (inner and outer) arranged in such an aspect that the output of one loop is the input for other loop as portrayed in Fig. 3 [5]. The FOPID controller is adopted as the inner measure which enhances the potency to control the supply disruption that may influence the outer process. The PD controller is adopted as the outer measure to regulate the output quality of the process. This controller has a vital advantage of eradication of noise which make the other parts of the system isolate from the noise.

Outer loop

This loop is characterized by concerning process output $Y(s)$, process of outer $G_1(s)$ and load distortion $d_1(s)$ as

$$Y(s) = G_1(s)U_1(s) + d_1(s) \quad (6)$$

Where $U_1(s)$ is the input to the process of outer which is equal to output of the inner loop. Outer loop is adopted to control the error associated with reference $R(s)$ or to track the reference.

Inner loop

The inner loop is characterized in equation (7) by concerning process of inner $G_2(s)$ as

$$y_2(s) = G_2(s)U_2(s) \quad (7)$$

Where output of the inner loop fed as input to the outer loop $y_2(s) = U_1(s)$.

The prime goal of the inner loop is to comprise the disturbances occurred inside the inner loop itself. The response of the cascade controller depends on fastness of inner controller. The overall transfer function of the cascade controller is characterized in equation (8).

$$Y(s) = \left[\frac{G_1(s)G_2(s)C_1(s)C_2(s)}{1 + G_2(s)C_2(s) + G_1(s)G_2(s)C_1(s)C_2(s)} \right] R(s) - \left[\frac{G_1(s)}{1 + G_2(s)C_2(s) + G_1(s)G_2(s)C_1(s)C_2(s)} \right] d_1(s) \quad (8)$$

In this paper, PD controller is adopted as outer loop controller and FOPID controller is adopted as inner loop.

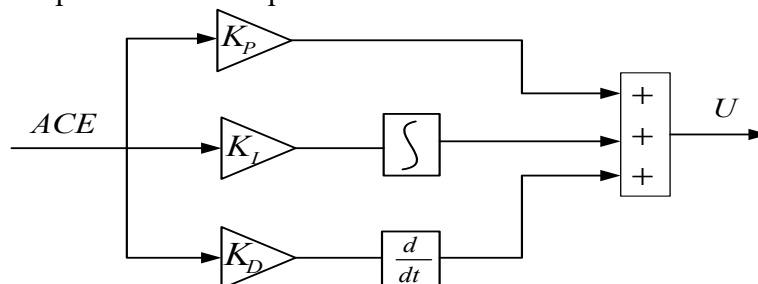


Figure 2(a). PID controller structure

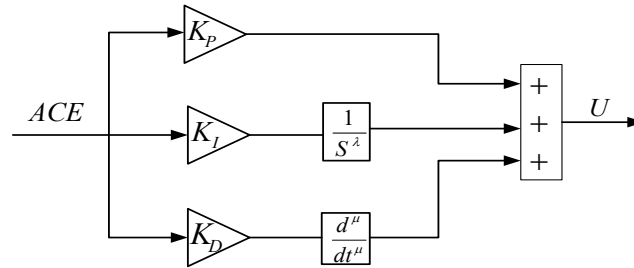


Figure 2(b). Fractional order PID controller structure

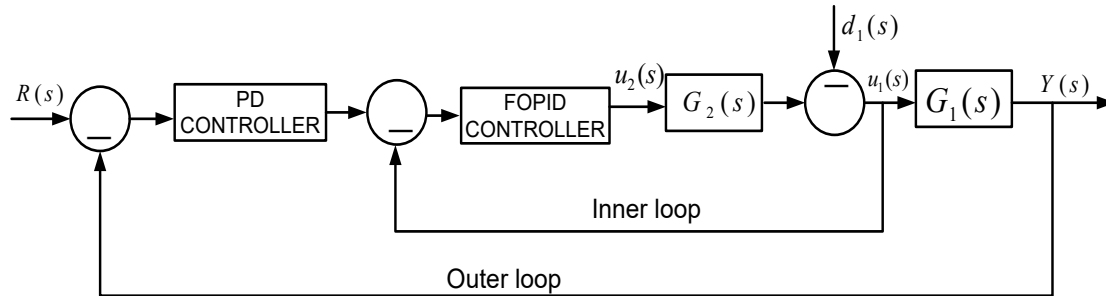


Figure 3. Cascade PD-FOPID controller structure [5]

Group Hunting Search (GHS) Algorithm

Optimization techniques play an influential aspect to enhance the performance of the controller by searching relevant pair of gain parameters of the controller. In this paper, GHS algorithm is adopted to tune the parameters of PID, FOPID, and PD-FOPID controllers individually to validate the performance of PD-FOPID controller. The basic purpose of optimization is to lessen ITAE by hunting the parameters of controllers within the specified limit as defined in equation (4).

The relation between predator (group hunters *i.e.*, Lions, wolves etc) and prey is beautifully expressed as optimization technique by r. Oftadeh *et.al.* [22]. GHS algorithm is derived from the strategy of hunting a prey by concerning the group hunting technique. Unity of group members adopts an approach to trap the prey by circumscribing it. The member of the group near to the prey is adopted as the leader and all other members follow the leader to move towards the prey (optimum solution). If any of the group members amends by a better position compared to the recent leader then it becomes the leader in the next generation. The hunter in each generation follows the leader by concerning maximum moments towards the leader (MML). MML affects the technique to counterbalance exploration and exploitation. The strides of the GHS are as

1. Initialize the group of hunters of size $X_{[NP \times D]}$ within the limit 0.001 to 2.
2. The best fitted hunters among the group is adopted as leader.
3. The hunter's positions are refurbished towards the leader. The mathematical expression is defined in equation (9).

$$X_i^{k+1} = X_i^k + rand \times MML \times (X_i^L - X_i^k) \quad (9)$$

$$MML = 0.6 - \left(it \times \left(\frac{0.6}{itermax} \right) \right)$$

Where ‘it’ is the current iteration, itermax is the maximum iterations and X_i^L is the position of leader.

4. The position of hunters are corrected by concerning Hunter’s Group Consideration Rate (HGCR) and distance radius (R_a) are represented in equation (10).

$$X_i^{k+1} = \begin{cases} X_i^{k+1} \in \{X_i^1, X_i^2, \Lambda, X_i^{HGS}\} \text{ with probability } HGCR \\ X_i^{k+1} \pm R_a \text{ with probability } (1-HGCR) \end{cases} \quad (10)$$

$$Ra(it) = Ra_{\min} (\max(X_i) - \min(X_i)) \exp \left(\frac{\ln \left(\frac{Ra_{\min}}{Ra_{\max}} \right) \times it}{iter \max} \right) \quad (11)$$

Ra is an exponential decay function and may be defined as in equation (11).

5. Identify the group to avoid the algorithm to be trapped into local optima. It may be characterized in equation (12).

$$X_i^{k+1} = X_i^L \pm rand(\max(X_i) - \min(X_i)) \times \alpha \exp(-\beta \times EN) \quad (12)$$

Where EN is the numbers of epochs. EN is estimated by matching the difference of leader and worst hunter with a small value.

6. Repeat steps 3 to 5 up to termination criteria satisfied. In this problem, maximum iteration (100) is treated as termination criteria

In appendix.2 all the specifications of GHS are portrayed.

Results and Discussion

Cascade PD-FOPID, FOPID and PID controllers are implemented in both areas individually. GHS algorithm is executed with 60 numbers of hunters for 100 iterations to tune the controller parameters by concerning ITAE as an objective function.

Table 1. GHS optimized gain parameters of different controllers

| Controllers | Gains of different Controllers | | |
|-------------|--------------------------------|--------|--------|
| | | Area1 | Area2 |
| PD-FOPID | K_1 | 2.0000 | 2.0000 |
| | K_2 | 0.2106 | 0.5617 |
| | K_3 | 0.0010 | 1.0715 |
| | K_4 | 0.1481 | 0.4265 |
| | K_5 | 1.5467 | 0.0010 |
| | μ | 0.4355 | 0.5003 |
| | λ | 0.7656 | 0.3372 |
| FOPID | K_1 | 0.5476 | 1.3368 |
| | K_2 | 0.8072 | 1.0391 |
| | K_3 | 1.5488 | 0.5526 |
| | μ | 0.9954 | 0.6808 |
| | λ | 0.8323 | 1.1300 |
| PID | K_1 | 0.3353 | 0.3086 |
| | K_2 | 1.2274 | 0.5837 |
| | K_3 | 0.2072 | 1.2178 |

The numbers of parameters to be tuned by GHS algorithm of PD-FOPID, FOPID, and PID controllers are 14, 10 and 6, respectively, and are tabulated in Table 1. The above parameters are within a specified perimeter of 0.001 to 2.

The convergence plot of GHS algorithm optimized PID, FOPID, and cascade PD-FOPID controllers is portrayed in Fig. 4 to validate the potency of PD-FOPID controller. The performance of GHS algorithm optimized PID controller is validated in Fig. 5 by comparing with [24] by implementing load change of 0.05 p.u in the area-1. The performance parameters (undershoot, overshoot and settling time) of tie-line power deviation of GHS optimized PID controller are relatively better over BFOA, GA, and ZN tuned PID controller.

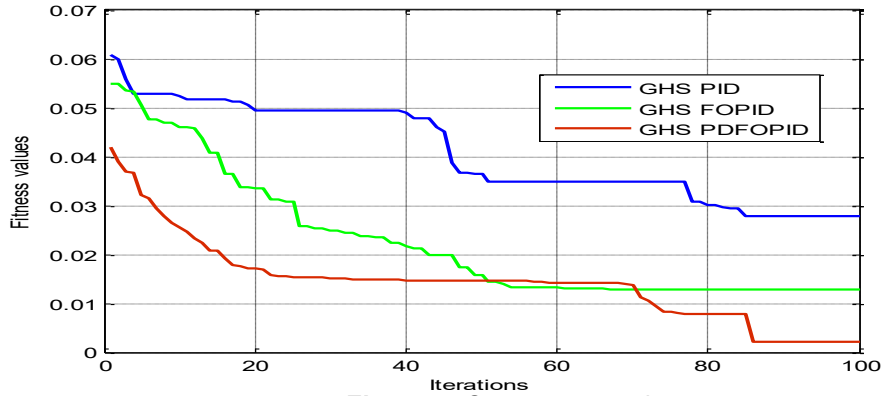


Figure 4. Convergence plot

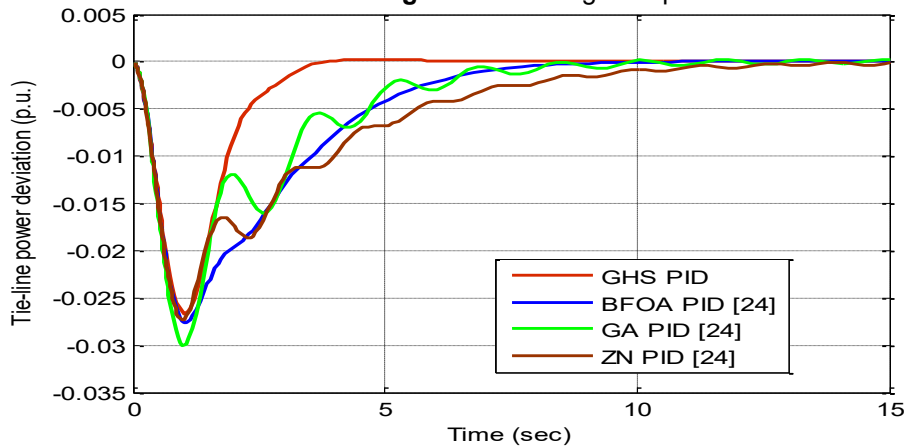


Figure 5. Tie-line power deviation due to 5% disturbance in area1

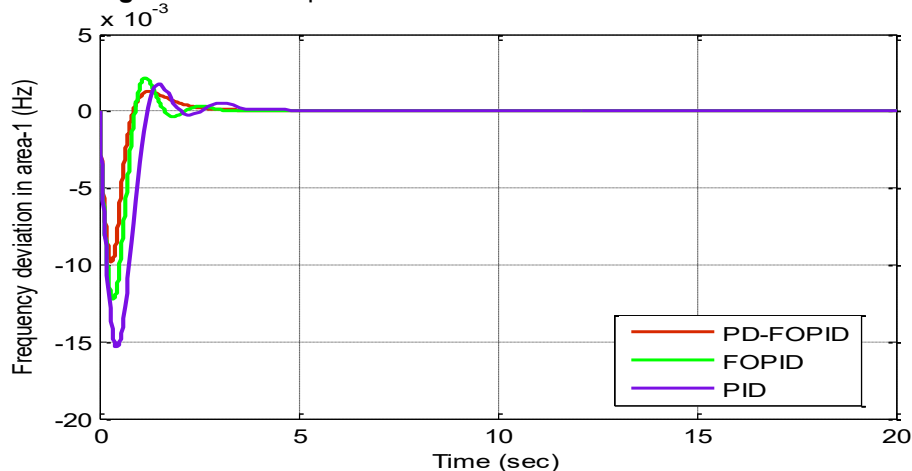


Figure 6. Frequency deviation in area-1

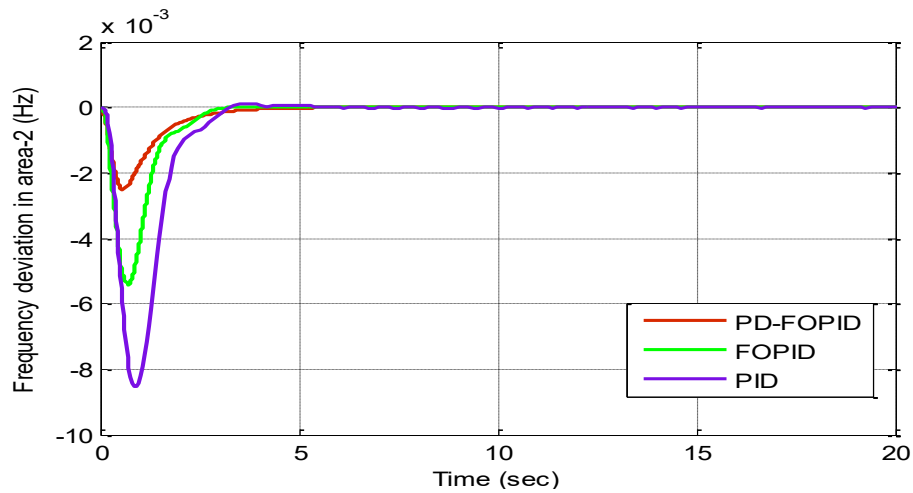


Figure 7. Frequency deviation in area-2

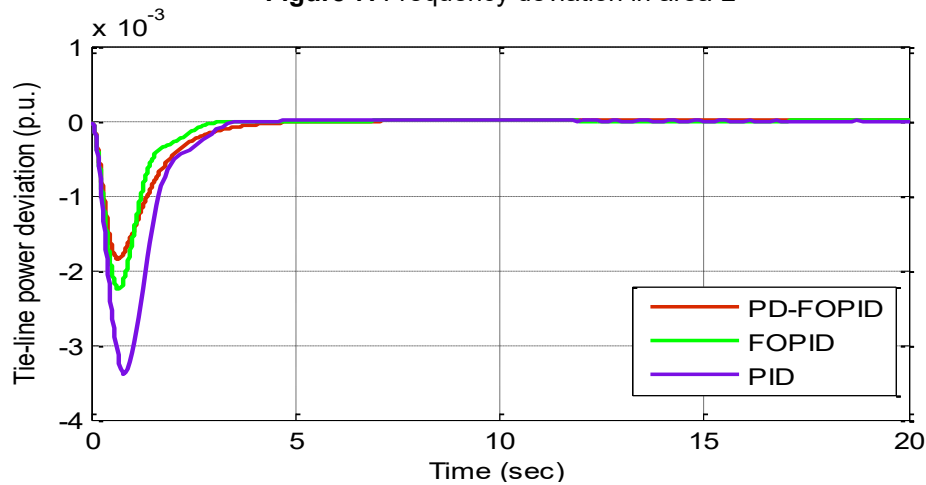


Figure 8. Tie-line power deviation

The frequency deviations of each area and power deviation in tie-line by implementing PD-FOPID, FOPID, and PID controllers optimized by GHS algorithm are portrayed in Fig. 6, Fig. 7 and Fig. 8, respectively.

The frequency deviation in the area-2 of the system by implementing variable step load change in the area-1 with different controllers optimized by GHS algorithm is illustrated in Fig. 9.

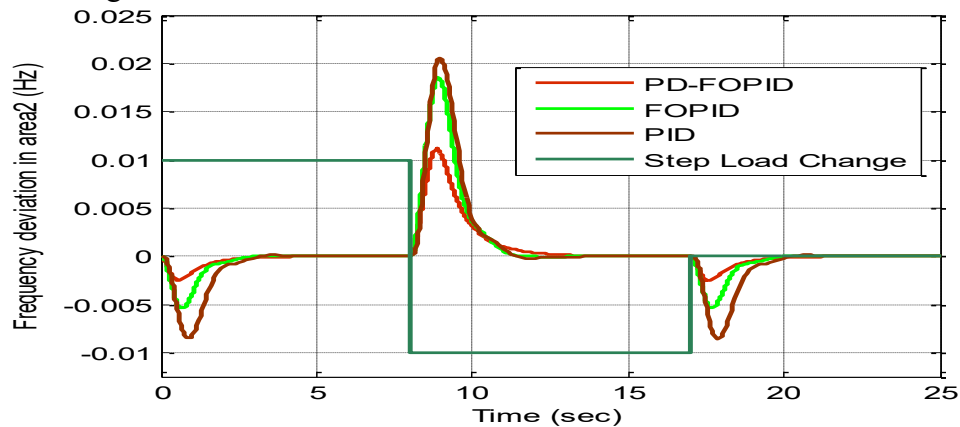


Figure 9. Frequency deviation in area-2 due to varying load disturbance in area-1

The objective function (ITAE) is adopted to lessen the settling time (T_s), peak overshoot (O_{sh}), and peak undershoot (U_{sh}) of the system. The performances of the controllers are discriminated by concerning these parameters and are mentioned below. ITAE value for GHS optimized PD-FOPID, FOPID, and PID controllers are 0.0022, 0.0128, and 0.0278, respectively.

Table 2. Peak undershoots (U_{sh}), peak overshoots (O_{sh}) and settling time (T_s) of Δf_1 , Δf_2 and ΔP_{tie}

| Controllers | Transient Responses | $\Delta f_1(\text{Hz})$ | $\Delta f_2(\text{Hz})$ | $\Delta P_{tie}(\text{p.u.})$ |
|-----------------|---------------------|-------------------------|-------------------------|-------------------------------|
| PD-FOPID | $U_{sh} (x10^{-4})$ | -98.1591 | -25.1317 | -18.3826 |
| | $O_{sh} (x10^{-4})$ | 12.7166 | 0 | 0 |
| | T_s | 2.7212 | 2.2901 | 2.7645 |
| FOPID | $U_{sh} (x10^{-4})$ | -122.6897 | -54.0853 | -22.4717 |
| | $O_{sh} (x10^{-4})$ | 21.5698 | 0 | 0 |
| | T_s | 2.8856 | 2.5455 | 2.3210 |
| PID | $U_{sh} (x10^{-4})$ | -153.4037 | -85.2842 | -33.8487 |
| | $O_{sh}(x10^{-4})$ | 17.7239 | 1.2366 | 0 |
| | T_s | 3.4721 | 2.9451 | 2.9315 |

Settling time is evaluated by considering a dimension of $\pm 0.05\%$ (5×10^{-4}) of final value. T_s , U_{sh} , and O_{sh} of the system are minimum with PD-FOPID controller optimized by GHS algorithm as reported in Table 2.

Cascade PD-FOPID controller optimized by GHS algorithm is validated as the better controller over PID and FOPID controllers.

Conclusion

The purpose of this paper is to validate the performance of cascade PD-FOPID controller optimized by GHS algorithm as an improved secondary controller of the interconnected thermal power system by concerning GRC. For this purpose, PID, FOPID, and cascade PD-FOPID controllers are applied individually in each area as AGC. All the controllers are optimized by GHS algorithm by conceding the termination criteria as maximum iterations (100). The minimum functional value is attained by cascade PD-FOPID controller optimized by GHS algorithm over PID and FOPID controllers. With 1% load disturbance in the area-1, PD-FOPID controller is validated better over PID and FOPID controllers to enhance the ability to get better control over tie-line power deviation and frequency deviations by considering their settling time, undershoots, and overshoot. The supremacy of PD-FOPID controller is validated over PID and FOPID controllers optimized by GHS algorithm.

Appendix.1 (power system parameters)

$K_{p1} = K_{p2} = 120 \text{ Hz/p.u. MW}$, $T_{p1} = T_{p2} = 20\text{s}$, $B_1 = B_2 = 0.4249$; $R_1 = R_2 = 2.4 \text{ Hz/p.u. MW}$;
 $T_{g1} = T_{g2} = 0.08 \text{ s}$; $T_{t1} = T_{t2} = 0.3 \text{ s}$;

Appendix.2 (Assumptions of algorithms)

$HGCR = 0.3$; $R_{a_{max}} = 0.0001$; $R_{a_{min}} = 1 \times 10^{-6}$;

CONFLICTS OF INTEREST

The authors declare that there is no conflict of interests regarding the publication of this paper.

References

- [1] P. S. Kundur, N.J. Balu, M.G. Lauby, Power system stability and control. Vol. 7. 1994: McGraw-hill New York.
- [2] N. Cohn, "Some Aspects of Tie-Line Bias Control on Interconnected Power Systems," AIEE Transactions, vol. 75, pp. 1415–1436, 1957.
- [3] A. Khodabakhshian, R. Hooshmand, "A new PID controller design for automatic generation control of hydro power systems," Int. J. Electr. Power Energy Syst., vol. 32, no. 5, pp. 375–382, 2010.
- [4] H. Shabani, B. Vahidi, M. Ebrahimpour, "A robust PID controller based on imperialist competitive algorithm for load-frequency control of power systems," ISA Trans., vol. 52, no. 1, pp. 88–95, 2013.
- [5] P. Dash, L. C. Saikia, N. Sinha, "Flower Pollination Algorithm Optimized PI-PD Cascade Controller in Automatic Generation Control of a Multi-area Power System," Int. J. Electr. Power Energy Syst., vol. 82, pp. 19–28, 2016.
- [6] P. Dash, L. C. Saikia, N. Sinha, "Comparison of performances of several Cuckoo search algorithm based 2DOF controllers in AGC of multi-area thermal system," Int. J. Electr. Power Energy Syst., vol. 55, pp. 429–436, 2014.
- [7] R. K. Sahu, S. Panda, U. K. Rout, D. K. Sahoo, "Teaching learning based optimization algorithm for automatic generation control of power system using 2-DOF PID controller," Int. J. Electr. Power Energy Syst., vol. 77, pp. 287–301, 2016.
- [8] S. P. Ghoshal, "Optimizations of PID gains by particle swarm optimizations in fuzzy based automatic generation control," Electr. Power Syst. Res., vol. 72, no. 3, pp. 203–212, 2004.
- [9] B.K. Sahu, T.K. Pati, J.R. Nayak, S. Panda, S.K. Kar, "A novel hybrid LUS-TLBO optimized fuzzy-PID controller for load frequency control of multi-source power system," Int. J. Electr. Power Energy Syst., vol. 74, pp. 58–69, 2016.
- [10] B.K. Sahu, S. Pati, P.K. Mohanty, S. Panda, "Teaching-learning based optimization algorithm based fuzzy-PID controller for automatic generation control of multi-area power system," *Appl. Soft Comput. J.*, vol. 27, pp. 240–249, 2015.
- [11] J. R. Nayak, B. Shaw, "Load frequency control of hydro-thermal power system using fuzzy PID controller optimized by hybrid DECPSO algorithm," IJPAM, vol. 114, no. 1, pp. 3–6, 2017.
- [12] R.K. Sahu, S. Panda, G.T. Chandra Sekhar, "A novel hybrid PSO-PS optimized fuzzy PI controller for AGC in multi area interconnected power systems," Int. J. Electr. Power Energy Syst., vol. 64, pp. 880–893, 2015.
- [13] D. Xue, Y.A. Chen, "Comparative Introduction of Four Fractional Order Controllers," in Proceedings of the 4th World Congress on Intelligent Control and Automation, Shanghai, P.R. China, pp. 3228-3235, 10-14 June 2002. DOI: 10.1109/WCICA.2002.1020131

- [14] I. Pan, S. Das, "Fractional Order AGC for Distributed Energy Resources Using Robust Optimization," *IEEE Transactions on Smart Grid*, vol. 7, no. 5, pp. 2175–2186, 2016.
- [15] V. H. Haji, C. A. Monje, "Fractional order fuzzy-PID control of a combined cycle power plant using Particle Swarm Optimization algorithm with an improved dynamic parameters selection," *Appl. Soft Comput.*, vol. 58, pp. 256–264, 2017.
- [16] A. Sikander, P. Thakur, R. C. Bansal, S. Rajasekar, "A novel technique to design cuckoo search based FOPID controller for AVR in power systems," *Comput. Electr. Eng.*, 2017. DOI: 10.1016/j.compeleceng.2017.07.005
- [17] J. Morsali, K. Zare, M.T. Hagh, "Comparative performance evaluation of fractional order controllers in LFC of two-area diverse-unit power system with considering GDB and GRC effects," *J. Electr. Syst. Inf. Technol.*, 2017. DOI: 10.1016/j.jesit.2017.05.002
- [18] P.N. Topno, S. Chanana, "Tilt Integral Derivative control for Two-area Load Frequency Control Problem," In: *Proc., 2015 2nd International Conference on Recent Advances in Engineering & Computational Sciences (RAECS)*, pp. 1-6, 2015. DOI: 10.1109/raecs.2015.7453361
- [19] M. Zamani, M. Karimi-Ghartemani, N. Sadati, M. Parniani, "Design of a fractional order PID controller for an AVR using particle swarm optimization," *Control Eng. Pract.*, vol. 17, no. 12, pp. 1380–1387, 2009.
- [20] R. Kumar Sahu, S. Panda, A. Biswal, G. T. Chandra Sekhar, "Design and analysis of tilt integral derivative controller with filter for load frequency control of multi-area interconnected power systems," *ISA Trans.*, vol. 61, pp. 251–264, 2016.
- [21] H. Senberber, A. Bagis, "Fractional PID controller design for fractional order systems using ABC algorithm," In: *Proc., 2017 Electronics*, pp. 1-7, 2017. DOI: 10.1109/electronics.2017.7995218
- [22] R. Oftadeh, M.J. Mahjoob, M. Shariatpanahi, "A novel meta-heuristic optimization algorithm inspired by group hunting of animals: Hunting search," *Comput. Math. with Appl.*, vol. 60, no. 7, pp. 2087–2098, 2010.
- [23] Y. Oysal, "A comparative study of adaptive load frequency controller designs in a power system with dynamic neural network models," *Energy Convers. Manag.*, vol. 46, no. 15–16, pp. 2656–2668, 2005.
- [24] E. S. Ali, S. M. Abd-Elazim, "Electrical Power and Energy Systems BFOA based design of PID controller for two area Load Frequency Control with nonlinearities," *Int. J. Electr. Power Energy Syst.*, vol. 51, pp. 224–231, 2013.
- [25] B. Shaw, A. Banerjee, V. Mukherjee, S. P. Ghoshal, "Solution of Optimal Power Flow by an Opposition-Based Gravitational Search Algorithm", *Intelligent Computing and Applications*, vol. 343, pp. 545–557, 2015.
- [26] B. Shaw, V. Mukherjee, S. P. Ghoshal, "Solution of reactive power dispatch of power systems by an opposition-based gravitational search algorithm," *Int. J. Electr. Power Energy Syst.*, vol. 55, pp. 29–40, 2014.
- [27] J. R. Nayak, B. Shaw, B. K. Sahu, "Application of adaptive-SOS (ASOS) algorithm based interval type-2 fuzzy-PID controller with derivative filter for automatic generation control of an interconnected power system," *Int. J. Engineering Science and Technology*, 2018. DOI: 10.1016/j.jestch.2018.03.010
- [28] J.R. Nayak, B. Shaw, S. Das, B.K. Sahu, "Design of MI fuzzy PID controller optimized by Modified Group Hunting Search algorithm for interconnected power system," *Microsyst. Technol.*, 2018. DOI: 10.1007/s00542-018-3788-3

Article copyright: © 2018 Jyoti Ranjan Nayak and Binod Shaw. This is an open access article distributed under the terms of the [Creative Commons Attribution 4.0 International License](https://creativecommons.org/licenses/by/4.0/), which permits unrestricted use and distribution provided the original author and source are credited.



Transient Analysis of Quasi Oppositional Based Lightning Search Algorithm Optimized PID Controller in Isolated Small Hydro Power Plant

Shashikant* and Binod Shaw

Department of Electrical Engineering, NIT, Raipur, C.G, India.

Received January 4, 2018; Accepted March 15, 2018; Published April 24, 2018

In this paper, Small Hydro Plant (SHP) of 1.3 MW is simulated with two conventional PID controllers in excitation system and governor to enhance the capability to handle the transiency of the generator. Excitation voltage control and turbine speed control are the two basic control schemes, to regulate reactive power or terminal voltage and real power or frequency respectively. The selection parameters of the PID controllers are significant to enhance the performance of the system. Quasi Oppositional Based Lightning Search Algorithm (QOLSA) is validated in this paper to optimize the PID controllers over LSA and PSO. Renewable energy source like SHP is environment friendly and very imperative to meet the vigorously growing load demand. The simulation of the SHP is established in MATLAB/SIMULINK environment. Finally, QOLSA optimized PID controller contributes better control in terminal voltage and power over LSA and PSO algorithms.

Keywords: Lightning Search Algorithm (LSA); Quasi Oppositional Based LSA (QOLSA); Small Hydro Power Plant (SHP); Proportional Integral Derivative(PID)

INTRODUCTION

For last two decades, the load demand of electricity is growing vigorously, due to this, power generation is unable to meet the load demand. In our power system network, most of the power is generated from conventional source of energy. The problem of using conventional sources of energy is: it is costly, creates pollution, and takes time to generate power and the huge requirement of raw materials which are extracted from fossil fuels. Earlier, we were enriched with natural resources and fossil fuels but due to extraction of fossil fuel it may get depleted in the near future. Providently, we have an alternate approach to generate electricity from non-conventional sources of energy. In this paper, an isolated Small Hydro Plant (SHP) is presented to meet the load less than 5MW. SHP has following advantages, which attract the interest of readers and industrialist.

- It is flexible.
- Under heavy load conditions gives supply to the grid.
- Standalone systems in rural areas.
- It is eco-friendly.

G. Baidya [1] has described a brief study about the advantages of SHP, current status of SHP in globe, government policies, and cost of installation & maintenance. The

*Corresponding author: shashikantkaushaley20@gmail.com

procedure to obtain the accurate governor model to improve the system stability, modeling of hydraulic turbine and their mathematical equations are well portrayed in [2]. Dewangan *et. al.* [3] enhanced the performance of the SHP by implementing craziness based particle swarm optimization (CRPSO) optimized PID controllers in both excitation and governor of the isolated alternator. Tenorio [4] presented a report on hydraulic governor and turbine model. They had also discussed the components of the various models of hydraulic governor and turbines. Kim and Schaefer [6] discussed the performance of excitation system and suggested the tuning methods for excitation parameter. Parameter for modeling synchronous machine designing is discussed in [7]. Enhancing the performance of the SHP by concerning frequency and terminal voltage has been attempted by many researchers in [8-18] by adopting some intelligent controller and some optimization techniques. Application of some adoptive algorithms in interconnected Hydro-Thermal power system are validated in [19, 20].

This present paper is an endeavor to design a SHP to enhance the terminal voltage and the power transient stability by implementing PID controllers in excitation and governor systems, respectively. The gain parameters of the PID controller have very vital aspects to enhance the performance of the system. Quasi Oppositional Based Lightning Search Algorithm (QOLSA) technique is adopted to hunt the best pair of parameters of PID controller to enhance the system performance. Lightning search algorithm (LSA) and particle swarm optimization (PSO) algorithm is adopted to validate the QOLSA technique to tune the PID controller.

SYSTEM DISCRPTION

SHP model consists of components like governor, servo motor, hydraulic turbine, salient pole alternator and excitation system. The block diagram of the SHP is illustrated in Figure 1. A DC regulated excitation voltage is enforced to the rotor of synchronous generator to enhance the transient response of the terminal voltage. Figure 2 represents the model of excitation system of the generator. Governor system is implemented to regulate the speed of the turbine. The controller in governor system regulates the valve of the gate of the water turbine to enhance the real power and frequency of the generator. The transfer function block of the governor system is portrayed in Figure 3. Servo motor controls the gate opening of water flow in the turbine. Servo motor action is governed by governor action. The simulation of SHP is done in MATLAB software to study its transient and dynamic response of the generator. Two different optimizing techniques (LSA and QOLSA) were executed to optimize PID controller in governor and excitation system. Each block in simulation is represented as a mathematical modeling of the system which is presented in [3].

The governor system has transient and permanent droop. Transient droop allows rotor to change the speed smoothly according to power demand. Droops generally allow generator to operate parallely according to their capacity and load sharing.

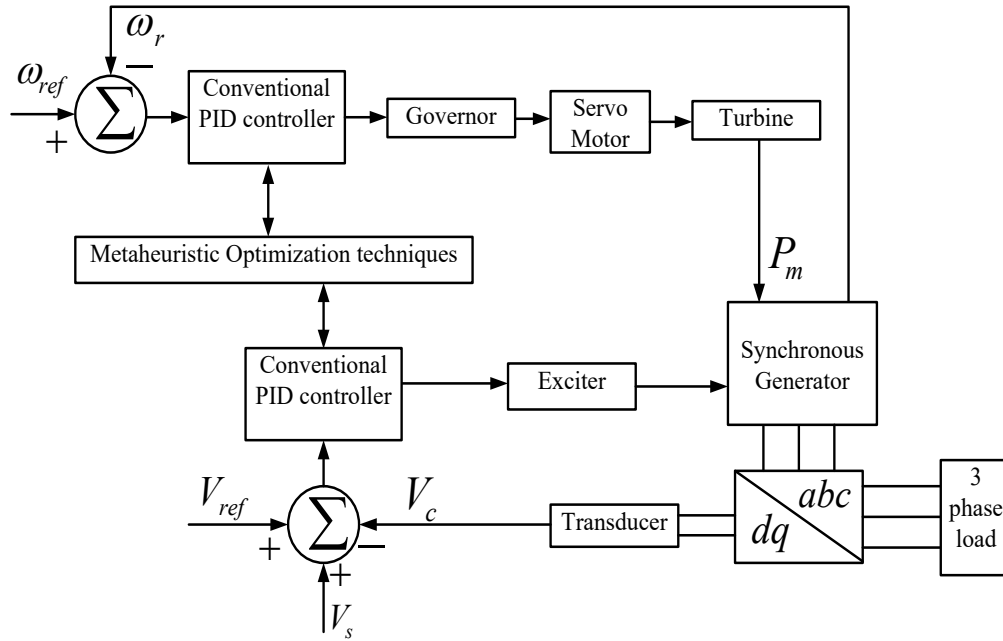


Figure 1. Block diagram of SHP

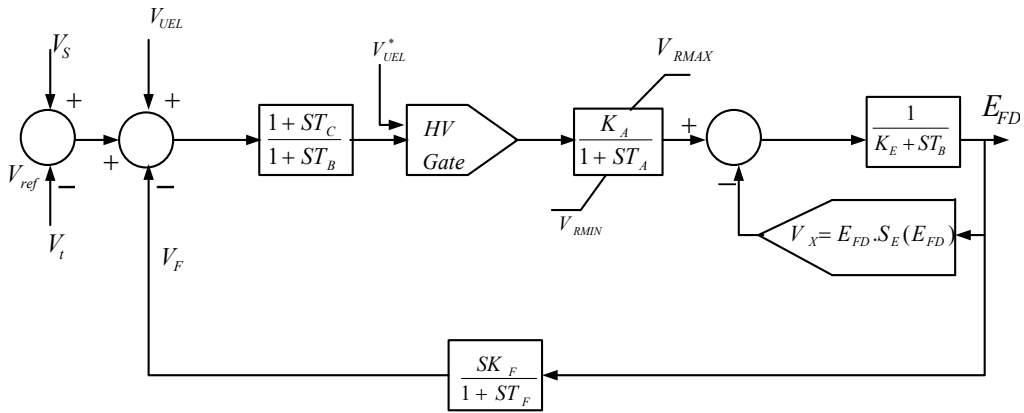


Figure 2. Excitation system transfer function block [5]

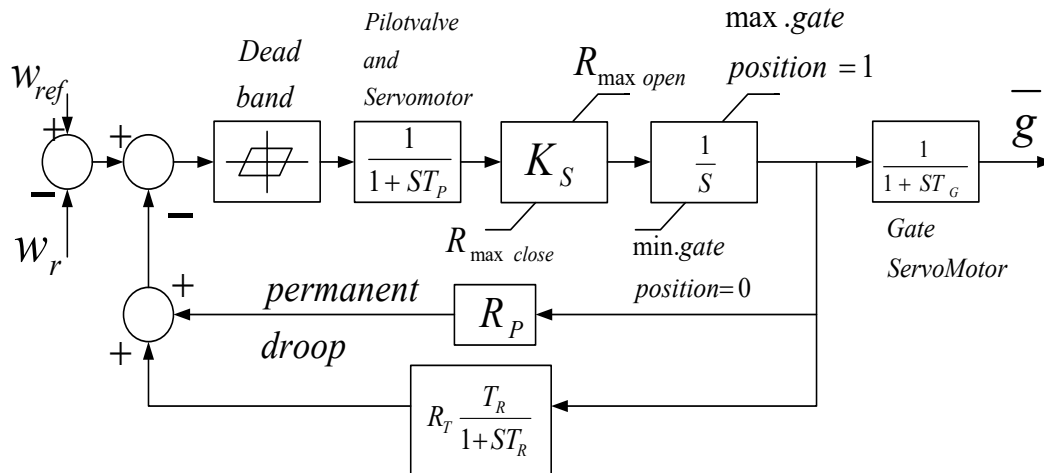


Figure 3. Governor system transfer function block [5]

PID CONTROLLER

The term PID controller refers to Proportional, Integrator and Derivative controller, which is a feedback control loop mechanism and widely used in industries. It generally calculates an error value $e(t)$ continuously. The error incorporated in the governor system by concerning the difference of desired speed and processed speed. PID controller gives desired result in an optimized way, without overshoot and time delay *i.e.*, its response is fast. Hence, it is applicable for automatic control. The difference between nominal terminal voltage and terminal voltage of generator is considered as an error, fed to the PID controller in the excitation system to control the terminal voltage. The block diagram of PID controller is portrayed in Figure. 4. The mathematical representation of PID controller may be expressed in equation (1).

$$u(t) = K_p e(t) + K_I \int_0^t e(t) dt + K_D \frac{d}{dt} e(t) \quad (1)$$

Its equivalent Laplace transform in Laplace domain can be written as equation (2).

$$U(s) = K_p E(s) + \frac{K_I}{s} E(s) + K_D s E(s) \quad (2)$$

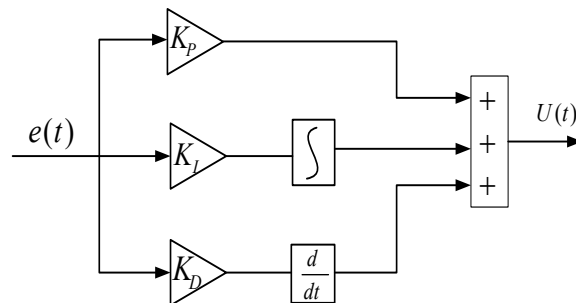


Figure 4. PID controller structure

QUASI OPPOSITIONAL BASED LIGHTNING SEARCH ALGORITHM (QOLSA)

This algorithm is inspired by a natural lightning phenomenon which occurs during bad weather condition. Lightning is visible for a few milliseconds (ms). Charge separation takes place within clouds during thunderstorm, and thus forms a strong electric field; due to this its surrounding gets ionized. Hence, more projectiles are generated with the original one. This projectile is being driven by an electric field and causes to form negative corona streamer. This streamer is formed at higher ionization region where attachment probability is less than ionization probability. The streamer or step leader progression is in discrete steps through a channel. A new channel is originated from an old channel forming a long channel whose tip energy is same as the old channel tip energy known as space leader. A current wave is produced when step leader propagates backwards until it connects to old channel. The corona burst out as the wave reaches to the tip of new leader and this process continues. Properties of projectiles and its equation are presented in [15, 16]. The Oppositional Based Learning (OBL) was introduced by Tizhoosh [17]. Harmony Search (HS) algorithm is modified to enhance the interconnected power system model in [18]. The fundamental purpose of this theory is to improve the accuracy of the result and to stimulate the diversity factor towards the optimal solution by concerning the opposite point of the particle.

Steps involving in QOLSA:

1. Initialize projectile matrix with number of population N as rows and number of variables D as columns ($P_{[N \times D]}$).
2. Initialize the quasi oppositional vector of same size *i.e.*, the mirror point of the initialized projectile vector ($QOP_{[N \times D]}$).
3. The projectile with best functional value is adopted as leader projectile.
4. Set max channel time and energy of leader tips.
5. Randomly generate transition projectiles.

Projectile speed is given in equation (3)

$$v_p = \left[1 - \left(\frac{1}{\sqrt{1 - \left(\frac{v_o}{c}\right)^2}} - SF_i / mc^2 \right)^{-2} \right]^{-0.5} \quad (3)$$

where,

v_p is current velocity, v_o is initial velocity, c is velocity of light, F_i is constant ionization rate, m is mass of projectile, S is path travelled.

The direction at which the projectile is travelling is given in equation (4)

$$\overline{P}_i = a + b - P_i \quad (4)$$

where,

\overline{P}_i And P_i is the two different original projectiles, a and b are boundary limits.

For a successful step leader transition, a channel is formed whose tip energy after several propagation trails is given as a probability density function in equation (5)

$$f(x^T) = \begin{cases} \frac{1}{b-a}, & a \leq x^T \leq b \\ 0, & x^T < a, x^T > b \end{cases} \quad (5)$$

X^T is a random number that may provide a solution or the initial tip energy.

Once the channel is formed, the step leader accelerates in the area of old channel to ionize the surroundings. The shape and position of the projectile to form corona streamer is given as a probability density function in equation (6)

$$f(x^S) = \begin{cases} \frac{1}{\mu} e^{-x^S/\mu}, & x^S \geq 0 \\ 0, & x^S \leq 0 \end{cases} \quad (6)$$

where, $f(x^S)$ represents the probability density function and μ represents shaping parameter

6. Evaluate performance (projectile energy).

Energy equation is given in (7)

$$\text{Energy} = 2.05 - 2e^{-\frac{5(T-t)}{T}} \quad (7)$$

where T is the maximum iteration and t is the current iteration.

7. Update leader tip energies.

New position and search space are updated when step leader energy is less than projectile energy. The new updated equations (8, 9, and 10) are given below:

$$P_{i_new}^S = P_i^S \pm \text{exprand}(\mu_i) \quad (8)$$

$$f(x^L) = \frac{1}{\sigma\sqrt{2\pi}} e^{-(x^L - \mu)^2 / 2\sigma^2} \quad (9)$$

$$P_{new}^L = P^L + \text{normrand}(\mu_L, \sigma_L) \quad (10)$$

where σ is scale parameter that describes about exploitation ability that decreases exponentially as it travels towards ground.

8. The mirror vector of new projectile vector is obtained from the P_{new} .

9. Update best and worst transition projectiles among both projectile and quasi oppositional projectile.

10. Repeat the steps from 5 to 9 until maximum iteration.

RESULT AND DISCUSSION

Simulation is carried out on MATLAB 2015a as per the block diagram shown in Figure 1. LSA and QOLSA algorithm are performed in SHP model to determine the gain parameters of the PID controller. Controllers are implemented in both excitation system and governor system to enhance the voltage and power profile. To extract the optimum parameters of the controller, both the algorithms are executed individually with 40 numbers of populations and for 50 iterations. Optimized parameters of PID controller implemented in governor system and excitation system are tabulated in Table 1. Figures

5 and 6 are the responses of terminal voltage and power of the system for these tunes parameters of the controller, respectively.

Table 1. The gain parameters of PID controller optimized by LSA and QOLSA

| Controllers | Gain | Excitation system | Governor System |
|-------------|-------|-------------------|-----------------|
| PSO [3] | K_P | 0.2095 | 1.7082 |
| | K_I | 0.1978 | 1.3472 |
| | K_D | 0.6202 | 1.2628 |
| LSA | K_P | 0.2475 | 0.8042 |
| | K_I | 0.3686 | 0.1529 |
| | K_D | 0.4807 | 0.4806 |
| QOLSA | K_P | 1.6618 | 0.0010 |
| | K_I | 1.1709 | 0.0010 |
| | K_D | 2.0000 | 0.7040 |

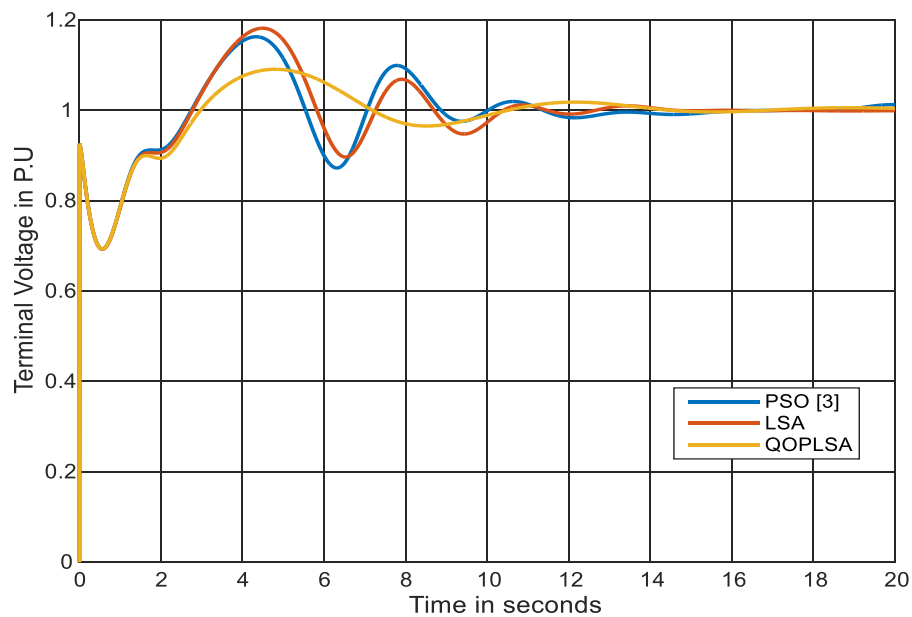


Figure 5. Terminal voltage response

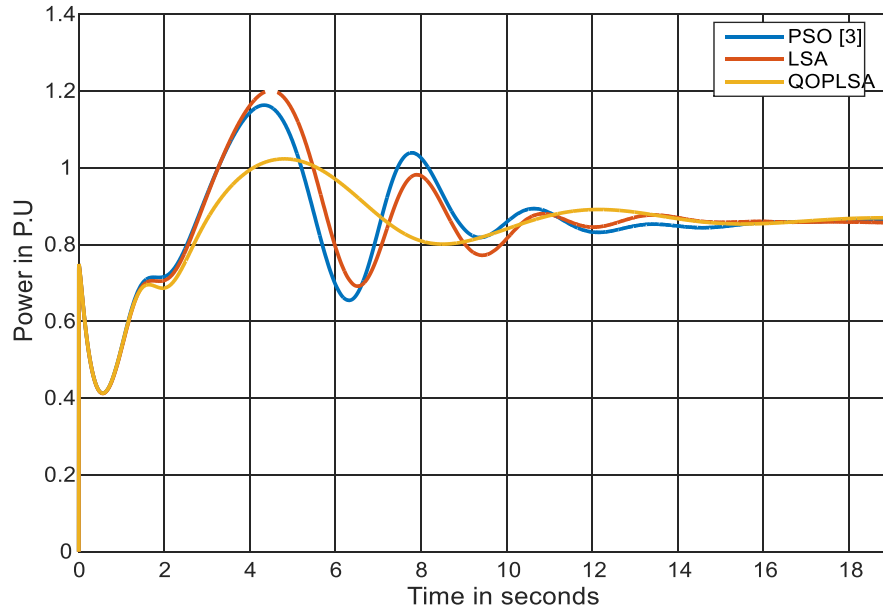


Figure 6. Real power response

Table 2. Peak undershoots (U_{sh}), peak overshoots (O_{sh}) and settling time (T_s) of terminal voltage and power.

| Controllers | Transient response | Terminal Voltage (P.U) | Power (P.U) |
|-------------|--------------------|------------------------|-------------|
| PSO | U_{sh} | 0.6900 | 0.4126 |
| | O_{sh} | 1.1630 | 1.1630 |
| | T_s | 8.4320 | 8.6350 |
| LSA | U_{sh} | 0.6925 | 0.4119 |
| | O_{sh} | 1.1820 | 1.2010 |
| | T_s | 8.2260 | 8.4900 |
| QOLSA | U_{sh} | 0.6931 | 0.4127 |
| | O_{sh} | 1.0910 | 1.023 |
| | T_s | 6.2080 | 6.7000 |

The numerical values of Undershoot (U_{sh}), overshoot (O_{sh}) and settling time (T_s) of the responses are tabulated in Table 2 to yield a fair contrast between the QOLSA and LSA optimized system. QOLSA optimized system contributes lesser functional value over LSA optimized system.

CONCLUSION

The proposed work is an approach to validate the QOLSA optimization technique over LSA and PSO [3] to optimize PID controller and to enhance the performance of the system by conceding terminal voltage and power of the generator. The transient response of the system is analyzed by conceding undershoot, overshoot and settling time of the

response. The undershoot of the system optimized by QOLSA, LSA and PSO are approximately equal. The response of QOLSA optimized PID controller system enhances the system response in terms of overshoot and settling time. The paper is concluded with validating QOLSA optimization technique over LSA and PSO to tune PID controller to yield better transient response of the system.

CONFLICTS OF INTEREST

The authors declare that there is no conflict of interests regarding the publication of this paper.

REFERENCE

- [1] G. Baidya, "Development of Small Hydro," *Himal. Small Hydropower Summit*, pp. 34–43, 2006.
http://ahec.org.in/links/HSHS/Presentations/Links/Technical%20Papers/Overview%20of%20SHP%20Development/Mr%20G%20Baidya_Development%20of%20SH.pdf (accessed on 4/26/2018)
- [2] L. N. Hannett, J. W. Feltes, and B. Fardanesh, "Field test to validate hydro-turbine governor model structure and parameters," *IEEE Trans. Power Syst.*, vol. 9, no. 4, pp. 1744–1751, 1994.
- [3] N. K. Dewangan, H. S. Sachdev, and B. Shaw, "An Analysis of Transient Response of Isolated Small Hydropower Plant with Application of CRPSO Optimized PID Controller," *International Journal of Pure and Applied Mathematics*, vol. 114, no. 9, pp. 137–145, 2017.
- [4] L. A. L. Tenorio, "Hydro Turbine and Governor Modelling: Electric - Hydraulic Interaction," Norwegian University of Science and Technology, Master Thesis, 2010.
<https://daim.idi.ntnu.no/masteroppgaver/005/5451/masteroppgave.pdf> (accessed on 4/26/2018)
- [5] P. Kundur, N.J. Balu, and M.G. Lauby, *Power system stability and control*. Vol. 7. 1994: McGraw-hill New York.
- [6] K. Kim and R. C. Schaefer, "Tuning a PID controller for a digital excitation control system," *Conf. Rec. 2004 Annu. Pulp Pap. Ind. Tech. Conf. (IEEE Cat. No.04CH37523)*, vol. 41, no. 2, pp. 485–492, 2004.
- [7] F. P. De Melo and R. J. Koessler, "Hydraulic Turbine and Turbine Control Models for System Dynamic Studies," *Trans. Power Syst.*, vol. 7, no. 1, pp. 167–179, 1992.
- [8] S. Syan and G. R. Biswal, "Frequency control of an isolated hydro power plant using artificial intelligence," *2015 IEEE Work. Comput. Intell. Theor. Appl. Futur. Dir.*, pp. 1–5, 2015. DOI: 10.1109/WCI.2015.7495537
- [9] H. Goyal, T. S. Bhatti, and D. P. Kothari, "A novel technique proposed for automatic control of small hydro power plants," *International Journal of Global Energy Issues*, vol. 24, pp. 29–46, 2005. DOI: 10.1504/IJGEI.2005.007076
- [10] M. G. Molina and M. Pacas, "Improved power conditioning system of micro-hydro power plant for distributed generation applications," *2010 IEEE Int. Conf. Ind. Technol.*, pp. 1733–1738, 2010. DOI: 10.1109/ICIT.2010.5472461

- [11] G. A. Aggidis, E. Luchinskaya, R. Rothschild, and D. C. Howard, "The costs of small-scale hydro power production: Impact on the development of existing potential," *Renew. Energy*, vol. 35, no. 12, pp. 2632–2638, 2010
- [12] R. Bhoi and D. S. M. Ali, "Potential of Hydro Power Plant in India and its Impact on Environment," *Int. J. Eng. Trends Technol.*, vol. 10, no. 3, pp. 114–119, 2014.
- [13] T. Abbasi and S. A. Abbasi, "Small hydro and the environmental implications of its extensive utilization," *Renew. Sustain. Energy Rev.*, vol. 15, no. 4, pp. 2134–2143, 2011.
- [14] J. R. Nayak, B. Shaw, and B. K. Shahu, "Load frequency control of hydro-thermal power system using fuzzy PID controller optimized by hybrid DECRPSO algorithm," *International Journal of Pure and Applied Mathematics*, vol. 114, no. 9, pp. 147–155, 2017.
- [15] H. Shareef, A. A. Ibrahim, and A. H. Mutlag, "Lightning search algorithm," *Appl. Soft Comput. J.*, vol. 36, pp. 315–333, 2015.
- [16] N. I. Petrov, G. N. Petrova, and F. D. Alessandro, "Quantification of the Probability of Lightning Strikes to Structures Using a Fractal Approach," *IEEE Transactions on Dielectrics and Electrical Insulation*, vol. 10, no. 4, pp. 641–654, 2003. DOI: 10.1109/TDEI.2003.1219649
- [17] H. R. Tizhoosh, "Opposition-Based Learning: A New Scheme for Machine Intelligence," *Comput. Intell. Model. Control Autom. 2005 Int. Conf. Intell. Agents, Web Technol. Internet Commer. Int. Conf.*, vol. 1, pp. 695–701, 2005.
- [18] C. K. Shiva and V. Mukherjee, "A novel quasi-oppositional harmony search algorithm for AGC optimization of three-area multi-unit power system after deregulation," *Eng. Sci. Technol. an Int. J.*, vol. 19, no. 1, pp. 395–420, 2016.
- [19] J. R. Nayak, B. Shaw, and B. K. Sahu, "Application of adaptive-SOS (ASOS) algorithm based interval type-2 fuzzy-PID controller with derivative filter for automatic generation control of an interconnected power system," *Int. J. Engineering Science and Technology*, 2018. DOI: 10.1016/j.jestch.2018.03.010.
- [20] J.R. Nayak, B. Shaw, S. Das, and B.K. Sahu, "Design of MI fuzzy PID controller optimized by Modified Group Hunting Search algorithm for interconnected power system," *Microsyst. Technol.*, 2018. DOI: 10.1007/s00542-018-3788-3.

Article copyright: © 2018 Shashikant and Binod Shaw. This is an open access article distributed under the terms of the [Creative Commons Attribution 4.0 International License](https://creativecommons.org/licenses/by/4.0/), which permits unrestricted use and distribution provided the original author and source are credited.



Design of Solar System by Implementing ALO Optimized PID Based MPPT Controller

Raj Kumar Sahu* and Binod Shaw

Department of Electrical Engineering, NIT, Raipur, C.G, India.

Received January 5, 2018; Accepted March 15, 2018; Published April 26, 2018

This paper is a strive approach to design offgrid solar system in association with DC-DC boost converter and MPPT. The tuned PID based MPPT technique is adopted to extract maximum power from the solar system under certain circumstances (temperature and irradiance). The design parameters of PID controller play an imperative aspect to enhance the performance of the system. Ant lion Optimizer (ALO) algorithm is adopted to optimize PID parameters to contribute relevant duty cycle for DC-DC boost converter to maximize output power and voltage. P and O based MPPT technique is implemented to validate the supremacy of PID based MPPT to enhance the response of the system. In this paper, the proposed ALO optimized PID controller based MPPT technique is performed better over conventional P & O technique by conceding the oscillation, time response, settling time and maximum values of voltage, current and power of the solar system.

Keywords: Photovoltaic system (PV); Maximum Power Point Tracking (MPPT); Perturb and Observe (P & O); Proportional-Integral-Derivative (PID) controller; Ant lion Optimizer (ALO) algorithm

INTRODUCTION

In the present scenario, renewable energy source plays a significant approach to meet the fast-growing load demand. Solar is an imperative concern among renewable energy due to its noise free, eco-friendly, and easy maintenance with impressive life span. Solar power is nonlinear and tough to guess. Solar energy falling on solar photovoltaic (PV) system can precisely disciple into electrical energy. Irradiation and temperature enormously influence the voltage and current which make them nonlinear. PV systems need to minimize cost, reduce the size and increase the efficiency. The maximum power point (MPP) is the extraction of power from solar cell under specific circumstances. Load current primarily relies upon radiation, ambient temperature, and cell temperature. Maximum Power Point Tracking (MPPT) is the process to track the maximum power by optimizing the load resistance properly in any environmental condition.

LITERATURE SURVEY

Many researchers have implemented various techniques to enhance the efficiency of the solar cell by enhancing the MPPT techniques during last few decades. Esram and Chapman [1] have contributed 19 different MPPT techniques and provided a fair

*Corresponding author: shashikantkaushaley20@gmail.com

interpretation for researchers to adopt relevant techniques. The P & O of variable step size is proposed by Al-Diab and Sourkounis [2], and the step size is tuned automatically and compared with the conventional method. Ishaque and Salam [3] have contributed a brief literature to the MPPT design by adopting soft computing methods during partial shading. The variable CS MPPT algorithm is validated by comparing with conventional P & O and PSO MPPT algorithm in three distinct case studies and is described in [4]. The efficiency of the partial shading PV module is enhanced up to 32% by using the current of non-shaded module in [5]. The fuzzy logic controller based MPPT algorithm with 8-bit microcontroller is compared with conventional P & O MPPT algorithm in [6]. Neural network based MPPT is implemented in 230-watt PV system in [7]. A brief literature survey on MPPT design is described beautifully in [8] and [9]. The P & O algorithm is optimized to enhance the efficiency of the MPPT technique in [10]. Adaptive Fuzzy-PI controller is implemented as MPPT and the role of climate change on PV module is well established in [10] and [11], respectively. Application of improved optimization techniques such as Adaptive Symbiotic Organism Search (ASOS) and Modified Group Hunting Search (MGHS) are validated in power system to tune controller parameters [12, 13]. Various soft computing techniques and optimization techniques are adopted to enhance the performance of MPPT of PV module in [14-19].

In this paper, Ant lion Optimizer (ALO) algorithm [20] optimized PID controller based MPPT technique is strived to validate over P & O technique to enhance the power and voltage of the system by contributing gate pulse of DC-DC boost converter. The proposed experiment is executed in MATLAB/SIMULINK environment.

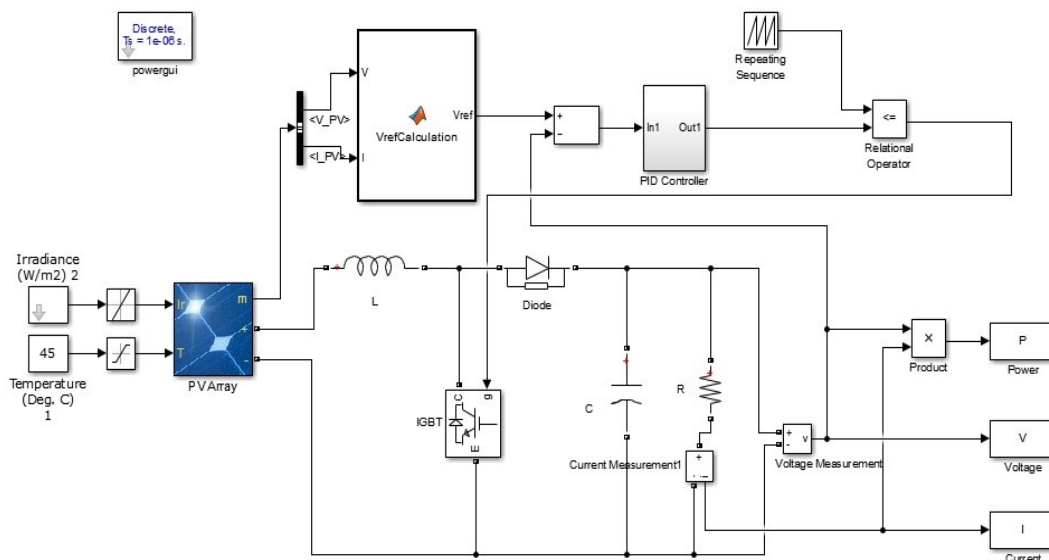


Figure 1. Simulink model of PID based solar system

SYSTEM INVESTIGATED

The Simulink model of PV module with PID based MPPT controller is portrayed in Figure 1. The proposed isolated solar system is portrayed in Figure 2, basically consisting of PV array, DC-DC Boost converter and MPPT controller. MPPT controller regulates gate pulse of boost converter by conceding the voltage and current of the PV module. The regulated pulse of the converter enhances the efficiency of the solar system.

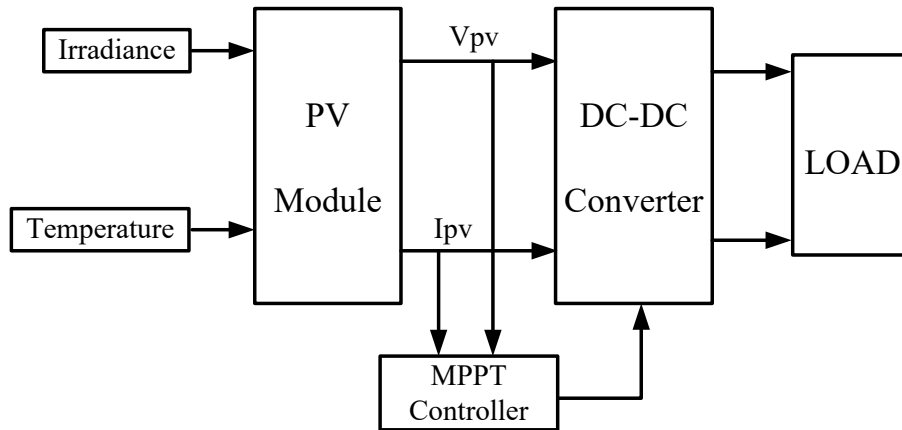


Figure 2. Block diagram of solar system

PV Module

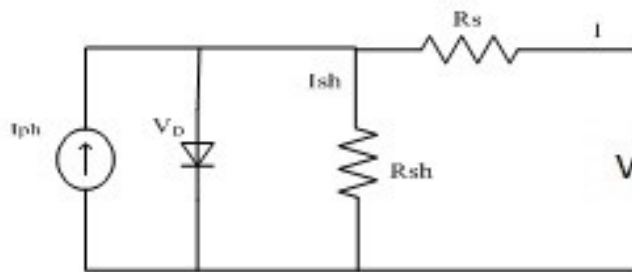


Figure 3. Equivalent circuit of solar cell

PV cells are associated in series and parallel to enhance the voltage and current. The equivalent circuit is portrayed in Figure 3.

The equivalent solar system may be explained through equations (1)-(4).

$$I_{rr} = I_{scr} e^{(qV_{oc}/KN_sAT_{rk})-1} \quad (1)$$

$$I_d = I_{rr} (T_{ak}/T_{rk})^3 e^{[(E_gK/KA)(1/T_{rk}-1/T_{ak})]} \quad (2)$$

$$I_{PH} = I_{scr} + (K_i(T_{ak} - T_{rk}))S/1000 \quad (3)$$

$$I_o = N_p I_{PH} - N_p I_d \{e^{(q/N_s AKT_{ak})(V_o + I_o R_s)} - 1\} \quad (4)$$

Where I_o = PV module current
 V_o = PV module voltage
 T_{rk} = Reference temperature in Kelvin
 T_{ak} = Operating temperature in Kelvin

S = Irradiance W/m^2
 q = Charge of electron, 1.6×10^{-19} C
 A = Ideality factor, 1.3
 K = Boltzman constant
 E_g = Band Gap
 I_{scr} = S.C current
 N_s = Cells connected in series
 N_p = Cells connected in parallel
 K_i = S.C temperature co-efficient
 R_s = Series Resistance
 I_{Ph} = Light generated current
 I_{rr} = Reverse Saturation current

DC-DC boost converter

The basic purpose of design of boost converter is to boost the output voltage of the dc system. The output of the converter is enormously influenced by the switching frequency (gate pulse). Figure 4 represents the boost converter and the output of the converter may be characterized in equation (5)

$$V_{out} = \frac{1}{1-D} V_{in} \quad (5)$$

D is the duty cycle of the converter and is characterized in equation (6).

$$D = \frac{t_{on}}{t_{on} + t_{off}} \quad (6)$$

On time and off time of the switch are expressed in equations (7) and (8), respectively, by conceding switching period (T_s).

$$t_{on} = DT_s \quad (7)$$

$$t_{off} = (1-D)T_s \quad (8)$$

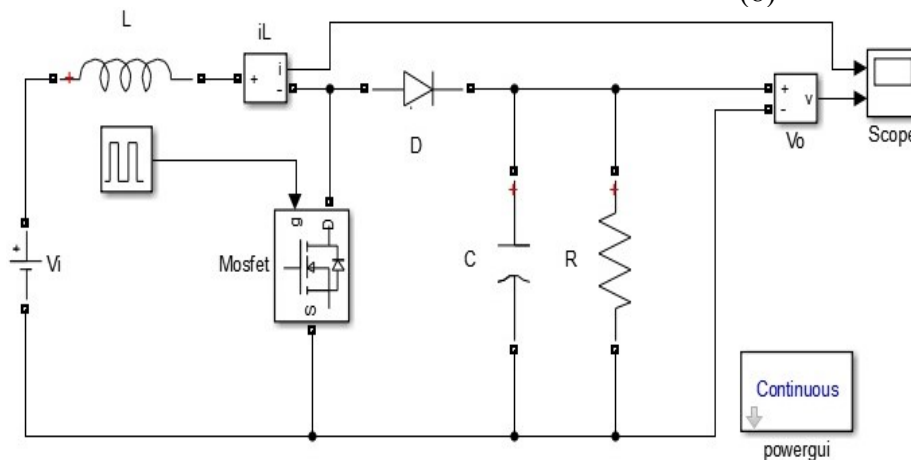


Figure 4. Boost converter

The parameters of boost converter are tabulated in Table 1.

Table 1. Boost converter parameters

| Model Components | Parameters |
|---------------------|--------------|
| Inductance, L | 1 μ H |
| Capacitance, C | 3000 μ F |
| Load, R | 24 Ω |
| DC voltage, Vdc | 12 V |
| Switching frequency | 10000 Hz |

PID based MPPT controller

The primary purpose of MPPT technique is to track the maximum power from the PV module by concerning the array voltage and power. In this paper, reference voltage (V_{ref}) is developed by correlating the instant power (P_k) and previous power (P_{k-1}) as portrayed in Figure 5.

The error signal achieved by comparing reference voltage with output voltage of boost converter is fed to the PID controller. The output of PID controller is used as gate pulse of the switch to enhance the power of the solar cell. The structure of PID controller is illustrated in Figure 6 and can be expressed as in equation (9).

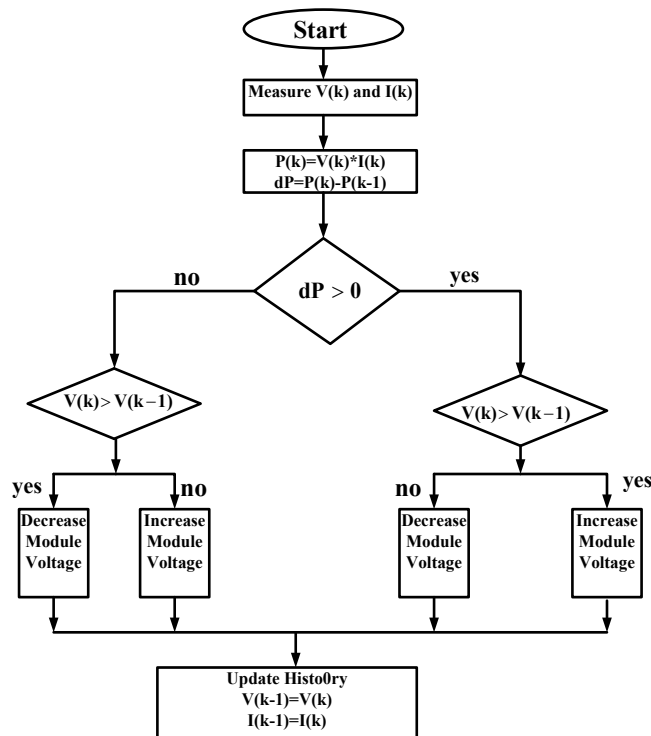


Figure 5. V_{ref} calculation algorithm

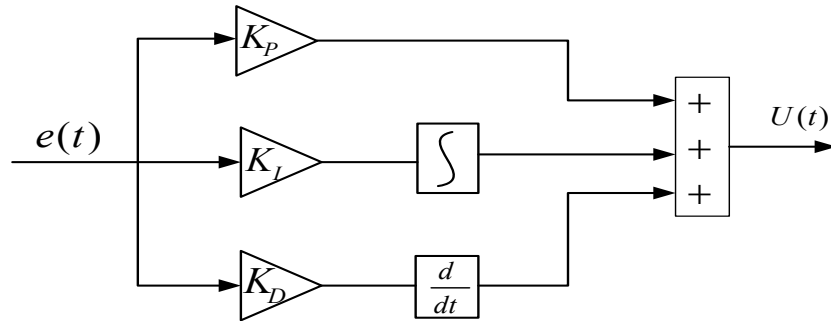


Figure 6. PID controller structure

$$u(t) = K_p \cdot e(t) + K_i \int_0^t e(t) \cdot dt + K_d \frac{d}{dt} e(t) \quad (9)$$

ANT LION OPTIMIZER ALGORITHM

The affiliation among predator (ant lion) and prey (ant) is intelligently portrayed as optimization technique by S. Mirjalili [21]. ALO algorithm is derivational from the planning of hawking of ant as food by ant lion to sustain and become capable. Ant lion creates reversed pyramid trap for the randomly moving ants to be captured into. Ant lion downtime in the ground of the soil constructs hole to trap ant or other bugs. Ants move randomly for searching food and sleep into the hole due to the pointed edge and loose sand of the hole. Here and there preys try to protect out from the opening however ant lion impels sands to the edge of the gap to make the prey slip into its jaw. The extent of opening is specifically relying on the starvation of antlion. The upgrade of the span of opening improves the likelihood to get nourishment. The steps followed for ALO algorithm is described as

1. The component of the framework which holds the places of preys is introduced arbitrarily with estimate $[M_{Prey}]_{NP \times D}$.

So introduction of ant lion position grid is resolved arbitrarily with same size $[M_{Antlion}]_{NP \times D}$, where NP and D are the population and measurement of plan factors, respectively. For this issue irregular in statement is in the middle of 0 to 2.

Useful estimations of the ant lion and prey are dictated by

$$F_{Prey} = f(M_{Prey})$$

$$F_{Antlion} = f(M_{Antlion})$$

Where F_{Prey} is a variety of wellness estimations of arbitrarily introduced M_{Prey} and $F_{Antlion}$ is the variety of wellness estimations of $M_{Antlion}$.

2. The antlion with the best fitness is allocated as the best.
3. Roulette wheel is utilized to choose antlions which give higher likelihood of fitting ant lions to chase preys.

4. The base and greatest vector of i^{th} factors c_i^g and d_i^g individually are modified as in equation (10) and (11) respectively.

$$c_i^g = AL_i^g + c^g \quad (10)$$

$$d_i^g = AL_i^g + d^g \quad (11)$$

Where AL_i^g is the position of i^{th} antlion at g^{th} generation. c^g and d^g might be described as

$$c^g = \frac{c^g}{I}, \quad d^g = \frac{d^g}{I}, \quad \text{and} \quad I = 10^w \frac{g}{n}$$

Where w is a round number chosen between 2 to 6 based on new generation.

5. The activities of preys are random in nature and may be shown in equation (12).

$$X(g) = [0, \text{cumsum}(2r(g1)-1), \text{cumsum}(2r(g2)-1), \dots, \text{cumsum}(2r(gn)-1)] \quad (12)$$

Where cumulative sum is found by cumsum . g and n are the generation and peak generation number respectively. r is a random probability distribution function described in equation (13).

$$r(g) = \begin{cases} 1 & \text{if } rand > 0.5 \\ 0 & \text{if } rand \leq 0.5 \end{cases} \quad (13)$$

6. The status of preys is modified by equation (14).

$$P_i^g = \frac{R_p^g + R_E^g}{2} \quad (14)$$

Where R_p^g and R_E^g are the strange changes around antlion and best respectively.

7. The functional values of preys are determined.
8. The antlion is updated by its analogous fitter prey as described in equation (15).

$$AL_i^g = P_i^g \quad \text{if } f(P_i^g) > f(AL_i^g) \quad (15)$$

9. The practical value of preys is determined as explain previously.
10. Elite value is updated by the antlion with fitness value better than elite.
11. Steps from 4 to 10 are repeated until maximum generation reached.

In the present work, the gains of PID controllers are tuned by ALO algorithm to enhance the power of the PV module.

RESULTS AND DISCUSSION

ALO algorithm is executed for 50 iterations with 50 populations to resolve the steps to discover the optimal gain parameters of PID controllers. The objective of the algorithm is to hunt the parameters within a specified limit as described in equation (16).

$$0.001 \leq K_p, K_I \text{ and } K_D \leq 2 \quad (16)$$

The optimal values of K_p , K_I , and K_D are 0.0711, 0.9079 and 1.1260, respectively. The performance of PV module by conceding power, voltage and current are portrayed in Figure 7, Figure 8 and Figure 9, respectively.

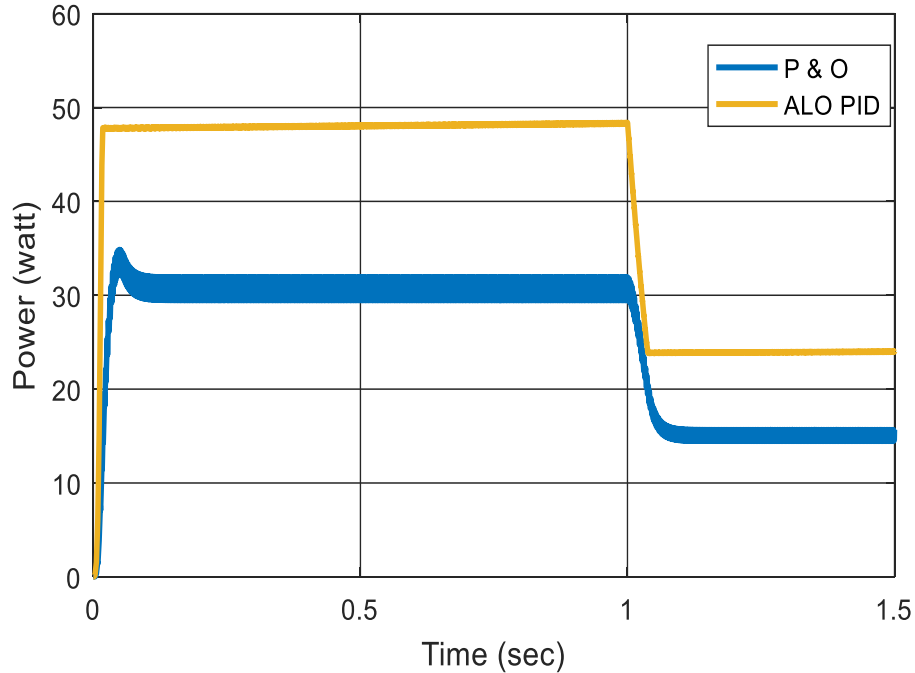


Figure 7. Power vs Time graph

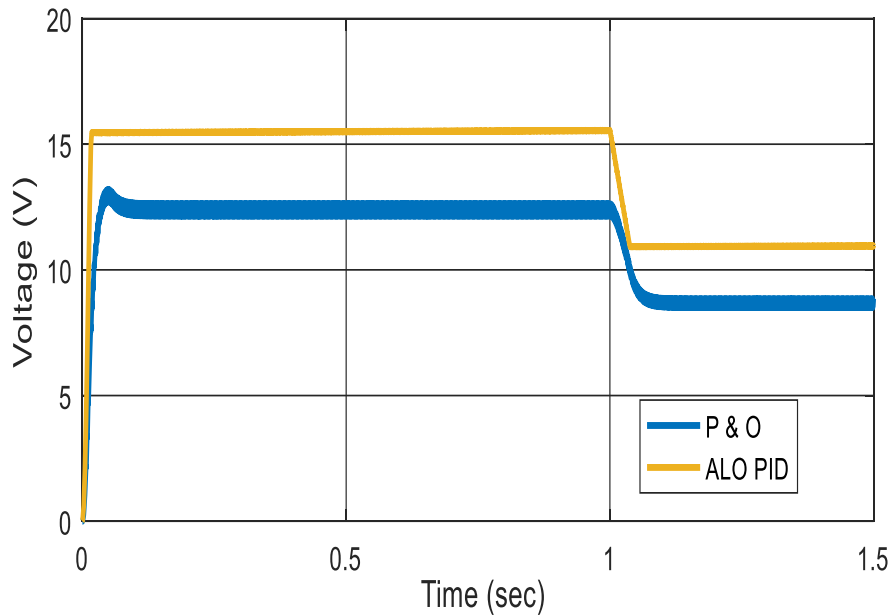


Figure 8. Voltage vs Time graph

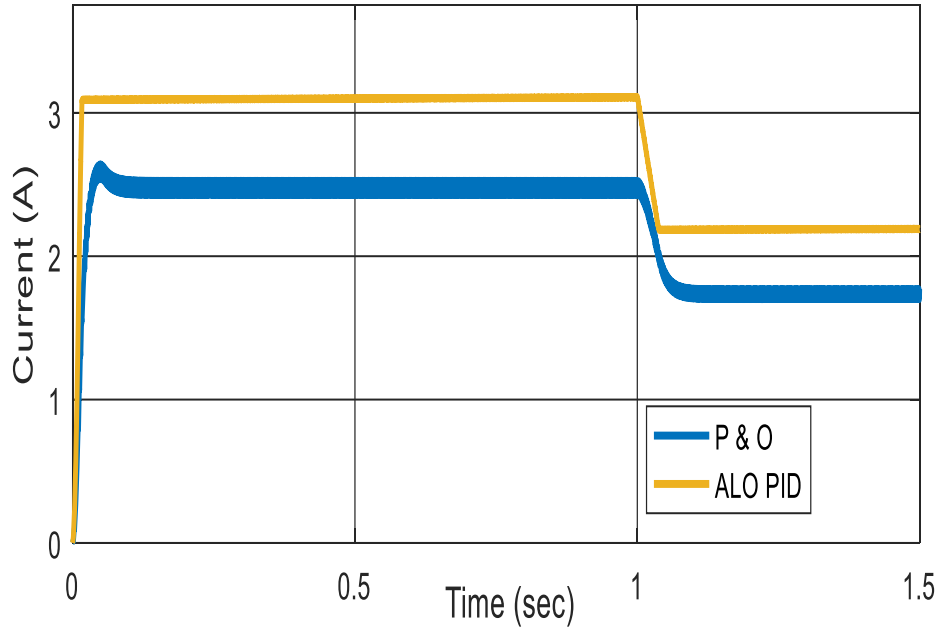


Figure 9. Current vs Time graph

The performance parameters of the output of PV module are tabulated in Table 2 to provide a fair supremacy of PID based MPPT controller over P & O technique.

Table 2. Performance response of output

| Performance Parameters | P&O based MPPT | | | PID based MPPT | | |
|------------------------|----------------|--------|-------|----------------|--------|-------|
| | P | V | I | P | V | I |
| Maximum | 30.55 | 12.385 | 2.477 | 48.02 | 15.465 | 3.094 |
| Overshoot | 2.94 | 0.56 | 0.12 | 0 | 0 | 0 |
| Settling time | 0.072 | 0.075 | 0.06 | 0.018 | 0.017 | 0.017 |
| Rise time | 0.032 | 0.0307 | 0.038 | 0.017 | 0.016 | 0.016 |
| Delay time | 0.019 | 0.012 | 0.013 | 0.012 | 0.011 | 0.010 |
| Oscillation | 2.432 | 0.492 | 0.098 | 0.061 | 0.012 | 0.002 |

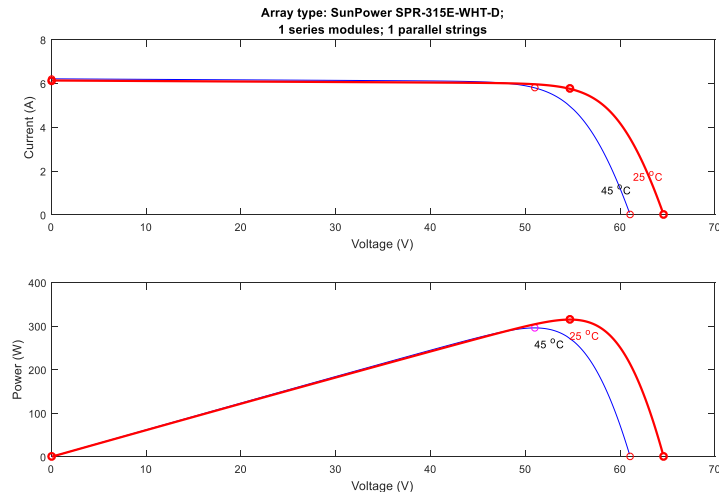


Figure 10. I-V and P-V characteristics of PV module

The I-V and P-V characteristics are illustrated in Figure 10. The settling time, rise time, delay time and oscillation of output responses (power, voltage and current) of PV module with ALO optimized PID based MPPT controller are lower than the P & O based MPPT technique. Overshoot evaluated by considering the difference between steady state maximum power and maximum power. Implementation of proposed MPPT technique enhances the responses of PV module remarkably. Finally, ALO optimized PID based MPPT technique is validated as a better technique over P & O based MPPT technique to enhance the efficiency of the PV module.

CONCLUSION

The purpose of this paper is to design a solar system and to enhance the efficiency of the system by implementing PID based MPPT technique. The PID based MPPT controller optimized by ALO algorithm is validated as an improved controller over P & O based MPPT controller of the solar system. Temperature, irradiance and load are the imperative factors which influence the current, voltage and power of the solar cell. This PID and P & O based MPPT controller is executed by diverging the irradiance (1000 W/m^2 to 700 W/m^2) and with constant temperature (45°C) and load (24Ω). The error signal is evaluated by the contrast of reference voltage and measured process voltage to achieve relevant gate pulse of the converter. The output voltage is enormously influenced by duty cycle of the gate pulse. The ALO optimized PID based MPPT techniques is validated over P & O technique to achieve maximum power, current and voltage with minimum oscillation, settling time, rise time and delay time.

CONFLICTS OF INTEREST

The authors declare that there is no conflict of interests regarding the publication of this paper.

REFERENCES

- [1] T. Eswam and P. L. Chapman, "Comparison of Photovoltaic Array Maximum Power Point Tracking Techniques," *IEEE Trans. Energy Convers.*, vol. 22, no. 2, pp. 439–449, 2007.
- [2] A. Al-Diab and C. Sourkounis, "Variable step size P&O MPPT algorithm for PV systems," *Proc. Int. Conf. Optim. Electr. Electron. Equipment, OPTIM*, pp. 1097–1102, 2010. DOI: 10.1109/OPTIM.2010.5510441
- [3] K. Ishaque and Z. Salam, "A review of maximum power point tracking techniques of PV system for uniform insolation and partial shading condition," *Renew. Sustain. Energy Rev.*, vol. 19, pp. 475–488, 2013.
- [4] J. Ahmed and Z. Salam, "A Maximum Power Point Tracking (MPPT) for PV system using Cuckoo Search with partial shading capability," *Appl. Energy*, vol. 119, pp. 118–130, 2014.

- [5] M. Z. Ramli and Z. Salam, "A simple energy recovery scheme to harvest the energy from shaded photovoltaic modules during partial shading," *IEEE Trans. Power Electron.*, vol. 29, no. 12, pp. 6458–6471, 2014.
- [6] Y. R. Yang, "A Fuzzy Logic Controller for Maximum Power Point Tracking with 8-Bit Microcontroller," In: *Proc., IECON 2010 - 36th Annual Conference on IEEE Industrial Electronics Society*, pp: 2895-2900, 2010. DOI: 10.1109/iecon.2010.5675084.
- [7] Y.H. Liu, C.L. Liu, J.W. Huang, and J.H. Chen, "Neural-network-based maximum power point tracking methods for photovoltaic systems operating under fast changing environments," *Sol. Energy*, vol. 89, pp. 42–53, 2013.
- [8] N. A. Kamarzaman and C. W. Tan, "A comprehensive review of maximum power point tracking algorithms for photovoltaic systems," *Renew. Sustain. Energy Rev.*, vol. 37, pp. 585–598, 2014.
- [9] A. Reza, M. Hassan, and S. Jamasb, "Classification and comparison of maximum power point tracking techniques for photovoltaic system: A review," *Renew. Sustain. Energy Rev.*, vol. 19, pp. 433–443, 2013.
- [10] N. Femia, G. Petrone, G. Spagnuolo, and M. Vitelli, "Optimization of Perturb and Observe Maximum Power Point Tracking Method," *IEEE Transactions on Power Electronics*, vol. 20, no. 4, pp. 963–973, 2005.
- [11] S. Hoffmann and M. Koehl, "Investigation on the Impact of Macro- and Micro-Climate on the Potential Induced Degradation," In: *Proc., 2013 IEEE 39th Photovoltaic Specialists Conference (PVSC)*, pp: 1822-1825, 2013. DOI: 10.1109/pvsc.2013.6744496
- [12] J. R. Nayak, B. Shaw, and B. K. Sahu, "Application of adaptive-SOS (ASOS) algorithm based interval type-2 fuzzy-PID controller with derivative filter for automatic generation control of an interconnected power system", *Int. J. Engineering Science and Technology*, 2018. DOI: 10.1016/j.jestch.2018.03.010.
- [13] J.R. Nayak, B. Shaw, S. Das, and B.K. Sahu, Design of MI fuzzy PID controller optimized by Modified Group Hunting Search algorithm for interconnected power system, *Microsyst. Technol.*, 2018. DOI: 10.1007/s00542-018-3788-3.
- [14] H. Shareef, A. H. Mutlag, and A. Mohamed, "A novel approach for fuzzy logic PV inverter controller optimization using lightning search algorithm," *Neuro computing*, vol. 168, pp. 435–453, 2015.
- [15] P.C. Cheng, B.R. Peng, Y.-H. Liu, Y.S. Cheng, and J.W. Huang, "Optimization of a Fuzzy-Logic-Control-Based MPPT Algorithm Using the Particle Swarm Optimization Technique," *Energies*, vol. 8, no. 6, pp. 5338–5360, 2015.
- [16] A. S. Oshaba, E. S. Ali, and S. M. Abdelazim, "PI controller design for MPPT of photovoltaic system supplying SRM via BAT search algorithm," *Neural Comput. Appl.*, vol. 28, no. 4, pp. 651–667, 2017.
- [17] R. Nagarajan, R. Yuvaraj, V. Hemalatha, S. Logapriya, A. Mekala, and S. Priyanga, "Implementation of PV - Based Boost Converter Using PI Controller with PSO Algorithm," *Int. J. Eng. Comput. Sci.*, vol. 6, no. 3, pp. 20479-20484, 2017. DOI: 10.18535/ijecs/v6i3.14
- [18] L. ZAGHBA, N. TERKI, A. BORN, A. BOUCHAKOUR "Robust maximum power point tracking technique and PI current controller design for grid connected PV system using MATLAB/SIMULINK," *Journal of Electrical Engineering*, vol. 15, pp. 315-320, 2015.

- [19] A. Neçaibia, S. Ladaci, A. Charef, and J. J. Loiseau, "Fractional order extremum seeking approach for maximum power point tracking of photovoltaic panels," *Front. Energy*, vol. 9, no. 1, pp. 43–53, 2015.
- [20] E. S. Ali, S. M. AbdElazim, and A. Y. Abdelaziz, "Ant Lion Optimization Algorithm for renewable Distributed Generations," *Energy*, vol. 116, pp. 445–458, 2016.
- [21] S. Mirjalili, "The Ant Lion Optimizer," *Adv. Eng. Softw.*, vol. 83, pp. 80–98, 2015.

Article copyright: © 2018 Raj Kumar Sahu and Binod Shaw. This is an open access article distributed under the terms of the [Creative Commons Attribution 4.0 International License](https://creativecommons.org/licenses/by/4.0/), which permits unrestricted use and distribution provided the original author and source are credited.



Heat Energy Recovery System

Ujjawal Kohli*, Vaibhav Mishra, and Sparsh Singh Kotwal

Department of Mechanical Engineering, Graphic Era University, Dehradun-248002, INDIA

Received January 22, 2018; Accepted March 26, 2018; Published April 27, 2018

Energy demands in today's world have increased and the main area of concerns is that approximately 90% of world's oil reserves are expected to be depleted within two generations. We are trying to build a technological system where the by-product of conventional fuel *i.e.*, exhaust heat of fuel, will be converted into another form so that it can further be used again. Mainly, recovery of heat energy is our prime motive. According to our motive, we are going to recover the heat of the hot exhaust gases from chimneys of factories which usually dissipate into the atmosphere and thus that exhaust heat left unused. So, we are making a water storing tank *i.e.*, water jacket that will surround the chimney through which heat from hot exhaust gases will come in contact with water present in water jacket. Through the process of conduction, heat transfer will take place. Therefore, due to heat, the temperature of the water will increase to a very high extent, and hot water can be used in boilers as a pre-heater for household or commercial purposes. Furthermore, global warming will also be controlled if we start implementing this technology at a huge scale.

Keywords: Chimneys; Conduction; Exhaust; Heat Recovery; Temperature; Water Jacket

I. Introduction

The majority of energy production from conventional and renewable resources is lost to the atmosphere due to onsite (equipment inefficiency and losses due to waste heat) and offsite (cable and transformers losses), which sums to be around 66% loss in electricity value [1-2]. The waste heat of different degrees could be found in final products of a certain process or as a by-product of industry such as from the exhaust producing from steel-making, glass making factories, etc. (Table 1). Heat is that amount of energy flowing from one body to another spontaneously due to their temperature difference or by means other than work or transfer of matter. Heat energy flows from an object of high temperature to an object with a lower temperature. It will never do the reverse until and unless any external force is applied.

In this project, we concentrated an approach towards the recovery *i.e.*, Recovery of waste heat. Approximately, there is a 30-50% heat energy loss in the form of heat dissipation *i.e.*, by cooling system and exhaust systems. This lost heat may contain heat energy and kinetic energy, which could be further employed for some applications. Extraction of heat energy is a somewhat easy process but recovering energy from an existing system to an extent that it can be used for useful work is difficult. Energy demands are increasing day by day and need a strong solution. No one thought over it for

*Corresponding author: kohliujjawal96@geu.ac.in, vaibhavamishra720@geu.ac.in, sparshkotwal@gmail.com

many years. So here we are introducing our Heat Energy Recovery System, which will use exhaust gases from chimneys of factories and use this waste energy again in another form. Our project is designed in such a way that it is durable and efficient with very low service requirement [3].

Concept of Waste Heat Recovery

Waste Heat Recovery means to utilize the heat energy in a better desired way which is expelled or exhausted to the atmosphere. This wasted heat energy can be recovered by coupling some secondary auxiliaries such as water jacket in electric chimneys to extract heat from exhaust gases generated by industries. This reduces wastage and improves efficient utilization of fuel *i.e.*, resources. The lost heat may be utilized for further energy requirements.

Table 1. Waste Exhaust Heat of Various Furnaces

| Types of Device | Temperature, °C |
|------------------------------|-----------------|
| Nickel Refining furnace | 1370-1650 |
| Aluminum Refining Furnace | 650-760 |
| Zinc Refining Furnace | 760-1100 |
| Copper Refining Furnace | 760-815 |
| Steel Refining Furnace | 925-1050 |
| Copper Reverberatory Furnace | 900-1100 |
| Open Hearth Furnace | 650-700 |
| Cement Kiln (Dry process) | 620-730 |
| Glass Melting Furnace | 1000-1550 |
| Hydrogen plants | 650-1000 |
| Solid Waste Incinerators | 650-1000 |
| Fume Incinerators | 650-1450 |

II. Objective

According to the United States Department of Energy, up to 50 percent of the energy from all fuels burned in the U.S. ends up in the atmosphere as waste heat. Research indicates that recovery of the waste energy from industrial facilities could fulfill up to 20 percent of total domestic electricity demand and simultaneously effect a 20 percent reduction in greenhouse gas emissions. Waste heat is a heat which is generated by a way of fuel combustion or chemical reaction and then dumped into the environment, even though it could still be reused for some useful and economic purpose. A large amount of hot flue gases is generated from boilers, glass factory, sugar factory, furnaces etc. The energy lost in waste gases cannot be fully recovered. If some of this waste heat could be recovered, a considerable amount of primary fuel could be saved [4]. Imagine if this waste heat can be recovered and adopted successfully there will be a revolutionary change in the world in terms of energy reusability. However, as per our analysis, much of the heat could be recovered and losses are minimized. So, the objective of our project is to establish a system which is strong enough to tackle present issues on a recovery of heat energy and efficient enough to make all facts into fiction.

III. Material Required

1. Water tank (at inlet and outlet)
2. Water jacket (around the chimney)
3. Motor
4. Piping system

IV. Construction

A schematic is designed to understand it in a better way (Fig. 1). Brick and cement made chimneys have low conduction ability. These materials nowadays have become obsolete and are no longer used for making chimneys. Modern chimneys are too way different from old chimneys. Water tank surrounds the chimney up to 80% of its height. High output is achieved at the storing end. This design is based on modern chimneys, which are now used everywhere and are called as “Electric Chimneys”. Electric chimneys are the chimneys which are held high in length, can work up to 24 hours, and it is best suited for our project to provide the output as per we planned [5].

The following standards and assumptions were taken to complete our research.

1. Thermal conductivity of chimney= 379 W/m K
2. Thickness of chimney= 0.25 m
3. Inlet exhaust gas temperature= 70 °C
4. Temperature of water before process= 20 °C
5. Mass flow rate= 1 kg/s
6. Specific heat at constant pressure= 4.180 KJ/Kg.K
7. Density of air= 2.017 kg/m³
8. Velocity of inside air= 1 m/s
9. Height of chimney=6 m
10. Dynamic viscosity of air=0.0000182 m²/s.

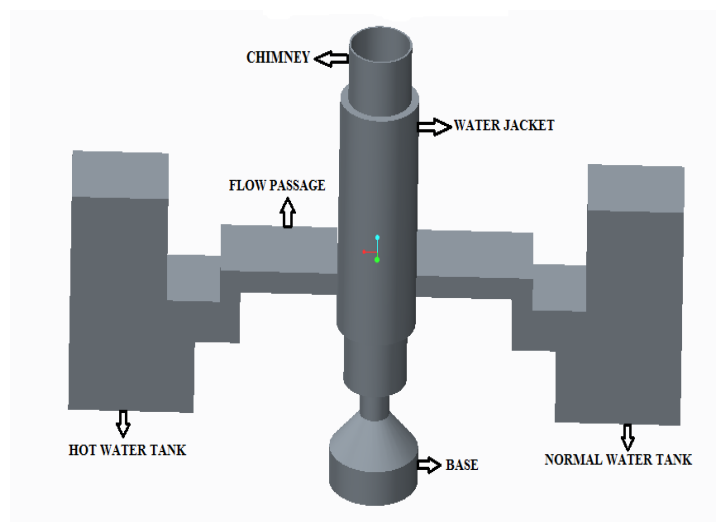


Fig. 1. Schematic of Actual Model

V. Code Methodology

In this project, we use 'C' program to create our code. We made our code to calculate the desired output temperature at the water jacket. Standards values are kept in mind while defining the code. All the standards are pre-defined and the actual output is obtained (Fig. 2). Following is the code used in our project.

```
#include<stdio.h>
int main()
{
    float
a1=0.19625,a2=4.56,dt=45,k=379,dx=0.25,h,ql,x,m=1,cp=4180,rho_air=2.017,v=1,l=6,u
=0.00001182,w,Pr=0.730,b=0.4,n,g,re;
    printf("Q=h.Am.(dt)    Q=-K.Am(dt/dx)\n\n");
    printf("h.Am.(dt)=K.Am(dt/dx)    (NEGLECT THE NEGATIVE)\n\n");
    printf("d=0.75 meter\nAm=(A0-Ai)/ln(A0/Ai)\nRo=0.75 m\nRi=0.5 m\n");
    printf("dt=(70-25)==>45\nK=379 w/mk\ndx=10*10^-3\n\n");
    h=(k)/(dx);
    printf("Convective heat transfer h=%f watt/m.sq.-K\n\n",h);
    printf("Q(loss)=h.A.dt\n");
    ql=h*a1*6*dt;
    printf("Heat loss Q(loss)=%f Joule\n\n",ql);
    printf("m=1\ncp=4.18*10^3 J/kg-K\nt=(70-x)\n");
    x=70-(ql/(m*cp));
    printf("Temperature of water jacket==>%f celcius\n\n",x);
    printf("Outlet temperature of air t=%f\n\n",(70-x));
    printf("rho_air=2.017 kg/m.cube\nVelocity of air v=1 m/sec.\nL=6
meter\nDyanamic viscosity u=1.182*10^-5 \n");
    w=(rho_air*v*l)/u;
    printf("Reynold number without water jacket=%f (Turbulent)\n\n",w);
    printf("Nu=h.L/k\nNu=(0.0233)*Re^0.8*Pr^0.4\n");
    n=(h*l)/k;
    g=n/(0.023*pow(Pr,b));
    re=pow(g,1.25);
    printf("Reynold number with water jacket=%f (Turbulent)\n\n",re);
    return(0);
}
```

```

Q=h.Am.(dt)          Q=-K.Am(dt/dx)
h.Am.(dt)=K.Am(dt/dx)      (NEGLECT THE NEGATIVE)
d=0.75 meter
Am=(A0-Ai)/ln(A0/Ai)
Ro=0.75 m
Ri=0.5 m
dt=(70-25)==>45
K=379 w/mk
dx=10*10^-3

Convective heat transfer h=1516.000000 watt/m.sq.-K

Q(loss)=h.A.dt
Heat loss Q(loss)=80329.054688 Joule

m=1
cp=4.18*10^3 J/kg-K
t=(70-x)
Temperature of water jacket==>50.782524 celcius

Outlet temperature of air t=19.217476

rho_air=2.017 kg/m.cube
Velocity of air v=1 m/sec.
L=6 meter
Dyanamic viscosity u=1.182*10^-5
Reynold number without water jacket=1023857.812500 (Turbulent)

Nu=h.L/k
Nu=(0.0233)*Re^0.8*Pr^0.4
Reynold number with water jacket=6941.331543 (Turbulent)

```

Fig. 2. Output of code

I. Working

The working of our project is very simple, *i.e.*, various factories such as glass factory, boilers, sugar factory, furnaces, etc. produce flue gases into the atmosphere through chimneys. So, we are setting up a water jacket surrounding the chimney which will be full of water. After setting up, the waste exhaust flue gases are made to flow through the heat exchanger unit. The temperature of flue gases at the exhaust is initially very high. Due to the flow of hot gases through a heat exchanger, there is an increase in temperature of water which is circulated from feed pump via the heat exchanger to water jacket. Water gets heated and gains temperature through conduction from hot exhaust gases, *i.e.*, waste heat is recovered and the flue gases are exhausted at reduced temperature [6-8]. The temperature of exhaust gases is considerably reduced; this also helps to control global warming. Due to recovery of energy, there will be a considerable reduction in fuel (such as CNG, LPG and other primary fuels) required to heat the water. Also, after that lukewarm or somewhat hot water is transferred to tank through motor which is transferred to household and commercial applications. It can also be used in boilers to work as a pre-heater in household, where it can be used for various purposes such as bathing, washing utensils and clothes, etc.

II. Applications

1. Waste heat of medium (120-650 °C) and high (>650 °C) temperature could be used for the generation of electricity or mechanical work via different capturing processes [9-11].
2. Waste heat recovery system can also be used to fulfill refrigeration requirements of a trailer (for example): The configuration is easy as only a waste heat recovery boiler with absorption cooler is required. Furthermore, only low pressures and temperatures needed to be handled.
3. Hot water can also be used for medical purposes such as sterilization of medical equipment. It can be used in household for washing clothes and bathing, and commercially it can be used in the same factories as a pre-heater which will also help in increasing its efficiency [12].
4. Usage of primary fuels will be reduced over a large extent.
5. Due to reduced exhaust gas temperature, it helps in lowering global warming.

III. Results Obtained

The proposed design of a plant layout has been analyzed. It's identified that the potential in cement, glass and automobile factories for generation of exhaust heat is the maximum.

As per calculations and research conducted, only reference standard values of all the materials are used as a sample and following results are obtained.

1. Temperature of water before entering in the water jacket = **25°C**.
2. Minimum temperature of exhaust gases entering in the chimney = **70°C**.
3. Rise in temperature exhaust gas comes in contact with water jacket = **50°C**
4. Reynolds's number for exhaust gases without using water jacket comes out to be = 10238.812500. [**TURBULENT FLOW**]
5. Reynolds's number for exhaust gases when the water jacket is used, comes out to be = 6941.331543. [**TURBULENT FLOW**]

NOTE: Value of Reynolds's number remains turbulent even when heat is extracted from exhaust gases by using a water jacket. Waste heat is successfully recovered, and our prime motto is achieved. Also, due to success of this research, various global warming gases will be greatly reduced.

IV. Conclusion and Future Scope

The waste heat energy of flue gases through chimney is recovered. This recovered heat can be utilized to generate *i.e.*, to heat the water and this water can be further used for pretreatment and conservation of various processes. Heat exchanger acts as a basic recovery device. In this application, there is an efficient utilization of heat *i.e.*, heat recovery. The approach of review of this research is towards the heat recovery technique and simple implementation for various systems in day to day life. These techniques have proven better, beneficial and eco-friendly. It is also a way and hope of energy saving.

CONFLICTS OF INTEREST

The authors declare that there is no conflict of interests regarding the publication of this paper.

REFERENCES

- [1] S. S. Thakare and J. A. Hole, "Review of analysis of heat recovery from top coat oven in paint shop", *International Journal of Engineering Research and Technology*, vol. 4, no. 2, pp.1085-1088, 2015.
- [2] R. Soltani, I. Dincer and M. A. Rosen, "Thermodynamic analysis of a novel multigeneration energy system based on heat recovery from a biomass CHP cycle", *Appl. Thermal Engineering*, vol 89, pp.90-100, 2015.
- [3] T. S. Jadhav and M. M. Lele, "A case study on energy saving in air conditioning system by heat recovery using heat pipe heat exchanger", *International Journal of Engineering Research and Technology*, vol. 3, no. 2, pp. 12-16, January 2014.
- [4] G. V. Pradeep Varma and T. Srinivas: "Design and analysis of a cogeneration plant using heat recovery of cement factory", *Case studies in Therm. Eng.*, vol. 5, pp. 24-31, 2015.
- [5] R. Saidur, W. K. Muzammil, S. Paria, M.H. Hassan, M. Rezaei and M. Hasanuzzaman, "Technologies to recover heat from internal combustion engines" *Renewable and Sustainable energy reviews*, vol. 16, pp.5649-5659, 2012.
- [6] F. Pask, J. Sadhukhan, P. Lake, S. McKenna, E.B. Perez and A. Yang: "Systematic approach to industrial oven optimization for energy saving", *Appl. Therm. Eng.*, vol. 71, no. 1, pp.72-77, 2014.
- [7] P. Ahmadi, M. A. Rose and I. Dincer: "Themodynamic modeling and multi-objective evolutionary-based optimization of new multigeneration energy system", *Energy Conver. Manag.*, vol. 76, pp. 282-300, 2013.
- [8] T.A.H. Ratlamwala, M. A. Gadalla and I. Dincer: "Performance analysis of a novel integrated geothermal-based system for multi generation applications", *Appl. Thermal Eng.*, vol. 40, pp. 71-79, 2012.
- [9] S. B. Riffat and A. Mardiana-Idayu, "Review on heat recovery technologies for building applications", *Renewable and Sustainable Energy Reviews*, vol. 16 pp. 1241-1255, 2012.
- [10] M. Ahamadzadehtlatapeh and Yau Y.H., "Predicting yearly energy recovery and dehumidification enhancement with a heat pipe heat exchanger using typical meteorological year data in tropics", *Journal of Mechanical Science and Technology*, vol. 25, no.4, pp. 847-853, 2011.
- [11] N.A. Madloola, N.A. Rahim, M.S. Hossiana and R. Saidutra: "A critical review on energy use and saving in cement industries", *Renewable and Sust. Energy Rev.*, vol. 15, pp. 2042-2060, 2011.
- [12] E. Wang, M. Ouyang, X. Li, J. Li and S. Xia, "Control system design for variable nozzle turbocharger", SAE (Society of Mechanical Engineers) paper no. 2009-01-1668. Presented at non-conference specific technical papers-2009, July 2010. Warrendale, PA, USA

Article copyright: © 2018 Ujjawal Kohli, Vaibhav Mishra and Sparsh Singh Kotwal. This is an open access article distributed under the terms of the [Creative Commons Attribution 4.0 International License](https://creativecommons.org/licenses/by/4.0/), which permits unrestricted use and distribution provided the original author and source are credited.



Operation of Symmetrical and Asymmetrical Two-Phase Induction Motor by Using 3-Leg Voltage Source Inverter

Sheetal Vishal Umredkar^{1*}, Abhishek Junghare², and M.M. Renge³

¹ Assistant Professor, Department of Electrical Engineering, Shri Ramdeobaba College of Engineering Nagpur-440013, India

² Assistant Professor, Department of Electrical Engineering, S.B Jain Institute of technology and research Nagpur-441501, India

³ Professor, Department of Electrical Engineering, Shri Ramdeobaba College of Engineering Nagpur-440013, India

Received January 27, 2018; Accepted March 15, 2018; Published April 30, 2018

The importance and demand of renewable energy have increased rapidly, especially due to the fact that the fossil fuels are reducing at an alarming rate. Out of the existing sources of renewable energies, solar energy has been very popular due to obvious abundance and convenience. The predominant use of electrical energy is heating, ventilation and air conditioning in residential and industrial sector. Single phase induction motor is widely used for such low-power appliances like pumps, compressors, agriculture equipment's and blowers. In order to avoid losses and low-starting torque, we intend to use the single-phase induction motor as an asymmetrical two-phase induction motor, which will run on a two-phase supply yielding better efficiency, speed control and power factor. If a three-phase supply is available, Scott-T transformer can be used to get two-phase supply. However, if there is only single-phase supply available, two-phase inverter with Sine Pulse Width Modulation (SPWM) technique can be used. This paper presents the method for two-phase supply using the 3-leg voltage source inverter (VSI) which is used to supply asymmetrical and symmetrical two-phase induction motor. The 16 bit microcontroller dsPIC is used for SPWM signal generation.

Keywords: Two-phase motor; Two-phase supply; Scott-T transformer; Sine PWM; 3-Leg voltage source Inverter (VSI)

Introduction

Single-phase induction motor is the most widely used motor in home appliances, agricultural equipment, pumps, compressors, blowers and industries for low-power applications. This motor is widely adopted for domestic applications because it uses single-phase AC source with constant frequency which is easily available. In domestic applications, it is used with great advantages, but its performance is menial compared to the poly-phase induction motor due to low-rated power, zero starting torque and high torque harmonics [1, 2].

Two different techniques are used to control single-phase induction motor: scalar control and vector control. In scalar control technique, two parameters are changed simultaneously. The speed can be varied by changing the supply frequency, but this

*Corresponding author: umredkars@rknec.edu

causes changes in the impedances which result in changes in the current. If the current is small, torque developed by the motor decreases. If the frequency decreases or the voltage increases, the coils may burn or saturation may occur in the iron of coils. To avoid these problems, it is necessary to vary the voltage and frequency at the same time. Scalar control is a more economical and simpler technique, but it gives unsatisfactory performance of the drives with dynamic behavior and slow transient response. In vector control, it is possible to control two parameters independently and satisfy the requirements of dynamic behavior of the drives. Its main drawback is complexity and higher cost. Vector control of three-phase induction motor is easy as compared to single phase-phase induction motor, because single-phase induction motor has different parameters of both the windings (*i.e.*, main and auxiliary winding) [3,4].

In the proposed system, we have designed symmetrical and asymmetrical two-phase induction motors. In symmetrical two-phase induction motor, parameters of both the windings are same, while they are different in case of asymmetrical motor. For this study, we used scalar control for both symmetrical and asymmetrical motors. However, vector control of symmetrical two-phase motor can be simple and more accurate and should be preferred over scalar method for better dynamic performance in actual industrial applications [5]. Performance of single-phase induction motor is improved by using voltage source inverter (VSI), and we should use the single-phase induction motor (SPIM) as an asymmetrical two-phase induction motor (TPIM) by removing capacitor. Two-phase motor can be introduced in the place of single-phase induction motor with additional advantages such as more efficiency, better power factor and better speed control. There is no need to replace the existing single-phase motor, because it can be tweaked to work as two-phase motor to improve the performance of the drive by removing capacitor connected in the circuit and fed by two-phase supply. Two-phase supply can be generated with the help of three-phase supply and Scott-T transformer. But for the domestic applications, household single-phase supply is already available. So either conversion of supply to three-phase is needed or any other suitable setup is required. This complexity can be reduced with the help of microcontroller. This paper presents the method to get two-phase supply using the 3-leg VSI, which is used to power asymmetrical and symmetrical two-phase induction motor. A dsPIC microcontroller [6] is used to generate Sine Pulse Width Modulation (SPWM) switching signal for running the two-phase induction motor and controlling the speed of motor. The control is performed by SPWM technique with voltage source inverter and tested by open loop control.

Two-phase Supply

The simple method to obtain two-phase supply is by using the Scott-T transformer from conventional three-phase supply. The Scott-T is made by two different single-phase transformers with different tapping ratios. The connections are made in such manner that Scott-T transformer gives two single-phase outputs which are called as Main output and Teaser output. The Main and Teaser output are 90° out of phase [7]. Connections consist of 1:1 center-tapped ratio of Main transformer T_1 , and 86.6% ratio of Teaser transformer T_2 . The center-tapped side of T_1 transformer is connected between two of the phases in the three-phase side. Centre tap is then connected to one end of higher turn side of T_2 , and the other ends to remaining phases [8]. The remaining side of transformers T_1 and T_2

is the side at which two-phase output is obtained and two-phase motor can be connected [7].

Two-phase induction motor is connected between phase-1 and phase-2. But these types of supply cause imbalance in the system side due to power quality issues. The devices are sensitive to the power quality connected in the system and can cause mal-operation. Also in the household applications, the three-phase supply is not available as per requirement of above circuitry. With respect to industrial applications, the high cost of Scott-T transformer is a concern. Thus, more efficient and low cost technique to obtain two-phase supply is by using micro-controller.

Modeling of Two-phase Induction Motor

Single phase induction motors are constructed in the form of two-phase motors, with two stator windings in space quadrature [8]. The main and auxiliary windings are quite different in the following aspects: different turns, wire size and turns distributions. These differences cause unbalanced winding currents. Under balanced operating conditions, a symmetrical two-phase motor can be analyzed using technique for three-phase motors with slight modification [9].

Under unbalanced conditions, the stator-mmF wave travels 90° in space in a time interval corresponding to a 90° phase change of applied voltage, with the direction of travel depending on the phase sequence of the currents.

Mathematical model of two-phase induction motor is given below,

$$\begin{bmatrix} \lambda_m \\ \lambda_a \\ \lambda_{r1} \\ \lambda_{r2} \end{bmatrix} = \begin{bmatrix} L_m & 0 & L_{m,r1}(\theta_{me}) & L_{m,r2}(\theta_{me}) \\ 0 & L_a & L_{a,r1}(\theta_{me}) & L_{a,r2}(\theta_{me}) \\ L_{m,r1}(\theta_{me}) & L_{a,r1}(\theta_{me}) & L_r & 0 \\ L_{m,r2}(\theta_{me}) & L_{a,r2}(\theta_{me}) & 0 & L_r \end{bmatrix} \begin{bmatrix} i_m \\ i_a \\ i_{r1} \\ i_{r2} \end{bmatrix} \quad (1)$$

where

θ_{me} : Rotor angle measured in electrical radians.

L_m & L_a : Self-inductance of the main and auxiliary winding resp.

$L_{m,r1}(\theta_{me})$: Mutual inductance between the main winding and equivalent rotor winding 1.

$L_{m,r2}(\theta_{me})$: Mutual inductance between the main winding and equivalent rotor winding 2.

$L_{a,r1}(\theta_{me})$: Mutual inductance between the auxiliary winding and equivalent rotor winding 1.

$L_{a,r2}(\theta_{me})$: Mutual inductance between the auxiliary winding and equivalent rotor winding 2.

Assume a sinusoidal distribution of air gap flux, the mutual inductance between the main winding and the rotor is

$$L_{m,r1}(\theta_{me}) = L_{m,r} \cos(\theta_{me}) \quad (2)$$

$$L_{m,r2}(\theta_{me}) = -L_{m,r} \sin(\theta_{me}) \quad (3)$$

where

$L_{m,r}$: Amplitude of mutual inductance

$$L_{a,r1}(\theta_{me}) = L_{a,r} \sin(\theta_{me}) \quad (4)$$

$$L_{a,r2}(\theta_{me}) = L_{a,r} \cos(\theta_{me}) \quad (5)$$

$$L_{a,r} = aL_{a,r} \quad (6)$$

Self-inductance of the magnetizing branch can be written as the sum of leakage inductance $L_{m,1}$ and a magnetizing inductance L_m

$$L_m = L_{m,1} + L_m \quad (7)$$

Then the self-inductance of the auxiliary winding can be written as

$$L_a = L_{a,1} + a^2 L_m \quad (8)$$

The voltage equations for this machine can be written in terms of the winding currents and flux linkage as

$$v_m = i_m R_m + \frac{d\lambda_m}{dt} \quad (9)$$

$$v_a = i_a R_a + \frac{d\lambda_a}{dt} \quad (10)$$

$$v_{r1} = 0 = i_{r1} R_r + \frac{d\lambda_{r1}}{dt} \quad (11)$$

$$v_{r2} = 0 = i_{r2} R_r + \frac{d\lambda_{r2}}{dt} \quad (12)$$

where R_m , R_a , and R_r are the resistances of the main, auxiliary and rotor windings, respectively.

Electro-magnetic torque of the motor can be written as

$$T_{mech} = i_m i_{r1} \frac{dL_{m,r1}(\theta_{me})}{d\theta_m} + i_m i_{r2} \frac{dL_{m,r2}(\theta_{me})}{d\theta_m} + i_a i_{r1} \frac{dL_{a,r1}(\theta_{me})}{d\theta_m} + i_a i_{r2} \frac{dL_{a,r2}(\theta_{me})}{d\theta_m} \quad (13)$$

$$T_{mech} = \left[\frac{\text{poles}}{2} \right] [-L_{m,r}(i_m i_{r1} \sin\theta_{me} + i_m i_{r2} \cos\theta_{me}) + (L_{a,r}(i_a i_{r1} \cos\theta_{me} - i_a i_{r2} \sin\theta_{me}))] \quad (14)$$

where

$$\theta_m = \left[\frac{2}{\text{poles}} \right] \theta_{me} \text{ is the rotor angle in radians.}$$

Assuming steady-state operation, with constant mechanical speed w_{me} , corresponding to slip s and constant supply frequency w_e . Using above assumption, the rotor currents will be at frequencies $w_r = w_e - w_{me} = s w_{me}$ (produced by the stator positive-sequences field) and $w_r = w_e + w_{me} = (2 - s) w_{me}$ (produced by the stator negative-sequences field).

Using equation (11) and (12) to eliminate the rotor currents, the main and auxiliary-winding flux-linkage/current relationships of equation (1) can be written as

$$\overline{\lambda_m} [L_m - jL_{m,r}^2(\overline{k^+} + \overline{k^-})] \overline{I_m} + L_{m,r} L_{a,r} (\overline{k^+} - \overline{k^-}) \overline{I_m} \quad (15)$$

$$\overline{\lambda_a} = -L_{m,r} L_{a,r} (\overline{k^+} - \overline{k^-}) \overline{I_m} + [L_a - jL_{a,r}^2(\overline{k^+} + \overline{k^-})] \overline{I_a} \quad (16)$$

where

$$\bar{k}^+ = \frac{sw_e}{2(R_r + jsw_e L_r)} \text{ and } \bar{k}^- = \frac{(2-s)w_e}{2(R_r + j(2-s)w_e L_r)} \quad (17)$$

The voltage equations using equation (9) and (10) as,

$$\bar{V}_m = \bar{I}_m R_m + jw_e \bar{\lambda}_m \quad (18)$$

$$\bar{V}_a = \bar{I}_a R_a + jw_e \bar{\lambda}_a \quad (19)$$

The rotor currents consist of positive and negative-sequence components. The complex amplitudes of the positive-sequence and negative-sequence components at frequency sw_e and $(2-s)w_e$, respectively, are given by

$$\bar{I}_{r1}^+ = \frac{-jsw_e [L_{m,r} \bar{I}_m + j] L_{a,r} \bar{I}_a}{2(R_r + jsw_e L_r)} \quad (20)$$

$$\bar{I}_{r2}^+ = \bar{I}_{r1}^+ \quad (21)$$

$$\bar{I}_{r1}^- = \frac{-j(2-s)w_e [L_{m,r} \bar{I}_m - j] L_{a,r} \bar{I}_a}{2(R_r + j(2-s)w_e L_r)} \quad (22)$$

$$\bar{I}_{r2}^- = j \bar{I}_{r1}^- \quad (23)$$

Equivalent Circuit of Two-Phase Induction Motor

The TPIM equivalent circuit models take into account core loss representing with (R_c) in parallel across the forward and backward field impedances as shown in Fig. 1 [9]. Design of the induction motor model depends on determination of the parameters. The parameters can be determined by performing direct current test, no-load test and locked rotor test on the motor.

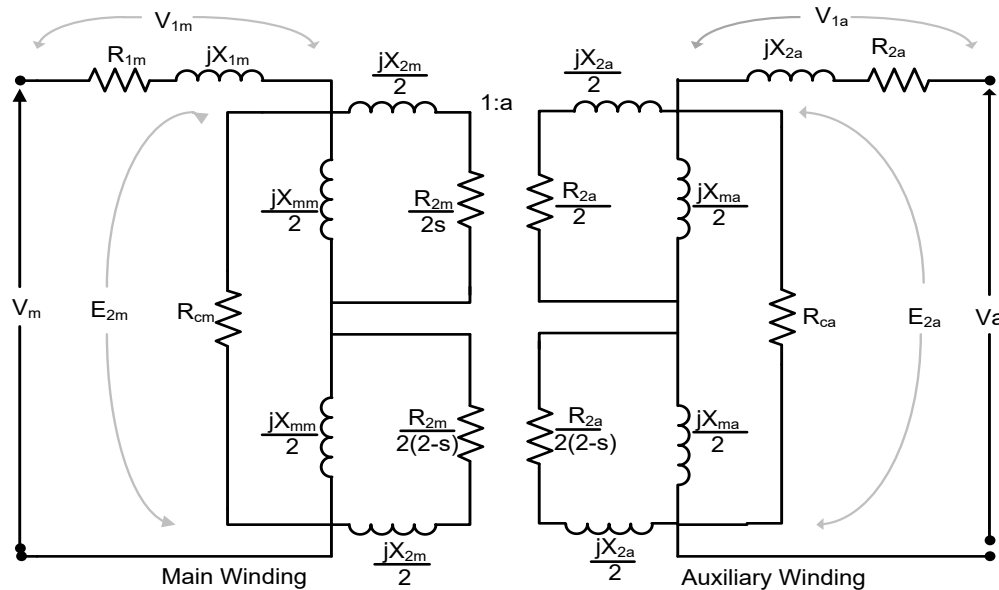


Fig. 1. Equivalent circuit of two-phase induction motor

Fig. 1 shows the equivalent circuit for TPIM. $V_m, I_m, V_a, I_a, s, a, R_{cm}, R_{ca}$ are main winding and auxiliary winding voltages, currents, slip, turn ratio, resistances showing the main and auxiliary winding core losses, respectively. Impedance calculation of main winding is given by following equations,

$$Z_m = Z_{1m} + Z_{2m} \quad (24)$$

$$Z_{1m} = (R_{1m} + jX_{1m}) \quad (25)$$

$$Z_{2m} = \frac{R_{cm}(Z_{fm} + Z_{bm})}{R_{cm} + Z_{fm} + Z_{bm}} \quad (26)$$

$$Z_{fm} = \frac{\frac{jX_{mm}}{2} \left(\frac{R_{2m}}{2s} + j \frac{X_{2m}}{2} \right)}{\frac{jX_{mm}}{2} + \left(\frac{R_{2m}}{2s} + j \frac{X_{2m}}{2} \right)} \quad (27)$$

$$Z_{bm} = \frac{\frac{jX_{mm}}{2} \left(\frac{R_{2m}}{2(2-s)} + j \frac{X_{2m}}{2} \right)}{\frac{jX_{mm}}{2} + \left(\frac{R_{2m}}{2(2-s)} + j \frac{X_{2m}}{2} \right)} \quad (28)$$

The main winding voltage and current equations of the circuit are

$$V_m = V_{1m} + E_{2m} \quad (29)$$

$$I_m = \frac{V_m}{Z_m} \quad (30)$$

Similar to main winding, impedance of the auxiliary winding is given by the following equations.

$$Z_a = Z_{1a} + Z_{2a} \quad (31)$$

$$Z_{1a} = (R_{1a} + jX_{1a}) \quad (32)$$

$$Z_{2a} = \frac{R_{ca}(Z_{fa} + Z_{ba})}{R_{ca} + Z_{fa} + Z_{ba}} \quad (33)$$

$$Z_{fa} = \frac{\frac{jX_{ma}}{2} \left(\frac{R_{2a}}{2s} + j \frac{X_{2a}}{2} \right)}{\frac{jX_{ma}}{2} + \left(\frac{R_{2a}}{2s} + j \frac{X_{2a}}{2} \right)} \quad (34)$$

$$Z_{ba} = \frac{\frac{jX_{ma}}{2} \left(\frac{R_{2a}}{2(2-s)} + j \frac{X_{2a}}{2} \right)}{\frac{jX_{ma}}{2} + \left(\frac{R_{2a}}{2(2-s)} + j \frac{X_{2a}}{2} \right)} \quad (35)$$

The main winding voltage and current equations of the circuit are,

$$V_a = V_{1a} + E_{2a} \quad (36)$$

$$I_a = \frac{V_a}{Z_a} \quad (37)$$

$$V_a = aV_m \quad (38)$$

Referring to the equivalent circuit, power loss equation can be written as

$$P_{cus} = P_{cum} + P_{cu_a} = I_m^2 R_{1m} + I_a^2 R_{1a} \quad (39)$$

$$P_c = P_{cm} + P_{ca} \quad (40)$$

where P_{cus} and P_c are the stator copper loss and core loss.

Inverter Circuit

The block diagram of proposed system is shown in Fig. 2. The single-phase AC supply can be converted to DC by simply using bridge rectifier and filter circuitry. The 3-leg voltage source inverter is used to convert DC to two-phase AC supply. The 3-leg voltage source inverter consists of six insulated-gate bipolar transistor (IGBT) switches. The switching pulses for the IGBT are obtained by dsPIC micro-controller. The SPWM is used as modulation technique for IGBT. By using the inverter, the TPIM can be made to operate over a wide range of speed by adjusting the frequency [5].

Proposed System

Fig. 2 shows the proposed system, in which 3-leg voltage source inverter is connected to two-phase induction motor that is developed in the core of single-phase induction motor [8]. The 3-leg voltage source inverter is used for conversion of DC to AC by using sinusoidal pulse width modulation (SPWM) technique. A dsPIC microcontroller is used to generate switching pulses for the switches of the inverter by using SPWM technique. With the advent of renewable energy resources, photovoltaic (PV) array is often considered as the best power source for DC supplies. The DC input to the inverter can be given by a solar panel through boost converters. The connected system can have various applications like solar based water pumping system, cooling system and many others. For this study, it is necessary to obtain higher voltage for three-leg VSI driving TPIM with rated flux. Therefore, a boost converter can be included to achieve sufficient DC link voltage and increase the system efficiency [10].

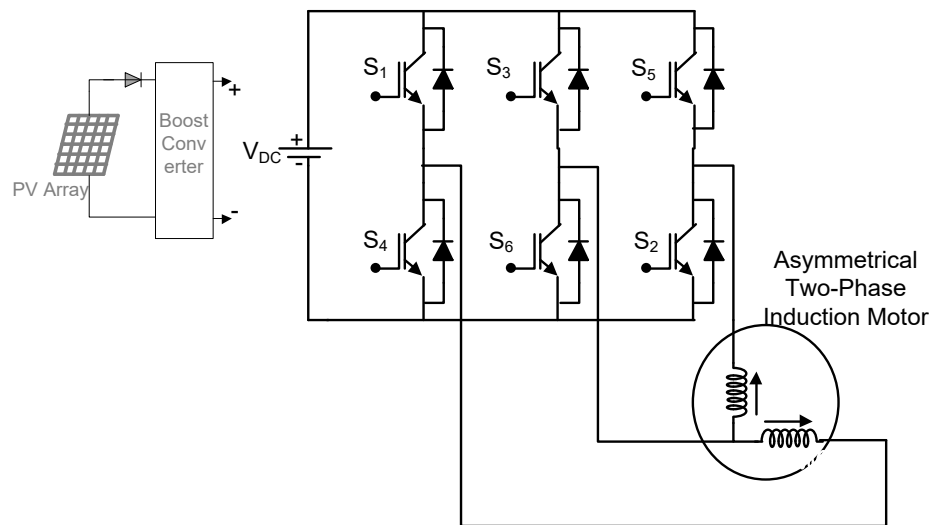


Fig. 2. Proposed System

Two-Leg Voltage Source Inverter

The two-leg two-phase inverter connected to two-phase Induction Motor, it consists of 4 switches with 2-leg inverter and center tapped capacitor supplied with DC supply [11, 12]. DC supply is either fed from solar panel with the help of boost converter or with the help of diode rectifier fed from single-phase AC supply. SPWM pulses fed to second leg has phase shift of 90° . Main winding and auxiliary winding of two-phase

induction motor are fed from two legs of two-phase voltage source inverter. The neutral or common is given to capacitor link.

Many researchers have worked on the 2-leg voltage source inverter but practically it has its own problem of total harmonic distortion of current. The output voltage obtained at phases of two-phase induction motor in case of 2-leg inverter is lower, which results in lower efficiency of motor.

Three-Leg Voltage Source Inverter

The modern technique is to use 3-leg voltage source inverter 3-leg voltage source inverter is constructed as shown in Fig. 2 [1]. The inverter consists of 6 IGBT switches. Two switches and two diodes are used for a boost rectifier for power factor correction, and the other four switches and four diodes are used for the 2-leg inverter. Such circuits have been applied to compact SPIM drives to improve the input power factor and reduce the output voltage harmonics. A 3-leg voltage source inverter providing two-phase outputs is increasingly attractive for two-phase drive applications due to good dc voltage utilization. When compared with the 2-leg voltage source inverter for a two-phase induction motor, the 3-leg voltage source inverter offers reduction in the motor current ripple and more or less 20% higher output phase voltages. Also, the problem of unbalanced voltages across two DC-link capacitors is absent for the 3-leg voltage source inverter.

The voltages V_{a0} , V_{b0} and V_{c0} are defined by following equations,

$$V_{a0} = m \sin(\omega_e t) \quad (41)$$

$$V_{b0} = m \sin(\omega_e t - \frac{\pi}{2}) \quad (42)$$

$$V_{c0} = m \sin(\omega_e t - \pi) \quad (43)$$

where

m: modulation index

The switching signal pattern of the three-phase reference voltages is derived from equation (41) to equation (43) and compared with the triangular carrier signal. If the reference voltage is lower than the triangular carrier, the status of switching is OFF. Otherwise if reference voltage is higher than or equal to the triangular reference voltage, the status of switch is ON. This modulation technique is called as Sine pulse width modulation (SPWM).

The reference voltage can be adjusted by varying values of modulation index m from 0 to 1, while the magnitude of triangular carrier voltage (V_{tri}) is to be 1. The modulation index is kept at 0.95. The switching frequency of IGBT switches is kept at 1000 Hz, which results in the output AC voltage at 50 Hz. The frequency of testing signal is kept at 50 Hz, as per Indian standard.

Gate Driver Circuit

The Gate driver circuit consists of main parts

1. AC supply
2. Rectifier
3. Filter Capacitor
4. dsPIC Microcontroller
5. Buffer SN7407

6. Driver TLP250

The rectifier circuit is used to convert AC to DC as per requirement. The dsPIC microcontroller works on the 3.3 volt DC and its output voltage is also a 3.3 volt DC. The buffer SN7407 works on 5 volt DC, while optocoupler TLP 250 needs 15 volt DC. The optocoupler IC provides necessary isolation between dsPIC microcontroller [6] circuit and IGBT switches. In this way, the gate pulse magnitude with voltage nearly equal to 14.5 volt is given to IGBT for its operation. The grounding of 15 volt supply for optocoupler TLP250, switches S_1 and S_4 , S_3 and S_6 , S_5 and S_2 should not be same, otherwise it would result in short-circuit. The grounding for switch S_4 , S_2 and S_6 can be made common for 15 volt DC.

Experimental Setup

Fig. 3 shows the experimental setup of the 3-leg voltage source inverter with following rating of asymmetrical two-phase Induction motor are 0.25 HP, 230 V, 50Hz, $R_{1m} = 2 \Omega$, $X_{1m} = X_{2m} = 3 \Omega$, $R_{2m} = 4 \Omega$, $X_{mm} = 60 \Omega$, $R_c = 600 \Omega$

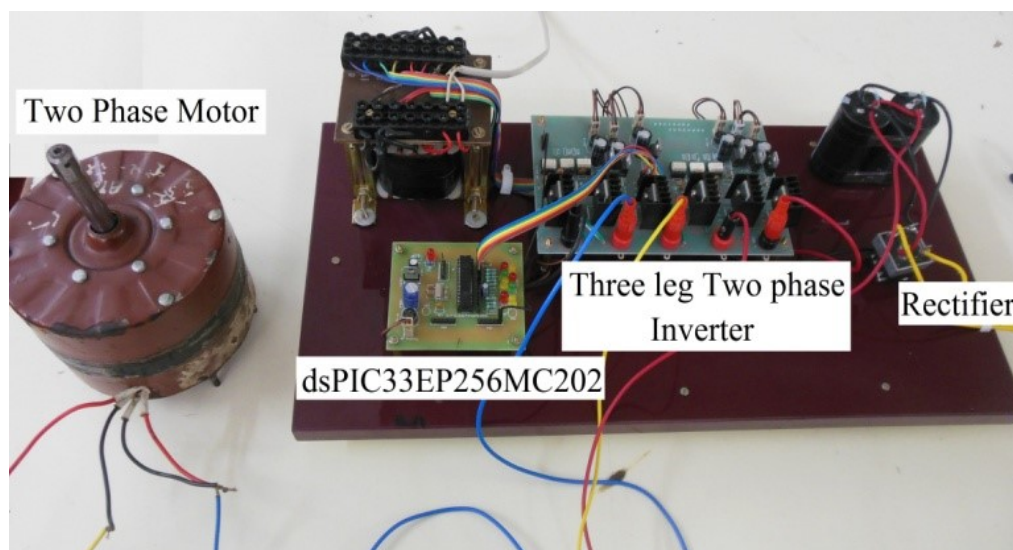


Fig. 3. Experimental setup

Single-phase supply is given to the rectifier, which is easily available in households and small factories. The rectifier converts it to DC and feeds DC supply to 3-leg two-phase inverter which converts it into two-phase AC supply. The IGBT switches are used in the inverter for switching, whose switching pulses are fed from dsPIC microcontroller IC.

Results

The switching pulses for upper switches S_1 , S_3 and S_5 are given in Fig. 4 and obtained with the help of the dsPIC microcontroller. The complementary pulses are given to S_4 , S_6 , and S_2 , respectively. The phase shift of 90° is obtained between two windings.

Fig. 5 shows the line voltage at the output terminal of inverter. Fig. 6 shows the speed signal of motor at no load. Motor is running at 1425 RPM.

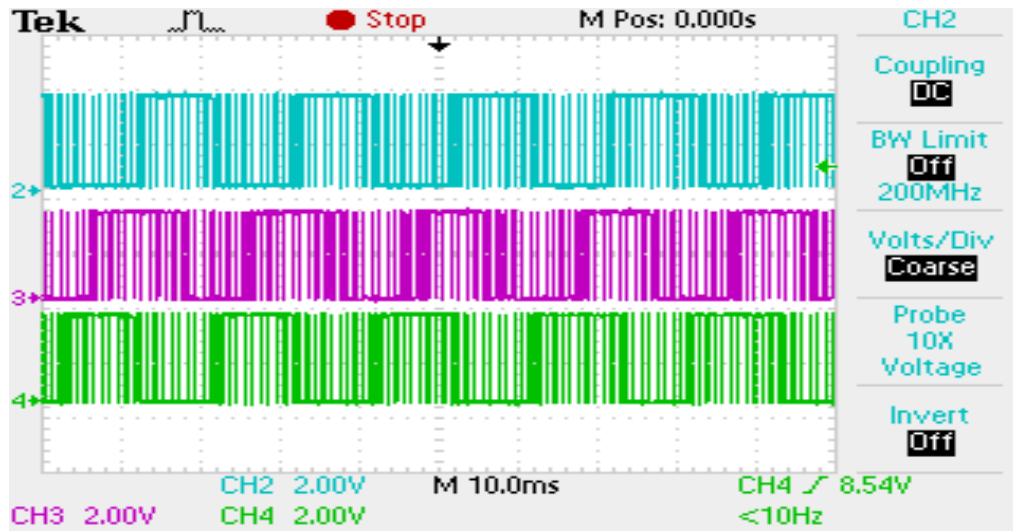


Fig. 4. Switching Signal for upper switches

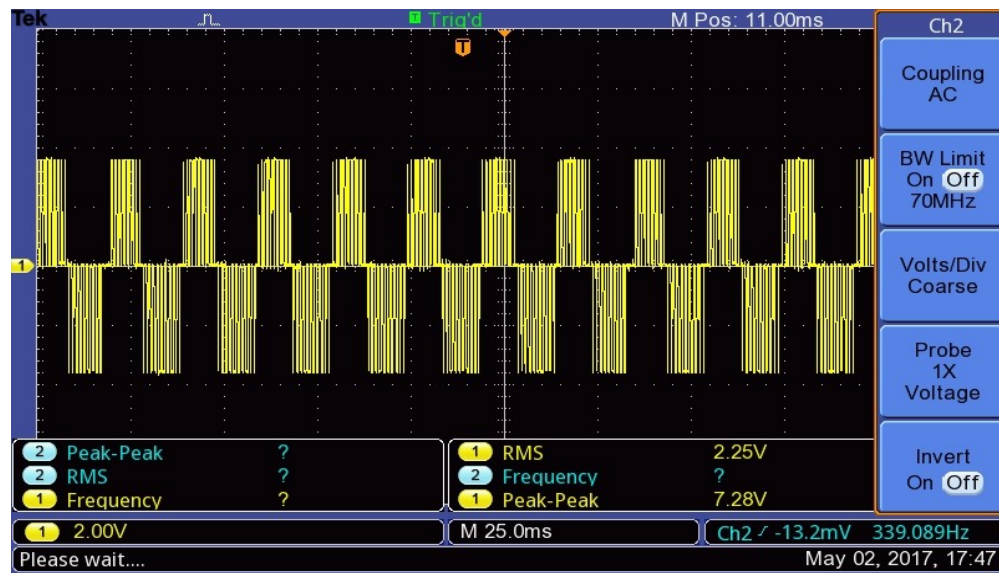


Fig. 5. Line Voltage

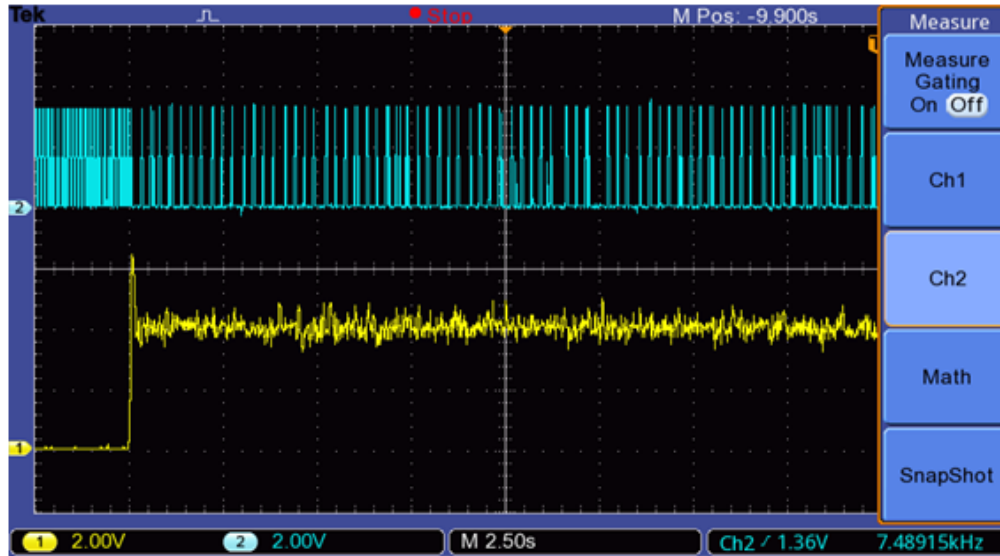


Fig. 6. Speed of two-phase induction motor at no load

Table 1. Results with asymmetrical induction motor

| Sr. No. | ASYMMETRICAL INDUCTION MOTOR | | | | |
|---------|------------------------------|----------------|-------------|-------------------|-------------|
| | Voltage (Volts) | With Capacitor | | Without Capacitor | |
| | | Power (Watts) | Speed (RPM) | Power (Watts) | Speed (RPM) |
| 1 | 120 | -- | -- | 54 | 360 |
| 2 | 130 | 62.77 | 580 | 64 | 570 |
| 3 | 150 | 79.66 | 790 | 78 | 770 |
| 4 | 190 | 108 | 1040 | 109 | 1062 |
| 5 | 210 | 133 | 1178 | 135.3 | 1198 |
| 6 | 230 | 139.5 | 1230 | 145 | 1320 |

Table 1 shows the readings of asymmetrical induction motor with and without capacitor. Table 2 shows the readings of symmetrical induction motor with and without capacitor.

Table 2. Results with symmetrical induction motor

| Sr. No. | SYMMETRICAL INDUCTION MOTOR | | | | |
|---------|-----------------------------|----------------|-------------|-------------------|-------------|
| | Voltage (Volts) | With Capacitor | | Without Capacitor | |
| | | Power (Watts) | Speed (RPM) | Power (Watts) | Speed (RPM) |
| 1 | 80 | -- | -- | 28.8 | 390 |
| 2 | 130 | 72.5 | 490 | 74.6 | 535 |
| 3 | 150 | 94 | 640 | 96.6 | 690 |
| 4 | 190 | 134.4 | 1050 | 136.6 | 1150 |
| 5 | 210 | 156.6 | 1156 | 159.8 | 1220 |
| 6 | 230 | 168 | 1226 | 172.3 | 1296 |

The experimental results shown in Table 1 and Table 2 indicate that the performance of symmetrical two-phase motor is satisfactory as compared to asymmetrical motor without capacitor.

The total costing was estimated from two conversion methods. It is clear that two-phase supply with 3-leg voltage source inverter system is very economical and efficient technique with huge difference of approximately \$22 than conventional Scott-T transformer system as shown in Table 3.

Table 3. Total Costing

| Two-Phase (With Scott-T Transformer) | | Two-Phase (With 3-Leg Inverter) | |
|---|--------------|------------------------------------|-------------|
| Motor Core, Stator and Rotor | \$ 12 | Motor Core, Stator and Rotor | \$ 12 |
| Winding Cost | \$ 8 | Winding Cost | \$ 8 |
| Scott-T Transformer | \$ 32 | 3-Leg Inverter | \$ 10 |
| Total | \$ 52 | Total | \$30 |

Conclusion

In the developing countries, the motor pumps consume substantial portion of total electricity. Single-phase induction motor is commonly used in household, industries and agriculture for pumping purpose. Same single-phase induction motor can be upgraded to two-phase motor by the technique described in this paper. The use of two-phase induction motor gives high starting torque, variable speed and high rated power. The two-phase mode of operation achieves increased rated torque causing more power in the same frame size and higher efficiency resulting in less running cost. By using a 3-leg voltage source inverter for obtaining two-phase supply, the supply for motor can be obtained more economically and efficiently.

CONFLICTS OF INTEREST

The authors declare that there is no conflict of interests regarding the publication of this paper.

REFERENCES

- [1] K. Kaenthong, V. Tipsuwanporn, A. Numsomran and A. Charean, "Asymmetrical Two-Phase Induction Motor Speed Controlled with 3-Leg Voltage Source Inverter," IEEE International Conference on Industrial Technology (ICIT), pp. 640-645, 2015. DOI: 10.1109/icit.2015.7125170
- [2] D.G. Holmes and A. kotsopoulos, "Variable speed control of single and two phase induction motors using a three phase voltage source inverter" IEEE Industrial

- Applications Society annual meeting conference records, pp.613-620, 1993. DOI: 10.1109/IAS.1993.298887
- [3] Md Ayubur Rahman Khan and Md Quamrul Ahsan, "Development and Performance Analysis of a Two-Phase Induction Motor in the Frame and Core of a Single-Phase Induction Motor," 8th International Conference on Electrical and Computer Engineering, pp. 469-472, 2014. DOI: 10.1109/ICECE.2014.7026982
- [4] F.A.S. Neves, E.B.S. Filho, J.M.S. Cruz, R.P. Landim, Z.D. Lins and A.G.H. Accioly, "Single-Phase Induction Motor Drives with Direct Torque Control," IEEE 2002 28th Annual Conference of the Industrial Electronics Society. IECON 02, pp.241-246, 2002. DOI: 10.1109/IECON.2002.1187514
- [5] Do-Hyun Jang "Problems Incurred in a Vector-Controlled Single-Phase Induction Motor, and a Proposal for a Vector-Controlled Two-Phase Induction Motor as Replacement," IEEE Transaction on Power Electronics, vol. 28, no. 1, pp. 526 – 536, 2013. DOI: 10.1109/TPEL.2012.2199772
- [6] Microchip Technology, "DS70000657H, 16-Bit Microcontrollers and Digital Signal Controllers with High-Speed PWM, Op Amps and Advanced Analog" , 2013. <http://ww1.microchip.com/downloads/en/DeviceDoc/70000657H.pdf> (accessed on 4/30/2018)
- [7] J. Parmar, "Scott-T Connection of Transformer", 2012. <https://electricalnotes.wordpress.com/2012/05/06/scott-t-connection-of-transformer/> (accessed on 4/30/2018)
- [8] P. Kongsuk and V. Kinnares, "Loss Modeling of Three-leg Voltage Source Inverter fed Asymmetrical Two-phase Induction Motor", 18th International Conference on Electrical Machines and systems(ICEMS), 2015. DOI: 10.1109/ICEMS.2015.7385130
- [9] A.E. Fitzgerald, C. Kingsley, S.D. Umans and B. James, Electric Machinery. New York: McGraw-Hill; 2003.
- [10] E. Hayakwong and V. Kinnares, "PV powered three-leg VSI fed asymmetrical parameter type two-phase induction motor," 2014 17th International Conference on Electrical Machines and Systems (ICEMS), Hangzhou, 2014, pp. 3220-3225. DOI: 10.1109/ICEMS.2014.7014047
- [11] D.H. Jang, "PWM methods for two-phase inverters," IEEE Ind. Appl. Mag., vol. 13, no. 2, pp.50-61, 2007. DOI: 10.1109/MIA.2007.322258
- [12] C.G. Veinott, Theory and Design of Small Induction Motors, New York: McGraw-Hill, 1959.

Article copyright: © 2018 Sheetal Vishal Umredkar, Abhishek Junghare and M. M. Renge. This is an open access article distributed under the terms of the Creative Commons Attribution 4.0 International License, which permits unrestricted use and distribution provided the original author and sources are credited.



Low Cost Device for Charging Mobile Phone using Another Smartphone

Vaibhav Aggarwal¹, Vaibhav Gupta¹, Kiran Sharma^{2*}, and Neetu Sharma³

¹ Department of Computer Science Engineering, Graphic Era University, Dehradun, Uttarakhand, India

² Department of Physics, Graphic Era University, Dehradun, Uttarakhand, India

³ Department of Chemistry, Graphic Era University, Dehradun, Uttarakhand, India

Received January 22, 2018; Accepted March 15, 2018; Published May 1, 2018

Mobile has been and will always remain one of the best companions for any human being. Mobile phones are considered as the live example of the advancement in technology on a daily basis. This era is marked by our complete dependence on this technology. The growing technology has introduced mobile phone, which plays an important role in communication. Since mobile phones have been made to be with the user all day and to carry out all the basic and high-performance task as per the demand of the user, the batteries need to be charged multiple times during a day. This imposes a burden on the user to carry a power bank while travelling; at times it becomes difficult if the power bank battery also drains out. This paper presents a small technique which may reduce this problem. The major components of the design are a capacitor of 2200 μF at 5.63 V and LED 1.5 V. The experimental data shows that the charging level of a mobile battery of 2100 mAh can be enhanced from 10-19 % in 35 minutes by consuming only 10% of the total energy of the other smart phone of battery 4000 mAh. Another experimental data shows that the charging level of a mobile battery of 2000 mAh can be enhanced from 14-37 % in 60 minutes by consuming only 20% of the total energy of the other smart phone of battery 4000 mAh. This low cost and simple designed USB On-the-Go (OTG) extension can now replace the necessity of carrying a power bank while travelling, which is expensive as compared to the above proposed technique as well.

Keywords: Mobile to mobile; Charging; On the Go (OTG); Low cost; Cable; Overcharging; Safe

Introduction

The advancement in science and technology has made mobile phones as an essential part in our life. Mobile phones have connected people living across the globe and had become a necessity in this advanced world. Due to the rapid increase functionality of mobile phone, the battery needs to be charged multiple times a day and moreover it cannot meet the increasing power demand [1, 2]. It becomes difficult to charge the battery of our mobile phone while traveling from place to place. Ali *et al.* [3] have proposed a portable mobile phone charger for travelling but it consists of a multidirectional wind turbine which can only be used in motorcycles. Manikandan *et al.* [4] created an energy storage system for mobile phone using super capacitors which can be charged in few seconds. This can be used to replace the batteries in the mobile phone,

*Corresponding author: kkiransharma@gmail.com

but most cell phones and electronic gadgets are powered by batteries [4]. Power banks have also been used as an extendable source of energy for mobile phones [5]. Many workers [6-9] have used renewable energy sources as the source to charge the mobile phone but this technique of charging mobile phones is not successful while travelling. Rewaskar and Datar [10] investigated a method of charging mobile phone with microwaves, but it can only be implemented within the microwave range transmitted from transmitter using antennas at a frequency is 2.45 GHz. Also wireless transmission causes harmful effect on human body and this method is very expensive. Varadarajan [11] used a coin-based technique as battery chargers. However, this technique requires pre-defined values and a suitably designed micro-controller for mobile phone of various configurations. Grid power or a solar energy [11] is used as source for charging mobile phone, which will not be convenient for users during travelling. A combination of wind power, human power and electrical power [12] have been used to charge mobile phone while traveling, but it can only be used with wind turbines for instant charging using a geared DC generator. Cao and Yin [13] introduced a USB protocol On the Go (OTG) chip for protocol transform high speed data transfer with the contradiction of duplicative function of data compression board in the USB transfer. The charging level can be increased by increasing the current in our circuit. For that we are going to use current booster circuit, and we will be able to apply fast charging technique. As we know that the power bank is little bit expensive and needs some space to carry. But the circuit we have made is cheaper as compared to the power bank and can be easily carried around. The power bank needs to be charged first and then to be used, but the circuit we had made can be used instantly. Moreover, we need not to carry around another mobile for this purpose, instead we can ask our neighbors to share their mobile charge which is more economical. While charging one phone from another phone, the current, voltage and charging percentages that show the enhancement are constantly checked.

In a portable device, the enhancement is greater, as the current in power bank is at higher rating. So, for the enhancement of that, we would apply fast charging technique. Various techniques have been proposed [1-13] to charge mobile phones while travelling. Mobiles have to be put to recharge after the batteries drain out. Normally the user carries a power bank; but at times it becomes difficult if the power bank battery also drains out.

Materials and Methods

Circuit Design

The design of this circuit keeps it easy to carry and use it (Figure 1). We have used the On the Go (OTG) extension to take the energy or the power from the other smart phone that we carry along and installed a circuit at the other end in order to make it more efficient and reliable. A-device acts as a USB host with the B-device acting as a USB peripheral. The host and peripheral modes may be exchanged later by using Host Negotiation Protocol (HNP). If an uncharged capacitor C is connected across the terminals of a battery of voltage V , the transient current flows as the capacitor plates charge up. However, the current stops flowing as soon as the charge Q on the positive plate reaches the value $Q=CV$. At this point, the electric field between the plates cancels the effect of the electric field generated by the battery, and there is no further movement of charge. Thus, if a capacitor is placed in a DC circuit then, as soon as its plates have charged up, the capacitor effectively behaves like a break in the circuit.

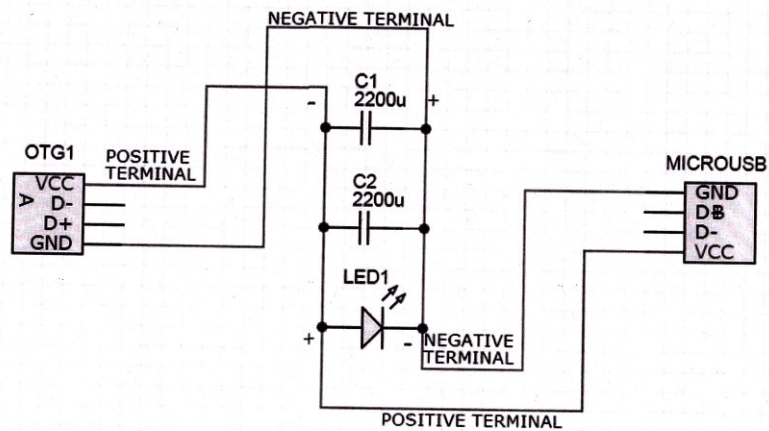


Fig. 1. Circuit design of OTG cable

The OTG cable can be used as the source to charge the mobile phones and also transfer high speed data [13]. This cheap, compact, and miniature circuit can be carried in pocket or bag and is light weight to carry it around. We took the required components and placed them on the printed circuit board (PCB) board as shown in the circuit diagram. Two capacitors of 2200 micro farad are connected in parallel. A since pin is used which is connected to the ground that helps in reverse charge or extract charge from the battery which is transferred to the other cell phone. The OTG cable is used to connect the mobile phone to the circuit having two capacitors connected in parallel. The charge flows through the OTG extension to the capacitors of 220 μ Farad, which are connected in parallel. The capacitors are connected in parallel in order to increase its capacitance to increase the safety of this device. Now once the charge flows through the capacitors it meets an LED of 1.5 V in the circuit, which is connected in parallel to the capacitors and helps determine the status of the circuit at the input end. It will depict whether our circuit is completely error free or it needs some rectifications. Now once the charge flows through the LED it will pass on through the micro USB cable attached at the other end in order to power other devices.

EXPERIMENTAL RESULTS & DISCUSSION

The designed OTG cable is used to charge the mobile phone from another smart phone. A mobile of 4000 mAh has been used to power a Samsung phone of 2100 mAh having 10% battery backup. It has been observed that in 30 min the battery of the phone can be enhanced up to 19% with only a loss of 20% charge of phone used at 5.63 V and 0.48 A. The charging and discharging percentage with time of both phones is represented in Figure 2.

Another set of phones are used. The charging time has been increased to 60 min, and the mobile phone charged is 2000 mAh and has 14% battery backup. The charging and discharging % with time of both the phone used has been shown in Figure 3. The results show that in 60 min the battery of the phone can be enhanced up to 34% with only a loss of 20% charge of phone of 4000 mAh used at 4.97 V and 0.44 A.

The proposed OTG cable has also been used to charge a completely discharged mobile phone of 1050 mAh for 60 min. The experimental results show that a very less battery discharge has been observed from 63% to 57% in a mobile phone of 4100 mAh used at 4.87 V and 0.54A. It has been observed that in 60 min the battery of the phone (Nokia-103) can be enhanced up to 31%. Figure 3 shows the graphical representation of charging and discharging % of both phones used with time. The loss of charge can be calculated by constantly checking of the current, voltage and charging percentages of another phone by using multimeter. The loss of charge is same as we have used the same mobile phone for charging other mobile phones so the loss in percentage is same as compared other.

From Figures 2-3, it is clear that the battery of a mobile can be increased up to 37% in 60 min with negligible loss in charging of the other smart phone used.

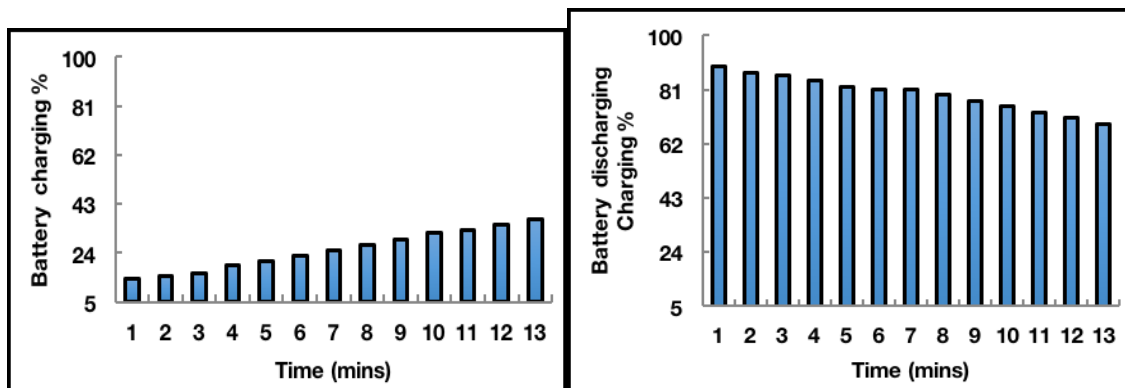


Fig. 2. (a) Battery charging % with respect to time of Samsung Core-2 used at 4.97 V and 0.44A

(b) The battery discharging % with respect to time of the smart phone used to drain charge.

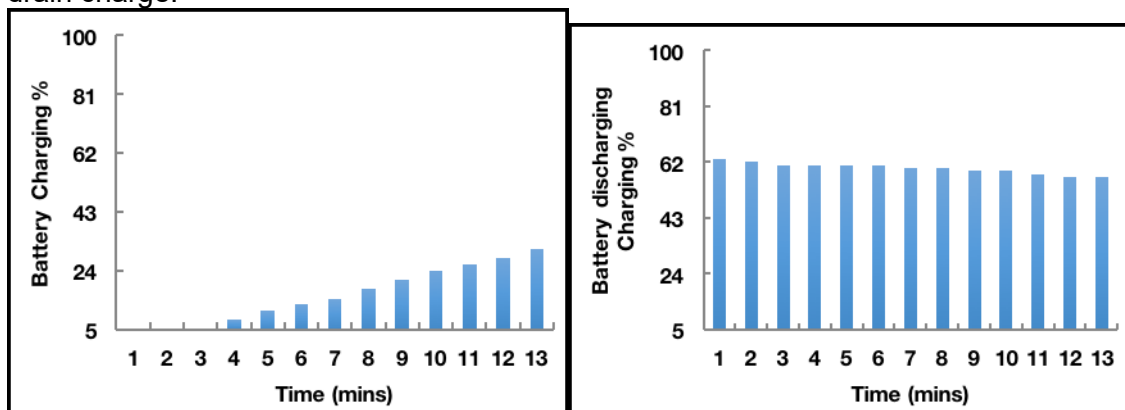


Fig. 3. (a) Battery charging % with respect to time of Nokia-103 used at 4.87 V and 0.54A

(b) The battery discharging % with respect to time of the smart phone used to drain charge.

CONCLUSIONS

In this paper, a low-cost method of charging mobile batteries has been designed for travelers, or people of rural and remote areas where the current supply is not available all the time. Now the necessity of carrying a power bank while travelling is also relaxed. This OTG is very useful in today's life because now days the necessity of communication is very important especially while moving from one place to another. Travelers can easily charge their phones by using this OTG cable simply by borrowing a Smartphone from the other passengers for few minutes. The proposed OTG cable is compact, simply designed and cheap.

CONFLICTS OF INTEREST

The authors declare that there is no conflict of interests regarding the publication of this paper.

REFERENCES

- [1] S.S. Shivakumar, K.N.S. Mohana, "Ziziphus mauritiana leaves extracts as corrosion inhibitor for mild steel in H₂SO₄ and HCl solutions", *European Journal of Chemistry*, 3(4), pp. 426-432, 2012.
- [2] P. Saikumar, D. Thamaraianna, G. Yuvaraj, C. Yuvaraj, "Wind energy based mobile phone battery charging and battery application", *International Journal for Research and Development in Engineering*, pp. 6-11, 2014.
- [3] K. Ali, W. S. W. Mohd, D. Rifai, M.I. Ahmed, A. Muzzakir, and T.A. Asyraf, "Design and Implementation of Portable Mobile Phone Charger Using Multidirectional Wind Turbine Extract", *Indian Journal of Science and Technology*, 9(9), pp. 1-6, 2016. DOI: 10.17485/ijst/2016/v9i9/88711
- [4] J. Manikandan, R.M. Priya, S. Pavithra, D. Sarathkumar, "Rapid Smart Phone Charging Using Super Capacitor", *International Journal of Advanced Research in Electrical, Electronics and instrumentation Engineering*, 4(4), pp. 2175-2180, 2015.
- [5] A. Joshi, "Low Cost, Portable and Extendable Power Bank", *International Journal of Scientific & Engineering Research*, 6(4), pp. 87-89, 2015.
- [6] S.B. Dhal, A. Agarwal, K. Agarwal, "Solar Powered Mobile Power Bank System", *American Journal of Electrical and Electronic Engineering*, 4(5), pp. 148-151, 2016.
- [7] R. Kamble, S. Yerolkar, D. Shirsath, B. Kulkarni, "Solar Mobile Charger", *International Journal of Innovative Research in Computer Science & Technology*, 2(4), 35-39, 2014.
- [8] T. Singh, P. Bhardwaj, B. Singh, A. Kumar, "Design and development of Portable Power Charger: A Green Energy Initiative", *International Journal of Electronics and Communication Technology*, 5(4), pp. 12-15, 2014.
- [9] A.N. Maroma, "Solar Powered Cell Phone Charging Station", *Open Access Library Journal*, 1(e1156), pp. 1-7, 2014.

- [10] P.A. Rewaskar, D. Datar, “Wireless Charging of Mobile Phone Using Microwave”, International Journal of Computer Science and Mobile Computing, 3(4), pp. 427-432, 2014.
- [11] M.S. Varadarajan, “Coin Based Universal Mobile Battery Charger”, IOSR Journal of Engineering, 2(6), pp. 1433-1438, 2012.
- [12] N.R.R. Reddy, Y. Sreekanth, M. Narayana “Mechanical and Electrical mobile charger”, Int. Journal of Engineering Research and Applications, 3(6), pp. 1705-1708, 2013.
- [13] M. Cao, P. Yin, “Research of USB OTG Technology in Image High-Speed Data Transfer”, Advanced Materials Research, 951, pp. 261-264, 2014.

Article copyright: © 2018 Vaibhav Aggarwal, Vaibhav Gupta, Kiran Sharma, and Neetu Sharma. This is an open access article distributed under the terms of the [Creative Commons Attribution 4.0 International License](https://creativecommons.org/licenses/by/4.0/), which permits unrestricted use and distribution provided the original author and source are credited.



Analysis and Design of Solar Power System Interface Utility Using ZVS Converter

R. G. Deshbhratar* and M. M. Renge

Electrical Department, Shri Ramdeobaba College of Engineering and Management, Nagpur, Maharashtra, India

Received January 16, 2018; Accepted March 15, 2018; Published May 9, 2018

The solar power generation system with minimal losses, high simplicity and easy control is attempted in this work, by developing a grid-tied zero-voltage switching (ZVS) inverter with a less number of power conversion stages and the least count of passive components, for single-phase applications that are suitable for conversion from low-voltage DC (40-60 V) to line voltage AC (230 VAC; RMS) at average power levels of 175 W and below. The ZVS full-bridge inverter fed from a PV panel is working on higher frequency with an asymmetric auxiliary circuit, which guarantees ZVS at the switching instants of the metal-oxide-semiconductor field-effect transistors (MOSFETs) by supplying the reactive current to these full-bridge semiconductor switches and reducing the switching losses. Checking of the constructional workability and analytical feasibility of the proposed topology with the highest efficiency and the simplest control was the target of this work, which was set on the basis of the results obtained in the MATLAB Simulink environment. The control strategies were planned for the optimum value of the reactive current injected by the auxiliary circuit to guarantee ZVS and use of phase shifted pulsewidth modulation (PWM) with varying frequencies for the full-bridge inverter and half-bridge cyclo-converter. The hybrid maximum power point tracking (MPPT) was part of this plan used to set the power at its maximum value against the environmental changes.

Keywords: Full-bridge inverter; Asymmetrical auxiliary circuit; Half-wave cycloconverter; Hybrid MPPT; Phase-shift control; Frequency modulation; Zero-voltage switching (ZVS)

I. Introduction

A. Motivation & Background

The solar energy generation is becoming the most promising day by day, as the conventional resources of energy are depleting swiftly and the rooftop grid tied photovoltaic (PV) panel with the inverter are developing with more and more efficiencies. It is necessary to reduce the complication in the design and control of this PV inverter to make it an economical, user friendly and strong alternative to the fossil fuel electricity. The main duty of the inverter is to convert the photovoltaic direct current (DC) power into grid-synchronized alternating current (AC) output. It may be central inverters, mini central inverters, string inverters, multi-string inverters, and microinverters [1, 2], according to the type of inverter topology. Among these inverter topologies, the microinverter is widely used, as it is suitable for integrating a single solar panel (40–400 W) to the grid. The inverter topology has a great role in deciding the cost

of the solar generation unit, which is now a day a main task behind many studies going on in this field [3-8]. The PV microinverter is very much suitable in this area in order to increase the efficiency by reducing the losses and thus reducing the cost.

The inverter topology receives the maximum DC power from the PV array (by imposing an optimal operating condition onto the solar panel through maximum power point tracking (MPPT)) and supplies this power into the grid at the AC line voltage. Operating the inverter at zero-voltage switching (ZVS) decreases the switching losses and provides a noise-free environment for the control circuit. ZVS is usually achieved by providing an inductive current flowing out of the full-bridge legs during the switch turn-on and by placing a snubber capacitor across each switch during the switch turn-off. An easy way to produce this inductive current is inserting an inductor in series or in parallel with the power transformer [1-8]. In this application, the efficiency and the compactness are the main driving design considerations. There is an extensive body of work on DC to AC power converters, specifically for the grid tied PV applications. A thorough overview and a topology classification are provided in some literature [12-14]. Topologies for different power levels and numbers of phases at the output are also presented in the literature [16-18]. In this paper, the topology of an inverter based on the architecture of Fig. 1, comprising a high frequency inverter, a high-frequency transformer, and a cycloconverter is presented. This general architecture is rarely investigated although it has been long known [2]. The improvement in this architecture that reduces device losses compared to other architectures along with flexible control, enabling very high efficiencies are attempted. All devices operate with resistive on-state drops (no diode drops) under ZVS to achieve high efficiency, and encompassing frequency control and inverter and cycloconverter phase shift control [2].

B. Objective

The main objective of this paper is to analyze and validate the topology and working conditions of the full-wave HF inverter with control strategies of phase shifted pulsewidth modulation (PWM) signal generation at automatically controlled frequencies. The power stage design and the simulation results of the proposed topology in MATLAB Simulink environment are discussed for the confirmation of an inverter that is suitable for utility interfacing, operating from low input voltages (40-60 V DC) to high output voltages (230 Vrms AC) at average power levels of 175 W. Operating at unity power factor, the power into the grid (averaged over a switching cycle) is given by Equation (1). The quantity P_{avg} represents the power injected into the grid, ω_l is the line angular frequency and V_p is the peak value of line voltage. This quantity can change (*e.g.*, based on solar panel insolation and shading) over a wide range of over 10 to 1.

$$P_O = \frac{V_p^2 \sin^2 \omega_l t}{R_{eqv}} = 2P_{avg} \sin^2 \omega_l t \quad (1)$$

II. Design

A. Topology

The proposed inverter topology in Fig. 1 shows a parallelly placed buffer capacitor bank (C_{bf}) with the solar panel providing the necessary twice-line-frequency energy buffering. This buffer may comprise the electrolytic capacitor, in parallel with high-frequency decoupling capacitance to carry the resonant current. The size of this

capacitance is given by (2) where, depending on the input voltage ' V_{in} ' and ripple voltage ' v_r ', the voltage ripple ratio on the input ' r ' is reasonably taken as 0.95. Hence, the required capacitance is approximately 7.38 mF (as dictated by the lowest nominal input voltage).

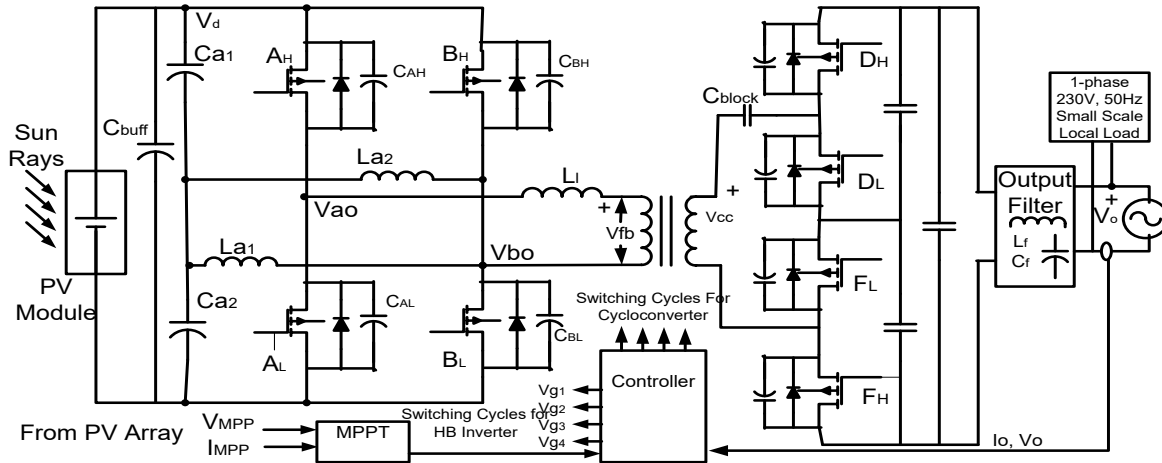


Fig.1. The Proposed Topology

$$r = \frac{V_{in} - v_r}{V_{in} + v_r} \quad (2a)$$

$$C_{bf} \approx \frac{P_{avg}}{2\omega_l V_{in}^2 (1-r)} \quad (2b)$$

A full-bridge inverter, using the reactive current supplied by the auxiliary circuit inductors that are just sufficient to achieve the ZVS at different loadings, is operated under variable-frequency phase-shift control, with the duty ratio controlled by MPPT. The reactive current is controlled by a control policy that regulates the switching frequency according to the varying load. It requires the switching frequency to decrease at low load and vice versa. The metal-oxide-semiconductor field-effect transistors (MOSFETs) A_H and A_L form the 'leading' half-bridge leg and B_H and B_L form the 'lagging' leg of the H-bridge inverter. In each half-bridge structure, the subscripts 'H' and 'L' refer to the high and low side device, respectively. These legs are lagging or leading with respect to the phase shift angle ' θ '. The parasitic capacitance and body diode are obtained across drain and source of each MOSFET [5]. However, to improve the ZVS characteristic of the H-inverter, some capacitance may be added across the switch (in the lagging leg more advantageous). The HF transformer (1:N) provides the galvanic isolation and voltage transformation. The capacitor C_{block} connected to the secondary side of this transformer at high-frequency quasi-sinusoidal voltage and current of V_{fb} and I_x (full-bridge inverter's output voltage and current), respectively. The high-frequency AC current is converted to the line frequency using a half-wave ZVS cycloconverter, yielding unity-power factor output current at line frequency. Also, the capacitor C_{block} placed on the secondary side of the HF transformer, restrict the entry of DC voltage if present in order to avoid the otherwise possible undue saturation of the transformer core. Its value chosen to be adequately large, so that it will not significantly affect the total effective capacitance of the main circuit. Its presence is intended in this design in such a manner that in the absence of any auxiliary circuit components (which are working as the

resonant components) on the secondary, this capacitance is absorbed into the overall capacitance across the cycloconverter. This cycloconverter improved greatly the layout for high frequency currents, providing reduced total device drop than conventional bidirectional-blocking-switch topologies. The operation of the cycloconverter can be outlined as follows. When the line (grid) voltage v_g is positive (with reference to the given polarity), the two switches F_H and F_L at the bottom of the cycloconverter (Fig. 1) remain on, while the two switches D_H and D_L at the top function as a half-bridge and modulate the average current (over a switching cycle) delivered into the AC line. Likewise, when v_g is negative, the two switches at the top remain on, whereas the two switches at the bottom modulate the average current for proper power delivery. A bypass capacitor is paralleled effectively to every pair of 'on' switches of cycloconverter half-bridge in a particular half cycle, resulting in reduced conduction losses, compared to a single switch of the same configuration. Hence, for this particular time, cycloconverter on state conduction loss results from 1.5 device resistances, as compared to two on state resistances of conventional 'back-to-back switch' half-wave cycloconverter [2, 10]. The cycloconverter switching and gating losses are considerably reduced, since one of the two half-bridges modulates at any given time in this topology. This means that the functional connectivity & the overall condensed nature of the layout of this cycloconverter topology are proven to be greatly advantageous over conventional 'back-to-back switch' cycloconverter topologies in the real life. These topological aspects are implemented in the lay-out of Fig. 1, which aims to achieve high efficiency as well as fewer component counts and yielding a small size, although achieving the large voltage transformation and isolation. As the full bridge inverter and half-wave cycloconverter topologies are able to reduce the required transformer turns ratio, they are compared to using a half-bridge inverter plus a full-wave cycloconverter, in order to achieve the improved efficiency. Similarly, the diode drops are eliminated from main operation of the converter, and by operating all of the devices under zero-voltage switching, low loss operation is achieved by scaling device areas up beyond that which is optimum for hard-switched topologies. For the sake of component count reduction and the integrated design, we are able to deploy the leakage and magnetizing inductances of transformer as part of the auxiliary circuit inductor.

B. Maximum Power Point Tracking

Due to the changes in direction of the sun, solar insolation level and ambient temperature, the output power of the PV module changes drastically. The PV characteristics of the PV module also show a single maximum power point for a particular operating condition. It is desired that the PV module operates close to this point, *i.e.*, the maximum output of the PV module is obtained near to the maximum power point (MPP). The process of tracking of this point in the operation of PV module is called as maximum power point tracking (MPPT). Maximization of PV power improves the utilization of the solar PV module [11]. According to the maximum power point theorem, the output power of any circuit can be maximized by adjusting source impedance equal to the load impedance, so the MPPT algorithm is equivalent to the problem of impedance matching. Many MPPT algorithms are in use now a day. The most common algorithms are the perturb and observe (P&O) and the incremental conductance (IC) method [9]. In the present work, the hybrid MPPT combining 'Perturb and Observe' and 'Incremental Conductance' methods is used. The perturb and observe is the simplest method. In this paper, we use only one sensor that is either voltage sensor or current

sensor to sense the PV array voltage or current, so the cost of implementation is less. The two main problems of the P&O are the oscillations around the MPP in steady state conditions, and poor tracking (possibly in the wrong direction, away from MPP) under rapidly-changing irradiances. The IC method has an advantage over the P&O method, because it can determine the MPP without oscillating around this value.

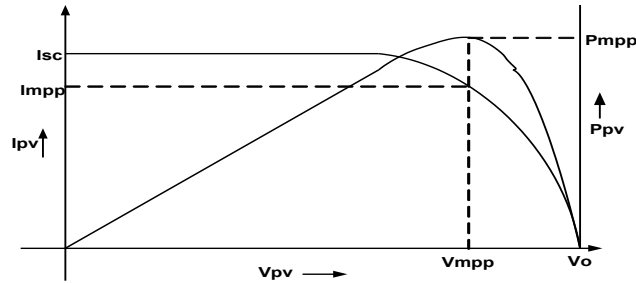


Fig. 2. The I_{pv} vs V_{pv} and P_{pv} vs V_{pv} Characteristic of Solar Panel Showing Maximum Power Point Voltage (V_{mpp}), Current (i_{mpp})

However, the IC method can produce unintentional oscillations and perform tracking erratically in wrong direction under rapidly changing atmospheric conditions and low irradiance. Due to higher complexity, the sampling frequency is reduced as compared to the P&O method. Perturb & Observe method and Incremental Conductance method have various advantages and disadvantages. So, our aim and innovation here were to club advantages of both the method and make the controller more flexible and sustainable to various adverse conditions.

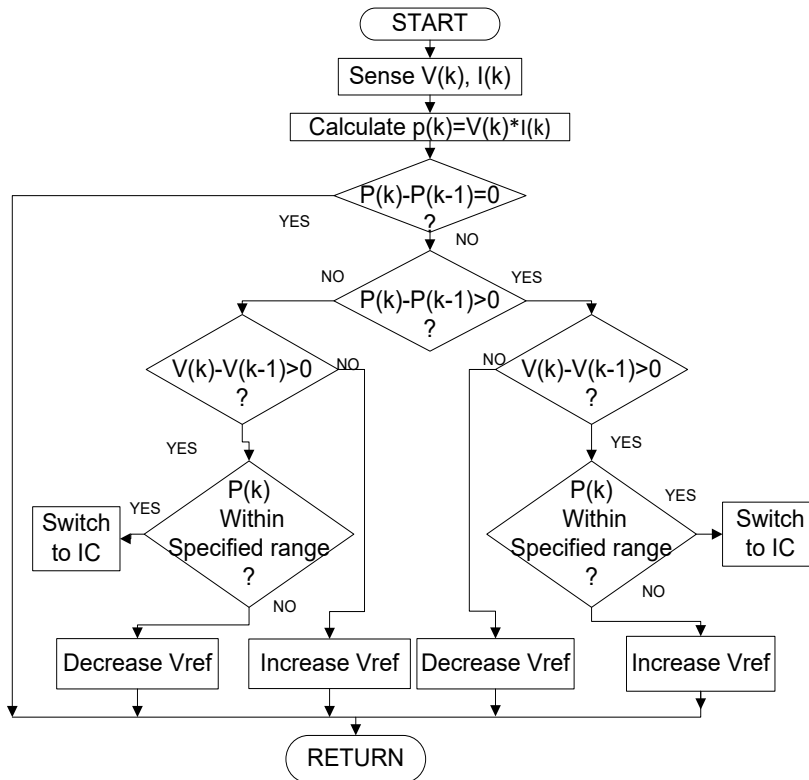


Fig.3. Hybrid Technique *i.e.*, combination of both PO and IC

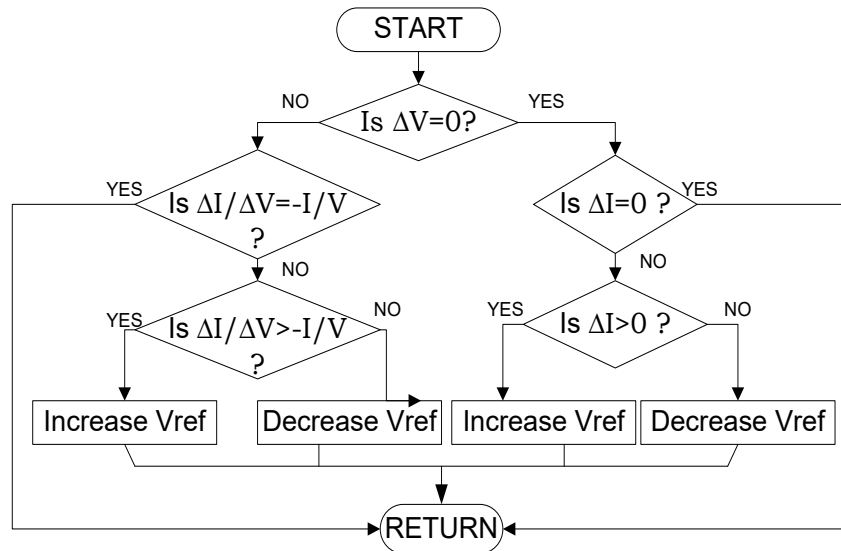


Fig. 4. Flow-chart for Incremental Conductance

The MPPT is tracked using criteria dP/dV (at V_{max} , I_{max}) = 0. A threshold error is normally allowed to make a tradeoff between the convergence speed and the allowable oscillations at the peak point limiting the sensitivity of the tracker. The simulation for MPP tracking is done for a step size of 0.5 V and a threshold acceptable error of 0.002 for an input irradiance of a trapezoidal pattern. The specified range of Pk is $0.95P_{max}$ used for the MPPT change from PO to IC.

Fig. 3 shows the flow chart of this hybrid MPPT, where the main body of flow chart is following the PO method. If the suggested criteria are fulfilled, it switches to the IC method (Fig. 4).

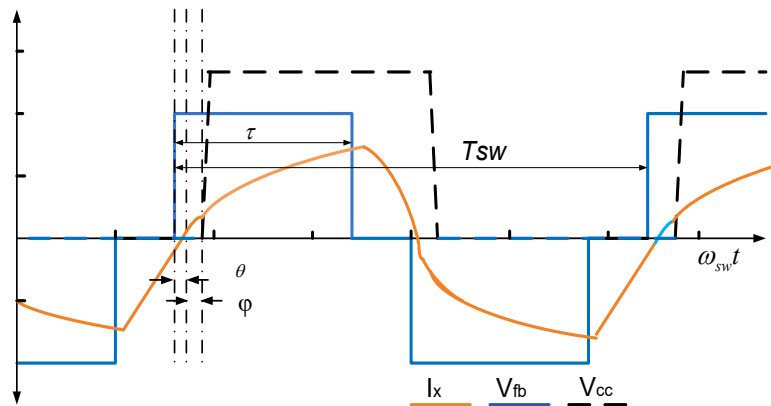


Fig. 5. Ideal waveforms in relationship with ideal angles

C. Idealized waveforms and ZVS

Fig. 5 shows the standard waveforms of interest for this topology, with their nomenclature declared in Fig. 1. For simplicity, the waveforms are dimensionally standardized for the sake of explaining their clear positional relations. So, no clear values are defined on y-axis and attempted to explain relative timing on x-axis. The figure demonstrates the waveforms of v_{fb} , I_x & V_{CC} on the time scale of the switching period ($T_{sw} = 1/f_{sw} = 2\pi/\omega_{sw}$). The instantaneous output voltage can be well approximated as constant, since the switching frequency is much greater than the line frequency during each

switching period. As the practical consequence of the control strategy, this is helpful to prove the proper transfer of power to the grid at any instant. The cycloconverter input voltage ' v_{cc} ' is a square wave with the minimum value of 0 and the maximum value of V_{out} (max of instantaneous v_{out}). The angular difference φ is the angle (normalized to the switching period) by which the zero-crossing of current I_x leads to the rise of ' v_{cc} '. The ' V_{fb} ' is a three-level stepped voltage waveform of the full-bridge inverter (as explained in Fig. 6). The three voltages of this waveform with respect to these three levels are $+v_{fb}$, 0 and $-v_{fb}$. This waveform leads to the zero crossing of the current I_x by angle θ . It should be very clear that the switching frequency of the converters is well above the resonant frequency of the equivalent circuit, and the equivalent impedance of this circuit seen by the full-bridge is inductive with positive angle θ . These optimal values are decided on the basis of iterative simulation results of peak current and input and output voltages, we call them θ_{main} and φ_{main} as the angles equivalent to the instant of time necessary to fully discharge the drain to source capacitance of the full-bridge inverter and the cycloconverter switches, respectively. Operating the inverter at $\theta \geq \theta_{main}$ and $\varphi \geq \varphi_{main}$ was the tentative adjustment for the better results. Operation of the inverter at $\theta \geq \theta_{main}$ and $\varphi \geq \varphi_{main}$ scrupulously implements ZVS on all eight MOSFETs, practically eliminating switching losses to the greater extent [9].

D. Power Transfer Strategy

The equation (3) shows the average power over a switching cycle. Here I_{x1} represents the fundamental (switching) frequency component of the inverter current for the expansion of the integral with Fourier series coefficient notation. The fundamental frequency component of current and the variable angle φ are related with the power transfer with the final approximation. The switching harmonics are neglected here. Since they account for less than 10% of total power transfer for the quality factors that are used here, ignoring harmonics is valid for qualitative purpose [2, 19].

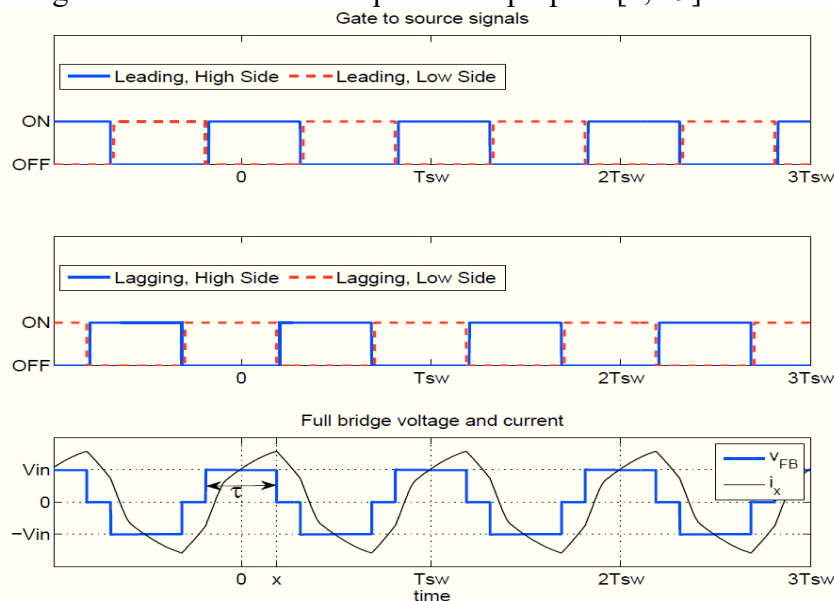


Fig. 6. Full-bridge timing and output voltage V_{fb} . The top two sub figures show the switching signals of the leading and lagging legs. Drain to source voltages (which can be deduced from the gating signals) combine to produce the waveform shown on the bottom figure. Here, τ is the overall 'width' of the positive and negative voltage pulses of V_{fb} .

$$P_{out} = \frac{1}{2\pi} \int_0^{2\pi} i_x(\tau) d\tau \quad (3a)$$

$$= \sum_n \frac{1}{n} \|V_{cc,n} I_{x,n}\| \cos(\angle V_{cc,n} - \angle I_{x,n}) \quad (3b)$$

Finally,

$$P_{out} \approx \frac{1}{\pi} i_{x,1} V_{out} \cos\varphi \quad (3c)$$

Following are the three ways used in combination, to implement the control strategies here to control the delivery of the quantity of power to the grid.

1. *Switching Frequency Control,*
2. *Inverter Phase Shift Control,*
3. *Cycloconverter phase Shift Control.*

In the present case, the H-bridge inverter connects two legs (leading leg and lagging leg) with the mid-points 'a' and 'b' bearing voltages ' V_{ao} ' and ' V_{bo} ', respectively, resulting in the inverter output voltage between a and b of V_{fb} ($V_{ao} - V_{bo}$). The inverter (Full-Bridge) phase shift takes the fundamental component of this V_{fb} as the phase reference for all waveforms of Fig. 5. The Fourier series coefficients of V_{fb} are given by Eq. (4), where $\delta = 2\tau/T$ (shown in Fig. 6). The phase of each component is therefore either 0 or π radians. Each leg of the full-bridge operates at 50% duty ratio. Changing phase shift of the full-bridge can be defined as changing the amount of time between the rise of the voltages of high sides of leading and lagging legs. This directly corresponds to changing τ , the overall 'width' of the positive and negative voltage pulses of V_{fb} , while also affecting θ (however, that relationship also depends on the frequency). According to Eq. (4), changing phase shift changes the magnitude of each harmonic component of the voltage, which in turn changes the current and the overall power transfer.

$$\begin{aligned} V_{fbn} &= 0 \text{ for } n = 2, 4, 6, \dots \\ &= \frac{4V_{in}}{n\pi} \sin \frac{n\delta\pi}{2} \text{ for } n = 1, 3, 5, \dots \end{aligned} \quad (4)$$

Using the cycloconverter phase shift changing technique, with a given current amplitude of the fundamental component and output voltage (Eq. 3c), it's evident that, the effect of increasing the cycloconverter phase shift φ is decreasing the instantaneous output power. For a given output power, operating at larger phase angle φ will result in a larger peak (and *rms*) resonant current.

And using the switching frequency control, the magnitude of the reactive current supplied by the auxiliary circuit inductors is controlled. This current supplied to the FB inverter switches should not be of high value, as it may lead to the high voltage spikes on the semiconductor switches due to the delay in the body diode turn-on. The work of the auxiliary circuit is totally independent, does not depend on the system operating conditions and is able to guarantee ZVS from no load to full load. Since the auxiliary circuit should provide enough reactive power to guarantee ZVS at all operating conditions, the peak value of the current flowing through the auxiliary inductor is regulated, which controls the MOSFET conduction losses essentially [5, 6].

Thus, these three techniques are used here simultaneously to regulate the power delivery to the grid as given by equation (3) and make it more efficient as per the requirement. And for achieving the high efficiency control, it is necessary to minimize

the total loss by satisfying the appropriate ZVS constraints. The maximum amount of power that the inverter can deliver (ignoring ZVS requirements) occurs, when it is operated at $\delta = 1$ and $\varphi = 0$. Decreasing the power delivery can be done by increasing f_{sw} or φ , or by decreasing δ [1]. An operating point determines the minimum required inverter current and the corresponding minimum cycloconverter phase shift $\varphi = \varphi_{main}$. Any extra cycloconverter phase shift will result in extra loss as a consequence of higher current [12]. The nominal control strategy that minimizes losses appears to operate at the lowest possible cycloconverter phase shift φ , as this results in the lowest *rms* current, while also switching at the lowest allowed frequency and consequently the narrowest pulse width τ on the full-bridge. Essentially the combination of frequency and phase shift modulation is more favorable in terms of loss than cycloconverter modulation, with the preference of lower frequency.

E: Auxiliary Circuit Components

The auxiliary inductor works as a constant reactive current source since the circuit current remains constant during the deadtime. This current discharges the capacitor across A_H and charges the capacitor across A_L . The value of this constant current source is derived as:

$$I_{AUX} = \frac{V_{in}}{8f_{sw} \cdot L_{aux}} \quad (5)$$

Therefore, the MOSFET capacitor voltage due to this constant current source is derived as,

$$V_{AH,aux}(t) = V_{in} - \frac{V_{in}}{8f_{sw} \cdot L_{aux}} (t - t_{\alpha}) \quad (6)$$

Here, V_{in} is the solar panel voltage, L_{aux} is the supplementary inductance, t_{α} is the starting instant of dead-time t_d between A_H & A_L and f_{sw} is the switching frequency. The inductor value is designed to provide enough current to make the voltage V_z (the value of V_a at the end of the dead-time) zero. Hence, the inductor is designed as,

$$I_{AUX1} = \frac{V_{in} \cdot t_d}{16f_{sw} \cdot C_{AH}(V_{in} + V_z)} \quad (7)$$

The lagging leg supplementary inductor, ' L_{aux2} ' could be designed by calculating the energy required to discharge the snubber capacitor C_{BH} . It is clear from the waveforms of Fig. 7(b) that, the primary current of the lagging leg is always a positive value, at the most it can be zero. The energy of discharging and charging the snubber capacitors is given by,

$$W_{Cs} = C_{BH} \cdot V_{in}^2 \quad (8)$$

The energy stored in the leakage and supplementary inductances and the peak current of the supplementary inductor are given by,

$$W_L = \frac{1}{2} \cdot L_{leak} \cdot I_p^2 + \frac{1}{2} \cdot L_{aux2} \cdot I_{aux2}^2 \quad (9)$$

Here I_p is the peak current of transformer primary. The peak current passing through the supplementary inductor is,

$$I_{aux} = \frac{V_{in}}{8f_{sw} \cdot L_{aux}} \quad (10)$$

In the worst case, I_p is equal to zero. Therefore, the lagging leg auxiliary inductance is derived as,

$$L_{aux2} = \frac{1}{128 \cdot C_{BH} \cdot f_{sw}^2} \quad (10a)$$

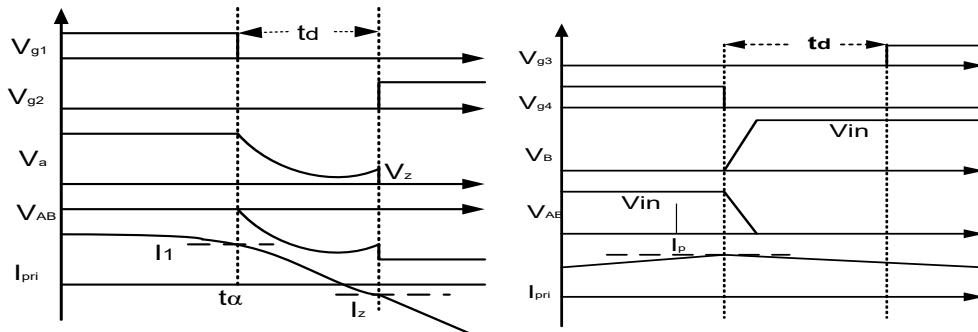


Fig. 7 (a). Key Waveforms of Leading Leg **Fig. 7(b).** Key Waveforms of Lagging Leg

Also, depending on the load conditions, the inductive current of the auxiliary inductor should be controlled, because excessive inductive current may overcharge the snubber capacitors due to the delayed body diode turn-on and result in an objectionable voltage spike on the MOSFETs. Therefore, a proper control approach is suggested to adaptively control the peak value of the auxiliary circuit current based on the load variations.

Table 1. Circuit Components & Their Values

| Component | It's Value | Component | It's Value |
|------------------------|-------------|-------------------------------|--------------|
| Input Voltage | 40-50 V | Cbf | 500 μ F |
| Output Voltage | 230 Vrms | Cblock | 1000 μ F |
| Output Power | 175 W | Lfilter | 0.1 μ FH |
| auxiliary Inductor -1 | 200 μ H | Cfilter | 4.0 μ F |
| auxiliary Inductor -2 | 100 μ H | Switching Frequency, f_{sw} | 55-350 kHz |
| Transformer Turn ratio | 1 : 7.66 | | |

The proposed closed-loop control system is shown in Fig. 8. The proposed control system consists of an internal current loop and an external voltage loop (Table 1). The frequency control loop regulates the frequency for the modulation depending upon the variations in loads as shown in Fig. 9. The peak value of the reactive current through the auxiliary circuit is controlled by the switching frequency, which is able to minimize the converter losses. At light loads, the switching frequency is lower to provide enough inductive current to ensure ZVS, and at higher loads, the switching frequency is higher to avoid too much reactive current and reduce the semiconductor conduction losses.

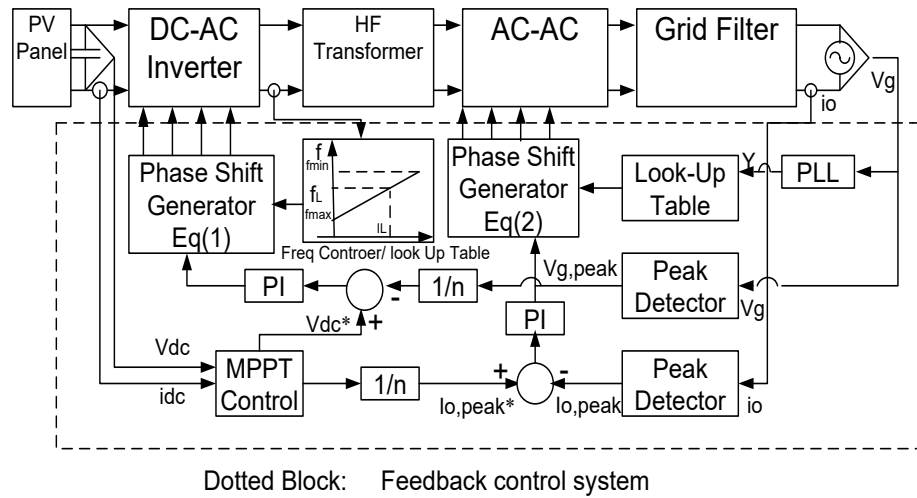


Fig. 8. Proposed Closed-Loop Control System

Fig. 10 shows how the frequency loop works. At light loads, the frequency is lower. Therefore, the voltage across the auxiliary inductor remains for a longer time, and the inductive current at the start of the switching transition is a larger value. For heavy loads, the frequency is higher, which decreases the peak value of the inductive current. The frequency control block is modeled by,

$$g(IL, t) = \mu \cdot IL(t) + f_{min} \quad (11)$$

$$f_{max} = \frac{V_{in} \cdot t_d}{16L_{aux1} \cdot C_{s1} \cdot (V_{in} + V_{Z,min})} \quad (12)$$

$$f_{min} = \frac{V_{in} \cdot t_d}{16L_{aux1} \cdot C_{s1} \cdot (V_{in} + V_{Z,max})} \quad (13)$$

$$\mu = \frac{f_{max} - f_{min}}{I_{L,max}} \quad (14)$$

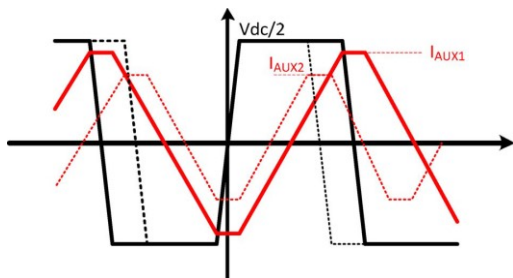


Fig. 9. Voltage and Current Waveform of Auxiliary Circuit Current (Output Current, I_o)

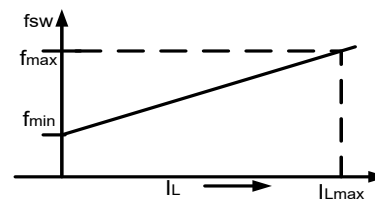


Fig.10. Frequency Control with Load

III. MATLAB SIMULATION MODEL

The micro-converter with the proposed topology along with the control strategy was simulated in the MATLAB Simulink environment. For the PV panel with PV cells, MPPT block was modeled using Simulink and SIM Power systems tool box in MATLAB.

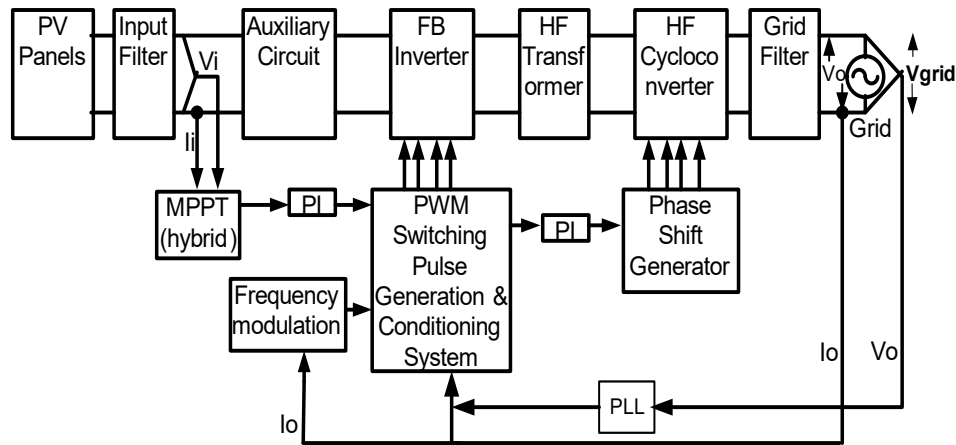


Fig. 11. MATLAB Simulation Block Diagram

The simulation with the Simulink model as shown in the Fig. 11 was carried iteratively for a large number of times with changing the controlling parameters, the frequency (f_{sw}), the FB Inverter phase shift angle (θ) and the cycloconverter phase shift angle (φ). The frequency control was implemented with the help of the PWM switching pulse generation and pulse conditioning system by changing the loading conditions, as it was explained in section II: *D, Power Transfer Strategy*. The FB Inverter phase shift angle (θ) and the cycloconverter phase shift angle (φ) control were implemented independently by assuming one of them constant while another is varying. For all the times the output power with Eq. (1) and the input power (DC power of solar panel) were measured and the efficiency was found (Table 2).

Table 2. Solar Module Parameters

| Parameters | Values |
|---------------------------------------|---------------|
| No. of Cells in Series, N_s | 46 |
| No. of Cells in Parallel, N_p | 02 |
| Open Circuit Voltage, V_o | 44.2V |
| Short Circuit Current, I_{sc} | 4.96 A |
| Series Resistance | 1 Ω |
| Shunt Resistance | 1000 Ω |
| Reverse Saturation Current | 1.1753e-8 A |
| Ideality Factor | 1.3 |
| Voltage at Max Power Point, V_{mpp} | 41.25 V |
| Current at Max Power Point, i_{mpp} | 4.242 A |
| Power at Max Power Point, P_{mpp} | 175 W |

IV. Results

The converter with the proposed topology was modeled using MATLAB Simulink and the control policy was implemented in the direction to minimize the losses of all the switches as well as all other components of the circuit. The iterative simulation

results were sequenced to study the orientation of the proposed set-up and identify the conditions for the satisfactory performance. The efficiency and the losses were studied for all these iterative results. The achievable efficiency, 98.73% found as a result of ZVS operated H-bridge inverter, is well above the inverter topologies used and reported in some papers [23, 24, 26, 27]. This is possible only due to the fact that, the reactive current is controlled and made sufficient for the loss-less switching of all the switches used in this topology. The different waveforms were plotted along with their angular relationship. It was found that, for the implementation of the ZVS to all the switches, the inverter current I_x should be lagging to the Inverter Voltage V_{fb} by optimal angle θ_{main} and leading to V_{cc} by the optimal angle ϕ_{main} . Fig. 12 shows this relationship. It also shows the maximum values of these quantities. Fig. 13 shows them in a Simplot mode of the GUI facility of Simulink. The use of Hybrid MPPT technique was useful to obtain the smooth and fast settling of the maximum power point which otherwise was very oscillating and sluggish using P&O MPPT as shown in Fig. 17. Hence the time of reaching the P_{max} point was reduced and thus power output and efficiency was increased as shown in Table 3.

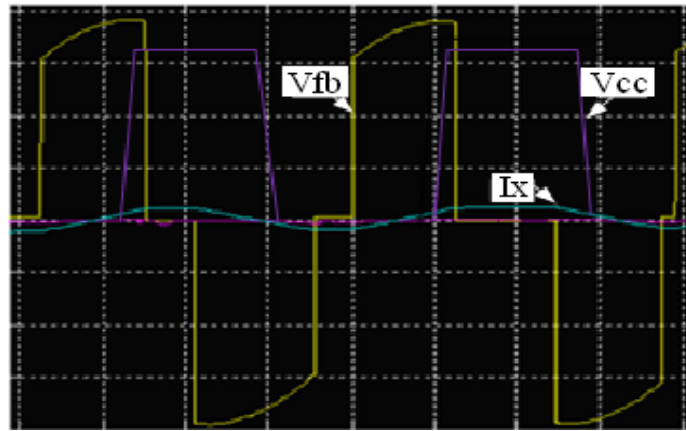


Fig. 12. MATLAB Simulation waveforms taken with the Simulink Model. V_{fb} : 38.6 V, $V_{cc,max}$ =335.09 V, Net efficiency: 98.73%. Switching frequency: 91.41 kHz, Inverter current: $I_{x,max}$ =3.59A, 5.66 A peak to peak.

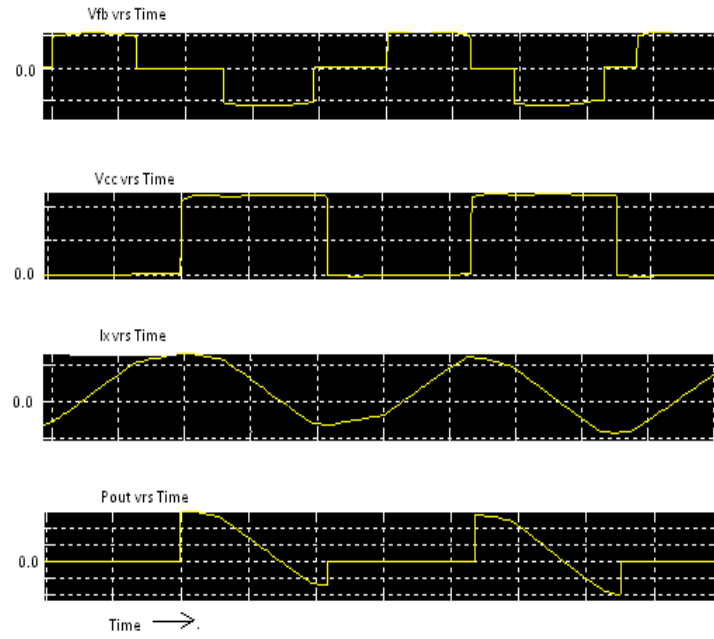


Fig.13. The Simulation resulted Waveforms: V_{fb} , V_{cc} (when V_g is positive half cycle), I_x , and P_o . It is the expanded version for explanation of their inter-relationship.

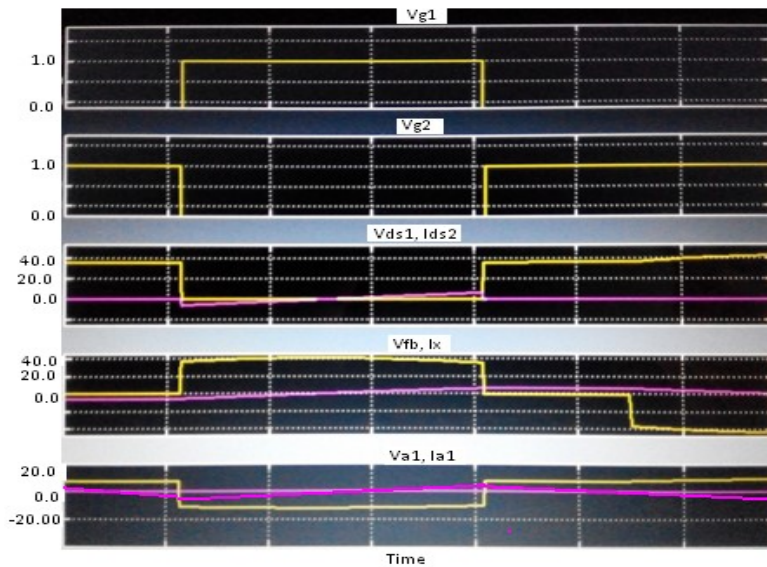


Fig.14. The Photograph of the Simulation Resulted Waveforms 1. V_{g1} , 2. V_{g2} ; 3. V_{ds1} & I_{ds1} ; 4. V_{fb} & I_x ; 5. V_{a1} & I_{a1} .

In the same way, Fig. 14 shows the variation of the % efficiency with the angle ϕ , $f_{sw}=94.41$ kHz, $\theta=22.35$ and full load. Fig. 14 shows the switching waveforms V_{g1} & V_{g2} , voltage V_{ds1} & current I_{ds1} of the MOSFET no.1, the inverter voltage V_{fb} & current I_x and the voltage across & current through the auxiliary inductor L_{a1} .

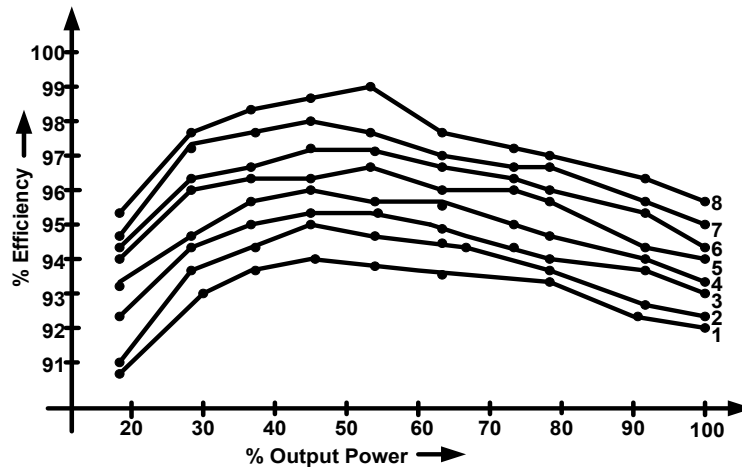


Fig. 15. The variations of % efficiency with respect to the % output power (The rated power of solar panel, 175 W assumed 100%), when the FB Inverter's phase shift angle θ (in degrees) takes values, 1: 106.06; 2: 91.35; 3: 80.15; 4: 63.40; 5: 45.75; 6: 36.15; 7: 16.6 (decreased by exceedingly greater degree than that for sr.no.8); 8: 22.35. Here $\phi = 12.55$ degrees with switching frequency of 94.41 kHz at full load.

ZVS of the cycloconverter depends on the switching sequence of the power switches, as it was explained in the section II Design: Topology. For studying the control, full-bridge phase shift θ is varied from its minimum to maximum value and cycloconverter phase shift ϕ is also varied from its minimum to maximum value at each step of θ . These variations are shown in the Figures 15 and 16, respectively. The changes in the FB inverter phase shift angle θ were implemented in the simulation with respect to the phase shift time and accordingly the results were obtained iteratively along with the % output power. The rated power of solar panel - 175 W was assumed 100%. The cycloconverter phase shift angle $\phi = 13.55$ degrees and switching frequency of 94.41 kHz were measured. The different angles, ' θ ' were taken starting from 126.15 to 16.6 degrees and it was found that highest efficiency achievable is at $\theta = 22.35$ degrees.

Table 3. The efficiency of the converter under different conditions

| Load | Efficiency with PO (%) | Efficiency with IC (%) | Efficiency with Hybrid (%) |
|------|------------------------|------------------------|----------------------------|
| 30% | 76.23 | 77.06 | 88.69 |
| 50% | 80.12 | 85.52 | 90.12 |
| 100% | 91.03 | 91.35 | 98.73 |

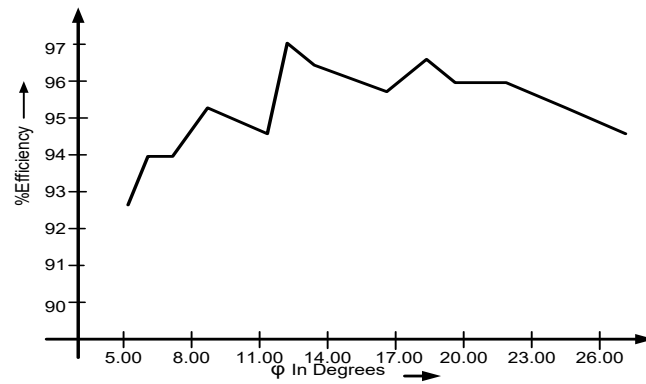


Fig. 16. The variations in efficiency for changes in Cycloconverter phase shift ' ϕ ', with $f_{sw}=94.41$ kHz, $\theta=22.35$ and full Load

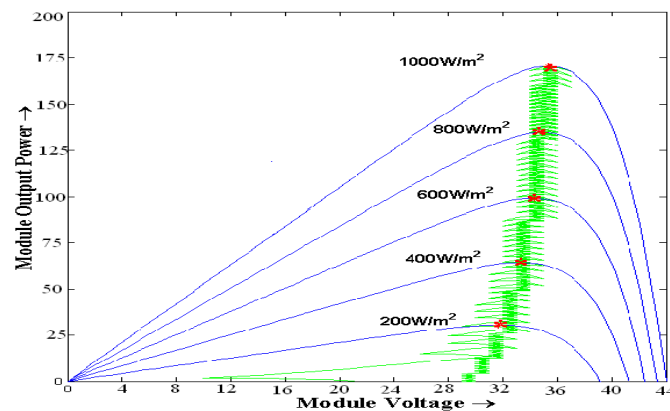


Fig. 17. Tracking of P&O MPPT method.

V. CONCLUSION

This paper introduces a microinverter for single-phase PV applications, which is suitable for conversion from low-voltage (35-50 V) DC to high voltage AC (*e.g.*, 230 V_{rms} AC). The topology is based on a full-bridge inverter with auxiliary circuit, a high-frequency transformer, and a novel half-wave cycloconverter. The losses are minimized to a large extent by the application of ZVS for the switches of the inverter and the cycloconverter. For this, the reactive current given by the auxiliary inductor is controlled to an optimum level by using the frequency modulation. The hybrid MPPT helped in fast control and increased efficiency. With the help of the MATLAB simulation, the operational characteristics are analyzed, and a multi-dimensional control technique is utilized to achieve high efficiency, applying the frequency control, inverter phase shift control and cycloconverter phase control, which suggests the highest achievable efficiency of 98.73%.

CONFLICTS OF INTEREST

The authors declare that there is no conflict of interests regarding the publication of this paper.

REFERENCES

- [1] D.R. Nayanisiri, D.M. Vilathgamuwa, D.L. Maskell, "Half-Wave Cycloconverter-Based Photovoltaic Microinverter Topology with Phase-Shift Power Modulation," *IEEE Transactions on Power Electronics*, vol. 28, no. 6, pp. 2700-2710, June 2013.
- [2] A. Trubitsyn, B.J. Pierquet, A.K. Hayman, G.E. Gamache, C.R. Sullivan, D.J. Perreault, "High-Efficiency Inverter for Photovoltaic Applications", *2010 IEEE Energy Conversion Congress and Exposition*, pp. 2803-2810, Sept. 2010. DOI: 10.1109/ECCE.2010.5618163
- [3] M. Pahlevaninezhad, J. Drobnik, P.K. Jain, A. Bakhshai, "A Load Adaptive Control Approach for a Zero-Voltage-Switching DC/DC Converter Used for Electric Vehicles," *IEEE Transactions on Industrial Electronics*, vol. 59, no. 2, pp. 920-933, February 2012.
- [4] P.K. Jain, W. Kang, H. Soin, Y. Xi, "Analysis and Design Considerations of a Load and Line Independent Zero Voltage Switching Full Bridge DC/DC Converter Topology," *IEEE Transactions on Power Electronics*, vol. 17, no. 5, pp. 649-657, September 2002.
- [5] F.Z. Peng, G.J. Su, L.M. Tolbert, "A Passive Soft-Switching Snubber for PWM Inverters," *IEEE Transactions on Power Electronics*, vol. 19, no. 2, pp. 363-370, March 2004.
- [6] Gwan-Bon Koo, Gun-Woo Moon, Myung-Joong Youn, "Analysis and Design of Phase Shift Full Bridge Converter with Series-Connected Two Transformers," *IEEE Transactions on Power Electronics*, vol. 19, no. 2, pp. 411- 419, March 2004.
- [7] A. Zahedi, "Solar photovoltaic (PV) energy; latest developments in the building integrated and hybrid PV systems," *Renew. Energy*, vol. 31, no. 5, pp. 711–718, Apr. 2006.
- [8] L. Zhang, K. Sun, Y. Xing, L. Feng, H. Ge, "A modular grid-connected photovoltaic generation system based on DC bus," *IEEE Trans. Power Electron.*, vol. 26, no. 2, pp. 523–531, Feb. 2011.
- [9] R. Teodorescu, M. Liserre, P. Rodr'iguez, "Grid Converters for Photovoltaic and Wind Power Systems", New York: Wiley, 2010.
- [10] H. Krishnaswami, "Photovoltaic microinverter using single-stage isolated high-frequency link series resonant topology," in *Proc. IEEE Energy Convers. Congr. Expo.*, vol. 1, no. 1, pp. 495–500, Sep. 2011.
- [11] A. Trubitsyn, B. Pierquet, A. Hayman, G. Gamache, C. Sullivan, D. Perreault, "High-efficiency inverter for photovoltaic applications," in *Proc. IEEE Energy Convers. Congr. Expo.*, vol. 1, pp. 2803–2810, Sep. 2010.
- [12] H. Patel, V. Agarwal, "A single-stage single-phase transformer-less doubly grounded grid-connected PV interface," *IEEE Trans. Energy Convers.*, vol. 24, no. 1, pp. 93–101, Mar. 2009.
- [13] T. Shimizu, K. Wada, "Flyback-type single-phase utility interactive inverter with power pulsation decoupling on the dc input for an ac photovoltaic module system," *IEEE Trans. Power Electron.*, vol. 21, no. 5, pp. 1264–1272, Sep. 2006.
- [14] F. Blaabjerg, Z. Chen, "Power electronics as efficient interface in dispersed power generation systems," *IEEE Trans. Power Electron.*, vol. 19, no. 5, pp. 1184–1194, Sep. 2004.

- [15] D. Cao, S. Jiang, X. Yu, "Low-cost semi-z-source inverter for single phase," *IEEE Trans. Power Electron.*, vol. 26, no. 12, pp. 3514–3523, Dec. 2011.
- [16] W. Yu, J. S. Lai, H. Qian, C. Hutchens, "High-efficiency MOSFET inverter with H6-type configuration for photovoltaic nonisolated AC-module applications," *IEEE Trans. Power Electron.*, vol. 26, no. 4, pp. 1253–1260, Apr. 2011.
- [17] K. Chomsuwan, P. Prisuwan, "Photovoltaic grid-connected inverter using two-switch buck-boost converter," in *Proc. IEEE Photovoltaic Spec. Conf.*, pp. 1527–1530, May 2002. DOI: 10.1109/PVSC.2002.1190902
- [18] B. Yang, W. Li, Y. Gu, W. Cui, X. He, "Improved transformerless inverter with common-mode leakage current elimination for a photovoltaic grid-connected power system," *IEEE Trans. Power Electron.*, vol. 27, no. 2, pp. 752–762, Feb. 2012.
- [19] S. Funabiki, T. Tanaka, "A new buck-boost-operation-based sinusoidal inverter circuit," in *Proc. IEEE Power Electron. Spec. Conf.*, vol. 4, pp. 1624–1629, 2002.
- [20] S.Y. Tseng, H.-Y. Wang, "A photovoltaic power system using a high step-up converter for DC load applications," *Energies*, vol.6, pp. 1068–1100, 2013.
- [21] L. Chen, A. Amirahmadi, Q. Zhang, N. Kutkut, I. Batarseh, "Design and Implementation of Three-Phase Two-Stage Grid-Connected Module Integrated Converter", *IEEE Transactions on Power Electronics*, vol. 29, no. 8, pp. 3881 – 3892, August 2014.
- [22] A. Mudassar, Y. Xu, H. Liu, L. Hang, G. Li, H. Hu, "Two-Stage Single-Phase Photovoltaic Grid-Tied Micro-Inverter Using Soft-Switching Techniques" *IEEE 2nd Annual Southern Power Electronics Conference (SPEC)*, pp. 1 - 6, 2016. DOI: 10.1109/SPEC.2016.7846048
- [23] Y. Zhang, J. Umuhoza, H. Liu, C. Farrell, H.A. Mantooh, "Optimizing efficiency and performance for single-phase photovoltaic inverter with dual-half bridge converter" *2015 IEEE Applied Power Electronics Conference and Exposition (APEC)*, pp. 1507-1511, 2015. DOI: 10.1109/APEC.2015.7104547
- [24] W.J. Cha, Y.W. Cho, J.M. Kwon, B.H. Kwon, "Highly Efficient Microinverter With Soft-Switching Step-Up Converter and Single-Switch-Modulation Inverter", *IEEE Transactions on Industrial Electronics*, vol. 62, no. 6, pp. 3516 – 3523, 2015.
- [25] Y. Chen; D. Xu, "Control of ZVS single-phase grid inverter with higher power quality", *2017 IEEE 18th Workshop on Control and Modeling for Power Electronics (COMPEL)*, pp. 1-8, 2017. DOI: 10.1109/COMPEL.2017.8013390
- [26] M. Tofighazary, M. Sabahi, E. Babaei, F.A.A. Meinagh, "Modified Single-Phase Single-Stage Grid-tied Flying Inductor Inverter with MPPT and Suppressed Leakage Current", *IEEE Transactions on Industrial Electronics*, vol. 65, no. 1, pp. 221 - 231, 2018. DOI: 10.1109/TIE.2017.2719610
- [27] M.I. Munir, T. Aldhanhani, K.H.A. Hosani, "Control of Grid Connected PV Array Using P&O MPPT Algorithm", *2017 Ninth Annual IEEE Green Technologies Conference (GreenTech)*, pp. 52-58, 2017. DOI: 10.1109/GreenTech.2017.14
- [28] A. Anzalchi, M. Moghaddami, A. Moghadasi, M.M. Pour, A. Sarwat, "Design and Analysis of a Higher Order Power Filter for Grid-Connected Renewable Energy Systems", *IEEE Transactions on Industry Applications*, vol. 53, no. 5, pp. 4149 - 4161, 2017

Article copyright: © 2018 R.G. Deshbhratar and M.M. Renge This is an open access article distributed under the terms of the [Creative Commons Attribution 4.0 International License](https://creativecommons.org/licenses/by/4.0/), which permits unrestricted use and distribution provided the original author and source are credited.



Design and Implementation of Analog Controller Based Single Phase Full Bridge Inverter for Photovoltaic Applications

Abhishek Ranjan*, Sunil Jalutharia, Harsh Garg, and Nitin Gupta

Department of Electrical Engineering, Malaviya National Institute of Technology Jaipur-302017, India

Received April 27, 2018; Accepted May 7, 2018; Published May 11, 2018

This paper presents a low-cost design of the analog controller for the photovoltaic driven single-phase inverter to generate desired output voltage. The hardware set-up mainly consists of an inverter and an analog controller. The developed controller controls the output voltage of the inverter using SPWM (Sinusoidal Pulse Width Modulation) technique. The inverter, which is designed using Metal-Oxide-Semiconductor Field Effect Transistor (MOSFET) as a switch, generates high-quality output with reduced ripple content and less filtering requirement, making the whole setup cost-effective and efficient. A gate driver circuit is also employed to provide isolation between the inverter and the analog controller. The closed loop analog controller for the photovoltaic driven inverter is implemented and tested for various loads. In all these cases, the output voltage waveforms are of high quality with a lesser number of lower order harmonics. In this way, the paper presents a low-cost design of the inverter that can be used for low-power domestic applications.

Keywords: Analog Controller; H-Bridge Inverter; Sinusoidal Pulse Width Modulation (SPWM); Metal-Oxide-Semiconductor Field Effect Transistor (MOSFET); Gate Driver

Introduction

Many parts of the world are still in darkness with no sources of power. The researchers and scholars are working hard on non-conventional renewable sources of energy to provide an energy source in those regions. As these are environmentally friendly and clean energy sources, it has become an area of interest to the whole world. New and improved technologies are being introduced every day in this field. One of the most common sources of energy is solar energy, which is proven to be the most challenging one.

To extract solar energy, the photovoltaic (PV) array is used. It is based on the technology that converts solar energy to electrical energy. The use of PV array is not favored much because of the high cost of the installation. In spite of the high cost of installation, the use of PV array is increasing in most parts of the world to pump water, to get hot water in winters and even for lightening purposes [1]. So, the main focus is to make its implementation cost effective in houses, colleges, hospitals, rural areas, public places and even in small scale industries. An analog circuit for generating sine pulse width modulation (SPWM) along with a single phase full bridge inverter is capable of converting the DC output of the PV array to AC. SPWM is a very effective technique

*Corresponding author: ranjanabhishek12345@gmail.com

used widely in power electronics applications such as motor driver, UPS and the renewable energy system [2, 3]. The controller helps maintain the power output as the radiation varies during the day. This AC output power can be used to run the various resistive and inductive loads. The analog controller has a proportional integrator (PI) controller that helps stabilize the output voltage at the motor. Even if the output voltage of the PV array fluctuates, the motor runs at a constant speed [4, 5]. A complete experimental setup has been built to demonstrate the utility of this project.

Proposed Scheme

The schematic diagram of the proposed scheme is shown in Figure 1.

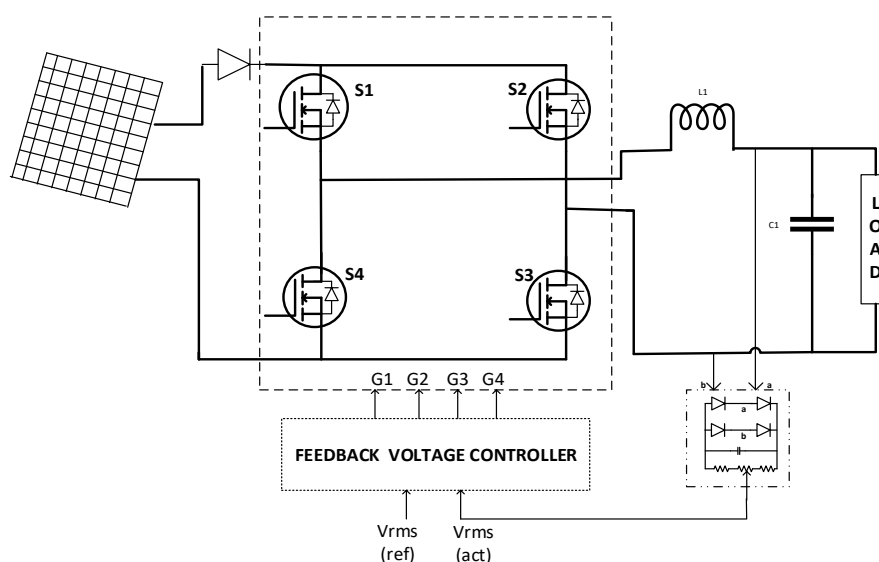


Figure 1. Schematic Diagram

The PV array is attached to a single phase full H-bridge inverter, which acts as a DC power source. An analog controller circuit is connected to the inverter, which provides the feedback to the system. This feedback helps in switching on and off of the power MOSFETs using SPWM technique. Hence, AC output is obtained from the inverter to drive an AC load. The output of the inverter depends on the solar radiation and its intensity. The components used in the circuit design are mentioned in Table 1. The major parts of the circuit are explained later.

Single Phase H-bridge Inverter

The inverter is a static power electronic circuit that converts the DC power to the AC power at desired output voltage and frequency. The most commonly used power transistors in inverters are MOSFETs and IGBTs. We used MOSFETs instead of IGBTs, because of the following reasons:

- 1) High switching frequency
- 2) Less switching power loss

3) Lesser cost with comparable efficiency

The single phase full bridge inverter is constructed by using two half-bridge inverters [6, 7]. The inverter circuit consists of four MOSFET (Metal oxide semiconductor field effect transistor) switches, four diodes, DC source and load. Each MOSFET is connected with an anti-parallel diode to support the reverse conduction. In the full H-bridge inverter circuit, the four switches S1, S2, S3 and S4 are connected as shown in the Figure 2. The gate pulses are shown in Figure 3 for S1 & S3 and S2 & S4, respectively.

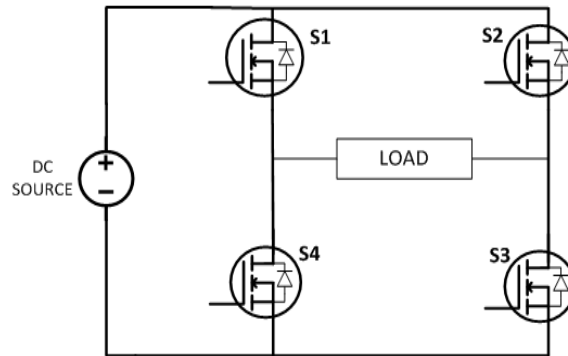


Figure 2. Single phase full H-bridge inverter

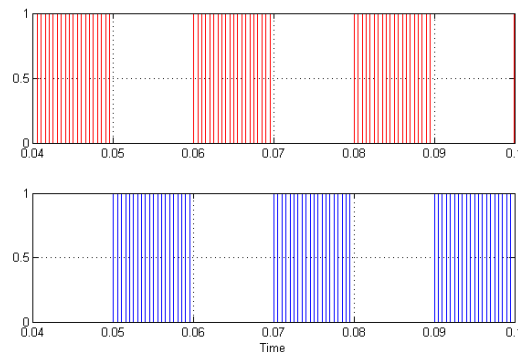


Figure 3. Gate Pulses (MATLAB)

The gate triggering pulses G_1 , G_2 , G_3 and G_4 are generated by using SPWM technique. The gate pulses G_1 , G_2 , G_3 and G_4 are used to control the MOSFET switches S1, S2, S3 and S4, respectively [8].

During the positive half cycle, the switches S1 & S3 will conduct, which are triggered simultaneously by gate triggering pulses G_1 and G_3 , respectively. During the remaining half cycle, the switches S2 & S4 will conduct and are triggered simultaneously by gate triggering pulses G_2 and G_4 , respectively.

Sinusoidal Pulse Width Modulation Technique

The sinusoidal pulse width modulation (SPWM) is an extension of multiple pulse modulation technique. In SPWM, several pulses per half cycle are used and the pulse-width is a sinusoidal function of the angular position of the pulse in a cycle as shown in Figure 4.

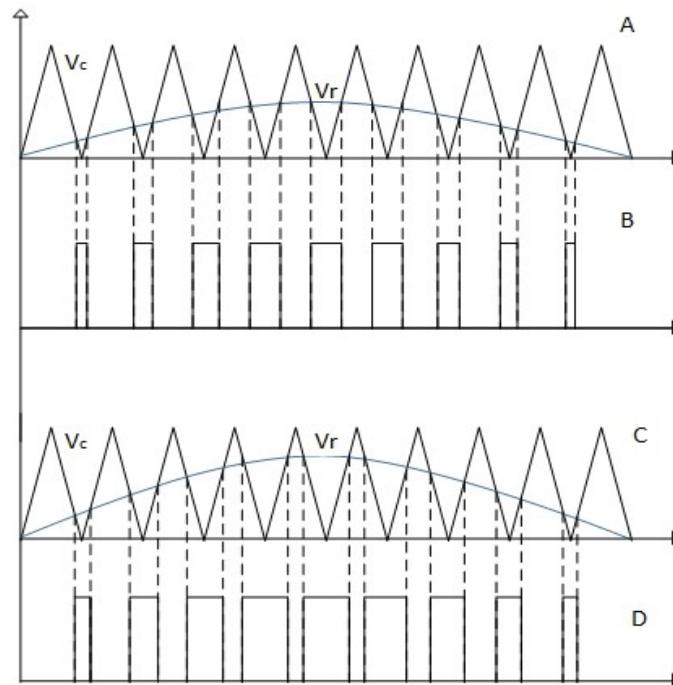


Figure 4. Generation of SPWM waveform

In this method, the high-frequency carrier signal (*i.e.*, the unipolar triangular wave) is compared with a reference or modulating signal (*i.e.*, the sinusoidal wave) to generate firing pulses. The firing pulses are generated, when the amplitude of the sine wave exceeds the amplitude of the repetitive signal. The generation of SPWM waveform for two different modulation index M_1 & M_2 is shown in part A, B, C and D of Figure 4 and it is also depicted below:

- A) Comparison of carrier wave V_c with modulation index M_1
- B) Firing pulses for modulation index M_1
- C) Comparison of carrier wave V_c with modulation index M_2 $\{M_2 > M_1\}$
- D) Firing pulses for modulation index M_2 $\{M_2 > M_1\}$

The output voltage and the output frequency of the inverter are regulated by SPWM technique. The output voltage can be varied by varying the amplitude of the modulating signal *i.e.*, the sine wave. The output frequency is decided by the frequency of the modulating signal *i.e.*, the sine wave. The quality of the output voltage waveform can be improved by increasing the number of pulses over each half cycle, which reduces the ripples and decreases the filtering requirement. This is made possible by varying the frequency of the carrier signal *i.e.*, the triangular wave.

Moreover, if we increase the frequency of the repetitive carrier signal, the frequency of the predominant harmonics increases, and their filtering becomes easier. Thus, the size of the required filter is reduced. Hence, the SPWM technique helps in reducing harmonic content and the cost of the set-up is significantly reduced due to the reduced size of the filter as mentioned in this document.

Analog Controller

The analog controller as shown in Figures 5 and 6 is an IC based analog circuit, which is used to produce desired AC supply from fluctuating DC supply *i.e.*, the PV array. It is used to vary the pulse width required to obtain a fixed AC supply for the smooth operation of AC loads.

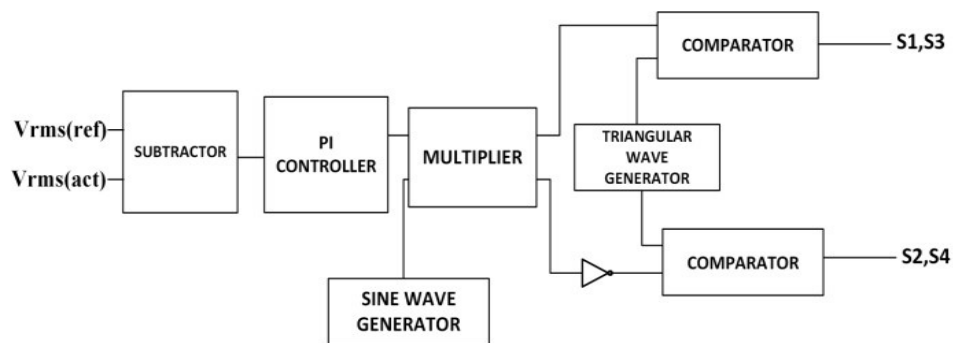


Figure 5. Block Diagram of an Analog Controller

The deviation of the actual root-mean-square (RMS) value from the set RMS value is fed to the PI controller. The amplitude of the sine wave is made proportional to the error signal by multiplying the output of the PI controller with the reference sine wave of the SPWM controller. The variable amplitude sine wave obtained from the multiplier AD633 is compared with the unipolar triangular wave to generate pulses for the gate triggering circuit of the inverter.

The analog controller is segmented into four stages as follows:

- 1) Difference amplifier
- 2) Proportional Integrator controller
- 3) Multiplier
- 4) Comparator

The reference RMS voltage (*i.e.*, the required constant output AC voltage) and the actual feedback RMS voltage are given as the inputs of the difference amplifiers.

The error signal generated from the first stage is fed to the Proportional-Integral Controller stage (Second stage). The PI controller continuously tries to minimize the error between the reference RMS voltage and the actual feedback RMS voltage. The output of the PI controller and the sine wave generated from the sine wave generator are fed to the inputs of a multiplier AD633 (Third stage). The output of the multiplier can be realized by the following equation

$$A_M = \frac{(A_{PI}) \times (A_{SINE})}{10} \quad (1)$$

where A_M , A_{PI} and A_{SINE} are the amplitude of the multiplier, PI controller, and sine wave, respectively.

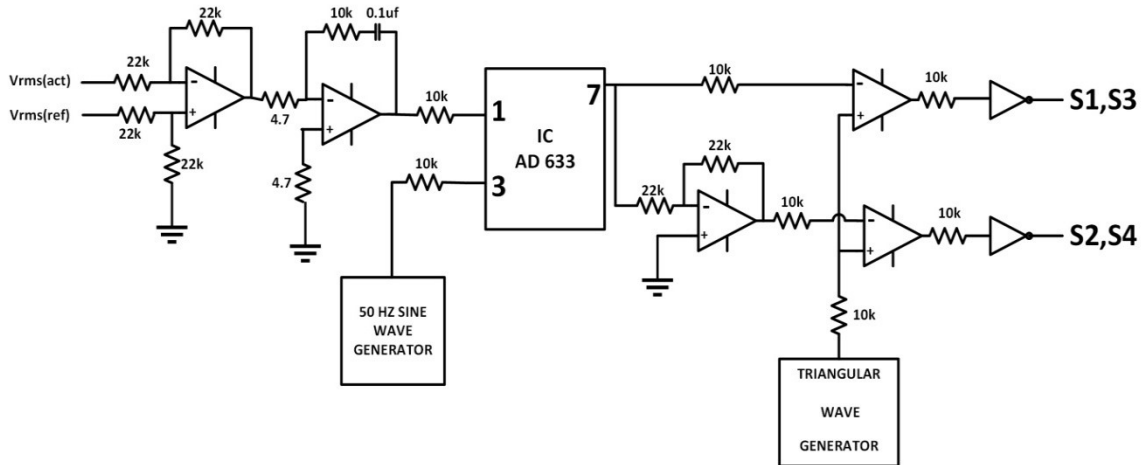


Figure 6. Circuit Diagram of Analog Controller

The output of the third stage is given to the inputs of the comparator (Fourth Stage). During the positive half cycle, the variable amplitude sine-wave is compared with the unipolar triangular wave generated from the triangular wave generator to generate the gate pulse. During the negative half cycle, the negative portion of the variable amplitude sine-wave is first inverted by inverting amplifier, and then compared with the unipolar triangular wave. Hence, the gate triggering pulses are generated for both positive and negative half cycles shown in Figure 16. The hardware implementation of the analog controller designed on the printed circuit board (PCB) is shown in Figure 7.

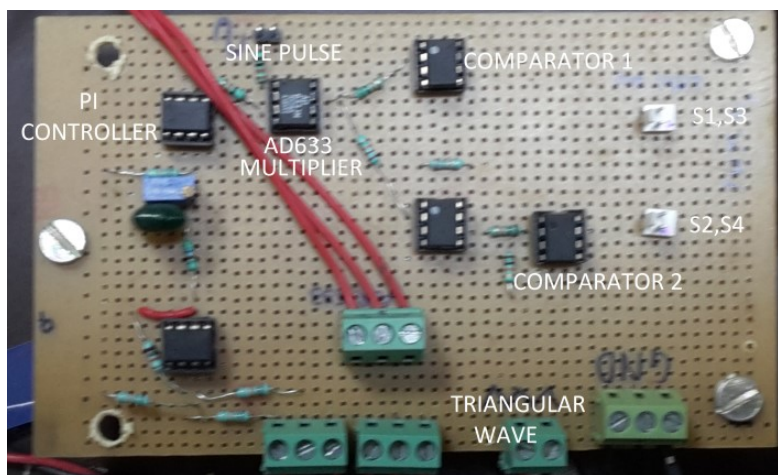


Figure 7. Hardware Design of Analog Controller

Gate Driver

A gate driver is an amplifier circuit employed to trigger the high-power transistor like IGBTs and MOSFETs from a low power output of the feedback voltage controller. The gate driver circuit is shown in Figure 8.

Isolation is required between the high-power circuit and the low-power control circuit in order to avoid the high-power circuit current to flow into the control circuit under faulty conditions. The isolation is provided by TLP250, which is an optocoupler device transferring electrical signals between two isolated circuits [9]. It is suitable for gate driving circuits for IGBT and power MOSFET. The input side has a LED and the receiving side has a photodetector. The propagation delay of the driver is relatively low, which typically lies between $0.15 \mu\text{s}$ to $0.5 \mu\text{s}$ as the input and output are optically isolated. The maximum operating frequency is around 25 kHz.

TLP250 receives 3V SPWM pulse generated by the analog controller. Then, TLP250 amplifies the 3V gate-pulse to more than 10V gate-pulse required to trigger MOSFET IRF540N as specified in its datasheet. Hence, TLP250 performs two main functions that are amplification of gate pulse and isolation of high power circuit from the controller circuit. The hardware implementation of the gate driver circuit is shown in Figure 9.

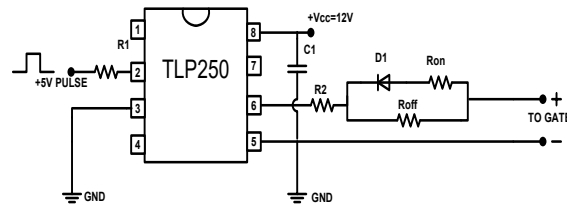


Figure 8. Schematic Circuit Diagram of TLP250 Gate Driver Circuit

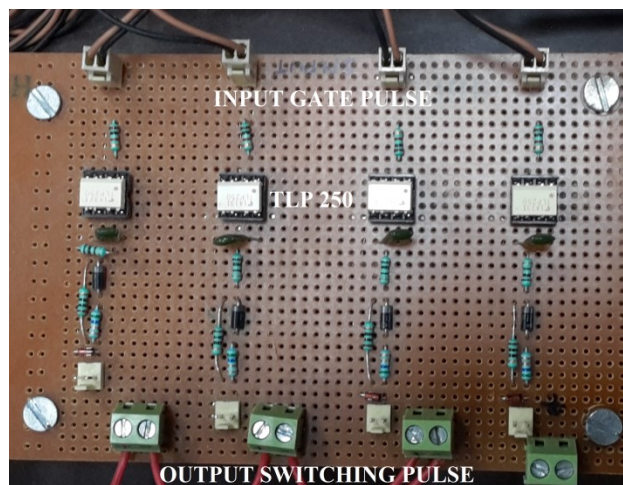


Figure 9. Hardware Design of Gate Driver Circuit

Sine Wave Generator

The Sine-Wave generator as shown in Figure 10 is used to generate a sinusoidal signal that is used as a reference signal for the generation of gate pulses using SPWM technique. This Sine-Wave generator utilizes the concept of the Wein's Bridge oscillator using op-amps. The Sine-Wave generator circuit generates repetitive waveforms of fixed frequency and amplitude without any external input signal.

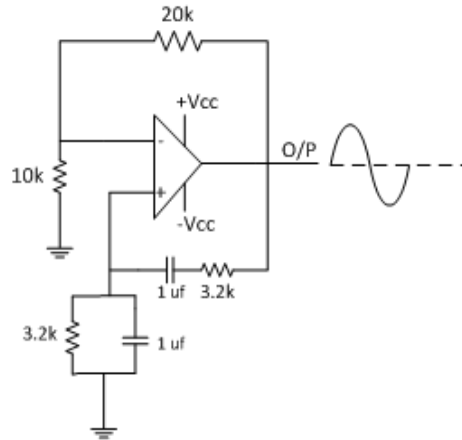


Figure 10. Schematic Circuit Diagram of Sine Wave Generator

The frequency is decided by the equation:

$$f = \frac{1}{2\pi RC} \quad (2)$$

The hardware implementation of the Sine-Wave generator is shown in Figure 11.

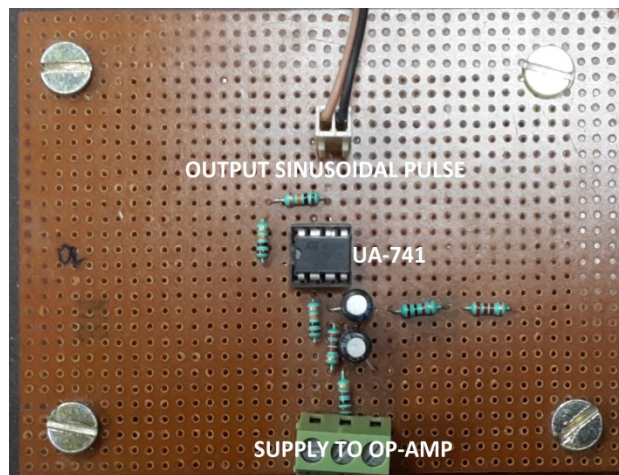


Figure 11. Hardware Design of Sine-Wave Generator

Experimental Results and Set-up

The laboratory prototype was constructed using a PV array, single phase MOSFET based inverter and a feedback analog controller. The overall hardware circuitry prepared for pulse generation is shown in Figure 12.

The D.C. output of the PV array is coupled to the input of single phase inverter in order to obtain AC output voltage (according to requirement) and frequency 50Hz. The output voltage of the inverter is controlled by generating suitable firing sequence for the inverter using an analog controller, which is present in feedback to the main power circuit.

In the analog controller, the output of the inverter is compared with the reference voltage to generate a suitable error signal. The error signal is passed to the PI controller and the output of the controller is then multiplied with the sine wave using a multiplier IC AD633. This is done to make the amplitude of sine wave proportional to the generated error signal.



Figure 12. Complete Experimental Set-Up

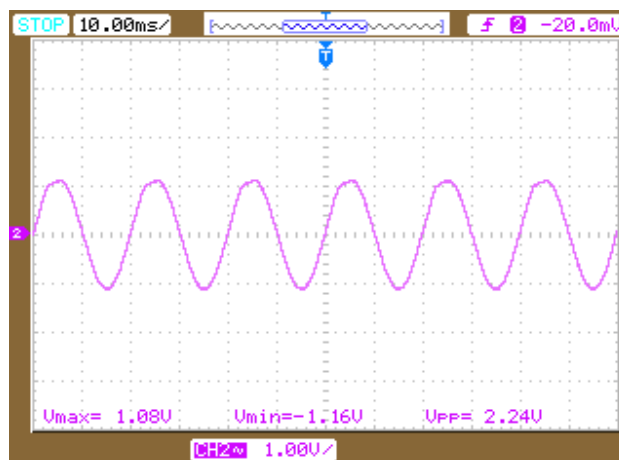


Figure 13. Sinusoidal Waveform

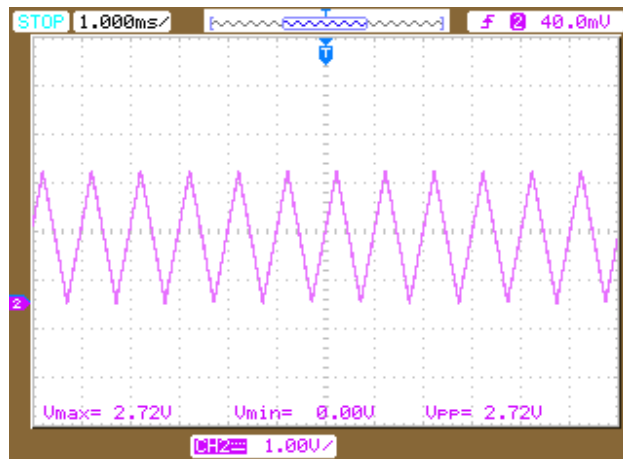


Figure 14. Unipolar Triangular Waveform

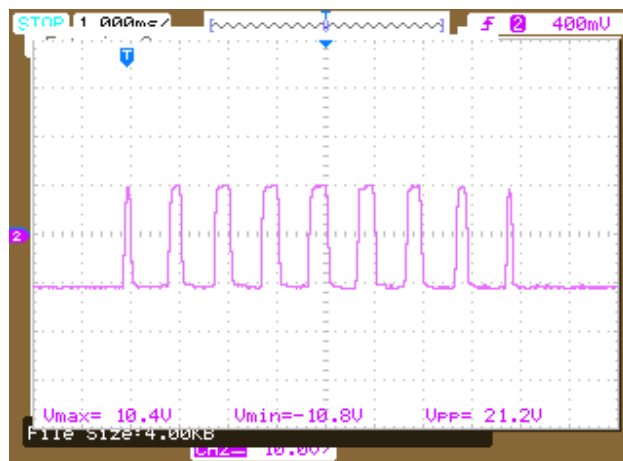


Figure 15. Generated SPWM Waveform

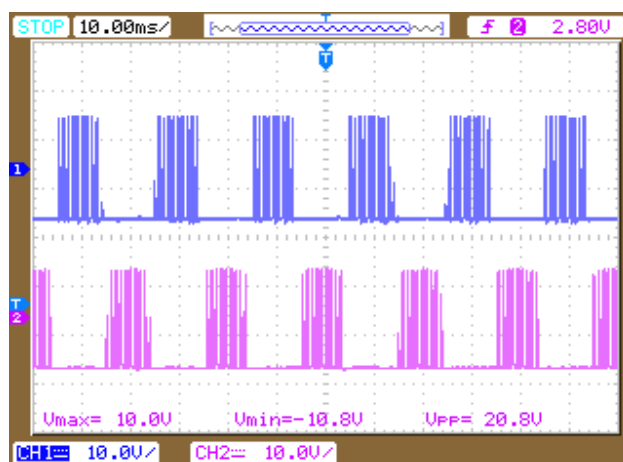


Figure 16. Triggering Gate Pulse



Figure 17. Output Voltage Waveform

Figure 13 shows the sinusoidal waveform generated by the Sine-Wave generator and Figure 14 shows the waveform of the triangular wave generator. The output of the multiplier is compared with a unipolar triangular wave to generate suitable firing gate pulse during both the positive and negative half cycle of the sinusoidal waveform.

The outputs of analog controller as shown in Figures 15 & 16, *i.e.*, G_1 , G_2 , G_3 & G_4 are given to the TLP250 driver circuit. The driver circuit forms a bridge between the analog controller and the inverter circuit. It provides the firing pulses to the gate terminal of the individual MOSFET switch. The output of the inverter is shown in the Figure 17.

The desired output voltage is obtained by giving suitable firing sequence generated by SPWM based analog controller. The output voltage and frequency have been mentioned in Table 2.

Table 1. Components Used in the Circuit

| S.No. | Component Name | Rating |
|-------|-----------------|----------------------|
| 1. | PV Array | 24V, 20W |
| 2. | MOSFET(IRF540N) | VDS= 100V,23-33A |
| 3. | Op-Amp(UA-741) | $\pm 18V, 1.7-2.8mA$ |
| 4. | AD633 | $\pm 15V, 4-6mA$ |

Table 2. Output Data

| S.No. | Parameter | Output values |
|-------|-----------|---------------|
| 1. | Voltage | 0-24V |
| 2. | Frequency | 50Hz |

CONCLUSIONS

In this paper, an efficient and cost-effective control strategy for the single phase full bridge inverter using an analog controller has been presented. The analog controller consisting of low-cost analog components is used to control the output voltage using SPWM technique. SPWM technique helps in reducing filtering requirement by eliminating predominant harmonics along with the output voltage control. Thus, the size

as well as the cost of the overall setup is reduced. This paper eliminates the requirement of a microcontroller. The overall system is first simulated using MATLAB, and then the hardware circuit is designed. The experimental results on the laboratory prototype are presented to validate the control strategy. The SPWM based single phase inverter is tested for various loads, where it is observed that the output current waveform is smooth due to less harmonic content and less total harmonic distortion (THD). THD can be reduced further by increasing the frequency of the carrier wave, and resulting in much smoother output waveforms. Thus, the paper presents the low-cost design and implementation of the analog components based control technique of a single phase inverter, which can be used to simplify many real life problems.

CONFLICTS OF INTEREST

We declare that there is no conflict of interests regarding the publication of this paper.

REFERENCES

- [1] J. Xu, K. Han, "The Single-Phase Inverter Design for Photovoltaic System" in Proceedings of International Symposium on Computer, Consumer and Control (IS3C), Xi'an, July 2016. DOI: 10.1109/IS3C.2016.95
- [2] P.S. Bimbhra, "Power Electronics", Khanna Publishers, 2012. pp. 309.
- [3] L. Umanand, "Power Electronics: Essentials & Applications", Wiley, 2009. pp. 80.
- [4] Y.C. Kuo, L.J. Liu, H.C. Lee, "Analog controller IC design for single-stage photovoltaic inverters" in Proceedings of International Conference on Fuzzy System Knowledge Discovery, China, July 2011. DOI: 10.1109/FSKD.2011.6020035
- [5] J. Luecke, "Analog and Digital Circuits for Electronic Control system applications", Elsevier, 2005. pp.43.
- [6] S.K. Mandal, "Power electronics", Edition India: Mc Graw Hill Education, 2014. pp. 81.
- [7] M.H. Rashid, "Power Electronics: Circuits, Devices, and Applications" Third Edition, Prentice Hall, 2011. pp. 226.
- [8] N. Sasidharan, J.G. Singh, "A Novel Single Stage Single Phase Reconfigurable Inverter Topology for a Solar Powered Hybrid AC/DC Home", IEEE Transaction on Industrial Electronics, vol. 64, pp. 2820-2828, 2016.
- [9] J.N. Khan, "Design considerations in using the inverter gate driver optocouplers for variable speed motor drives", White Paper, Avago Technologies, 2010.

Article copyright: © 2018 Abhishek Ranjan, Sunil Jalutharia, Harsh Garg and Nitin Gupta. This is an open access article distributed under the terms of the [Creative Commons Attribution 4.0 International License](https://creativecommons.org/licenses/by/4.0/), which permits unrestricted use and distribution provided the original author and source are credited.



Establishing Contingency Analysis with FACTS Devices Using Power World Simulator

B. Monisha^{1,2,*} and K. Balamurugan²

¹ Department of Electrical Engineering, Sastra University, Thanjavur, India

² Department of Electrical Engineering, Dr. Magalingam College of Engineering and Technology, Pollachi, India

Received January 18, 2018; Accepted March 15, 2018; Published 5/12/2018

Contingency analysis is the protection of power system operation under the loss of one or more of the major power system components. It is widely used to predict the effect of outages of transmission lines and generators. To calculate the number of violation, contingency analysis is the most preferable choice. Power systems use contingency analysis to foretell the result of any component failure. Contingency analysis is an application that uses a simulated model of power system to judge the result and calculate any overload. The proposed method approaches the flexible AC transmission system (FACTS) device to reduce the power flow in heavily loaded line and also increase the system performance. In this work, FACTS devices were implemented in IEEE 6-bus and IEEE 14-bus system and it is simulated by using Power World Simulator Software.

Keywords: Contingency analysis; Flexible AC transmission system (FACTS); Single contingency; Multiple contingency; Line outage distribution factors (LODFs)

Introduction

The power system security is the most difficult work because of great rivalry in open approach network. The most challenging task in security estimation is that gives knowledge about the system state in the event of contingency. By designing and operation, the main role is to control all areas in order to give protection, because any outage of equipment leads to transient instability. By using the line outage distribution factor (LODF), the outage of second line can cause small changes in the power flow. As compared with the pre-contingency taken with LODF with similar data [1], usually contingency analysis is segregated in three parts of contingency definition, selection and evaluation [2]. Contingency analysis results in line flow, voltage or reactive power violations that are simulated with hypothetical tests [3].

The effective way that we use is Flexible AC Transmission System (FACTS), which can make smaller the transmission congestion and control the devices by modeling their approximate sizes, optimal locations, settings and cost. A series compensator (Thyristor-Controlled Series Compensation, TCSC) is connected in series with transmission line in order to control the line impedance with much faster response compared to conventional control devices. To determine the suitable location for FACTS devices, a loss sensitivity method is used [4].

*Corresponding author: moni210494@gmail.com

In present work, the effort has been given on contingency analysis with D-FACTS devices in order to reduce the number of violations that take place in transmission line by a respond based on current. The respond based on current has auto configure characteristic curve parameters, like max compensation, initial current and limit current. In this paper two different bus systems are compared with different cases and it results in multiple contingency that will be more effective than single in each system.

Contingency Analysis

Contingency analysis classifies the power system into two stages as secure and insecure states. When the number of contingency is more, contingency analysis took a time-consuming process. Contingency may possibly cause harmful disturbances that exit under the control state of power system. Contingency referring to interrupts like generator, transformer and transmission line outages will cause quick and big changes in both the outline and the state of the system [4, 5]. The contingency list is chosen by the help of contingency ranking.

The main objective is to find out the line overload and violations under such contingencies and to mitigate the violations. Voltage violation will take place in two methods, namely single contingency and multi contingency. AC load flow is more accurate than DC load flow analysis [6]. Single contingency will take less time as compared to thousands of outages that take place in the system. Contingency analysis is studies in two types of tools namely on line and off line analysis [5]. In contingency analysis, two types of contingency are generator contingency and line contingency, which can occur due to two types of violations.

1. Low voltage violation
2. Line MVA limit violation.

Low voltage violation occurs due to insufficient reactive power, while line MVA limit violation takes place when it goes beyond its actual rating.

The line outage distribution factors are also defined similarly. The LODF is defined by,

$$\beta_{ij,mn} = \frac{\Delta f_{ij}}{f(0)_{mn}}$$

where $\beta_{ij,mn}$ is the line outage distribution factor for line 'i-j' under outage of line 'm-n', and $f(0)_{mn}$ is the power flow over line 'm-n' in the pre-outage condition. Therefore, for the outage of line 'm-n', the new flow over line 'i-j' is given.

Static Modelling of FACTS Devices

FACTS is a power electronic based system and other static equipment that provide control of one or more AC transmission system parameters to enhance controllability and increase power transfer capability [7]. Some benefits of FACTS devices are

- Increase the loading of line to thermal capability.
- Reduce power flow in heavily loaded line.
- Improve the stability, quality of supply, availability, reliability and load ability of the power system.
- Reduce reactive power flows and load flows.
- Limit the short circuit current and overloads.

Series compensator (TCSC) is used in system for reducing the violation. It is connected to the transmission line where the voltage rating is beyond its rating in order to reduce the rating.

Thyristor Controlled Series Compensator (TCSC)

In transmission line, it is connected in series where it improves the voltage profile of the system line [8]. A basic setup of TCSC is shown in Figure 1.

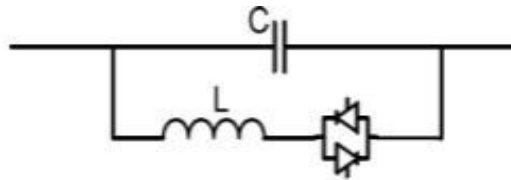


Figure 1. Basic setup of TCSC

The impedance of this circuit is

$$X_{TCSC}(\alpha) = \frac{X_c X_L(\alpha)}{X_L(\alpha) - X_c}$$

Where α is the firing angle, X_L is the inductor reactance and $X_L(\alpha)$ is inductor effective reactance at firing angle α

$$X_L \leq X_L(\alpha) \leq \infty$$

Let the complex power flowing from bus m to bus n can be expressed as

$$S_{mn}^* = P_{mn} - jQ_{mn} = V_m^* I_{mn}$$

$$= V_m^2 [G_{mn} + j(B_{mn} + B_{sh})] - V_m^* V_n (G_{mn} + jB_{mn})$$

The real and reactive power flows from bus m to bus n can be expressed as

$$P_{mn} = V_m^2 G_{mn} - V_m V_n G_{mn} \cos(\delta_m - \delta_n) + V_m V_n B_{ij} \sin(\delta_m - \delta_n)$$

$$Q_{mn} = -V_m^2 (B_{mn} + B_{sh}) + V_m V_n G_{mn} \sin(\delta_m - \delta_n) + V_m V_n B_{mn} \cos(\delta_m - \delta_n)$$

The active and reactive power losses in the line can be calculated as

$$P_L = P_{mn} + P_{nm}$$

$$Q_L = Q_{mn} + Q_{nm}$$

TCSC have two modes of operation in direction of the circuit resonance depending on the value of firing angle. Main purposes of the TCSC are to minimize the total power loss, generation cost and reactive power generation limits [9, 10].

Power World Simulator

Power world simulator was founded in 1996 by professor Thomas J. Overbye of the University of Illinois at Urbana-Champaign [11]. Simulator 5.0 is the first version. Recently, simulator 17 is used with new ribbon interface and it is a very advanced version used in all type of systems.

The steps taken for optimal power flow in power world simulator include [12]:

STEP 1: In 'Edit Mode', sketch single line diagram of given power system network with specified data.

STEP 2: During 'Run Mode', run the optimal power flow and find out the power flow in each transmission line.

STEP 3: Single Contingency is applied to power system and number of violations found in each transmission line without connecting FACTS devices.

STEP 4: Optimal placement of FACTS device can be found, in which the number of violations is in line.

STEP 5: After placing FACTS devices, run the power system with single contingency and compare the results.

STEP 6: The above steps are repeated for multi contingency case also.

The main advantage of contingency in power world simulator is that it automatically runs through a list of 1000's of contingency, creates a list of system overloads and voltage problems seen during these contingencies and compares the results of two contingencies runs [13, 14].

Results and Discussion

The IEEE-6 bus system and IEEE-14 bus system are simulated in the power world simulator, which involve contingency analysis. There are different cases in bus systems and it is differentiated below.

Case I

IEEE 6 Bus System- Single Contingency (without D-FACTS)

The single line diagram for IEEE-6 bus system is shown in Figure 2 and the bus output data, generator data and load data values are given in Table 1.

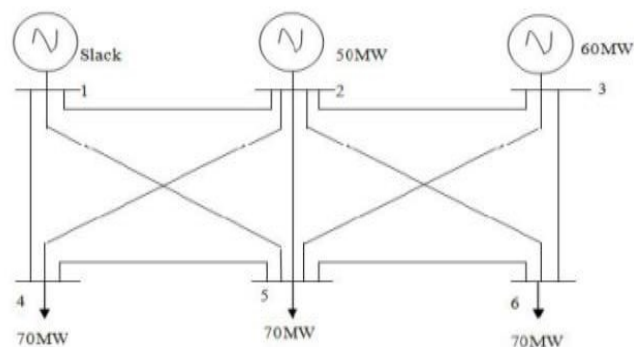


Figure 2. One line diagram of 6-bus system

Table 1. Bus data of IEEE 6-bus system

| Bus no | Bus type | V(p.u) | Pd (MW) | Qd (Mvar) | Pg (MW) | Qg (Mvar) |
|--------|----------|--------|---------|-----------|---------|-----------|
| 1 | Slack | 1.05 | 0 | 0 | 0 | 0 |
| 2 | PV | 1.05 | 0 | 0 | 50 | 0 |
| 3 | PV | 1.07 | 0 | 0 | 60 | 0 |
| 4 | PQ | 1.0 | 70 | 70 | 0 | 0 |
| 5 | PQ | 1.0 | 70 | 70 | 0 | 0 |
| 6 | PQ | 1.0 | 70 | 70 | 0 | 0 |

The generator real and reactive power outputs for the test system is shown in Table 2. The maximum and minimum MW and MVR ranges are also specified in this table.

Table 2. Generator data of IEEE 6-bus system

| BUS NO | P min (MW) | P max (MW) | Q min (Mvar) | Q max (Mvar) | ai \$/MW ² - h | bi \$/MW ² - h | ci \$/MW ² - h |
|--------|------------|------------|--------------|--------------|---------------------------|---------------------------|---------------------------|
| 1 | 50 | 200 | -20 | 100 | 0.0107 | 11.669 | 213.1 |
| 2 | 37.5 | 150 | -20 | 100 | 0.0178 | 10.333 | 200 |
| 3 | 45 | 180 | -15 | 100 | 0.0148 | 10.833 | 240 |

The line data of IEEE-6 for the test system is shown in Table 3. The real, reactive power and susceptance values are specified in this table.

Table 3. Line data for IEEE-6 bus system

| FROM BUS | TO BUS | R(p.u) | X(p.u) | Half line charging susceptance (p.u) | Thermal limit (MVA) |
|----------|--------|--------|--------|--------------------------------------|---------------------|
| 1 | 2 | 0.1 | 0.2 | 0.02 | 40 |
| 1 | 4 | 0.05 | 0.2 | 0.02 | 60 |
| 1 | 5 | 0.08 | 0.3 | 0.03 | 50 |
| 2 | 3 | 0.05 | 0.25 | 0.03 | 40 |
| 2 | 4 | 0.05 | 0.1 | 0.01 | 70 |
| 2 | 5 | 0.10 | 0.3 | 0.02 | 30 |
| 2 | 6 | 0.07 | 0.2 | 0.025 | 90 |
| 3 | 5 | 0.12 | 0.26 | 0.025 | 70 |
| 3 | 6 | 0.02 | 0.1 | 0.01 | 80 |
| 4 | 5 | 0.2 | 0.4 | 0.04 | 20 |
| 5 | 6 | 0.1 | 0.3 | 0.03 | 40 |

The contingency analysis of 6-bus test system is shown in Figure 3, when the power flow is running on the power world simulator.

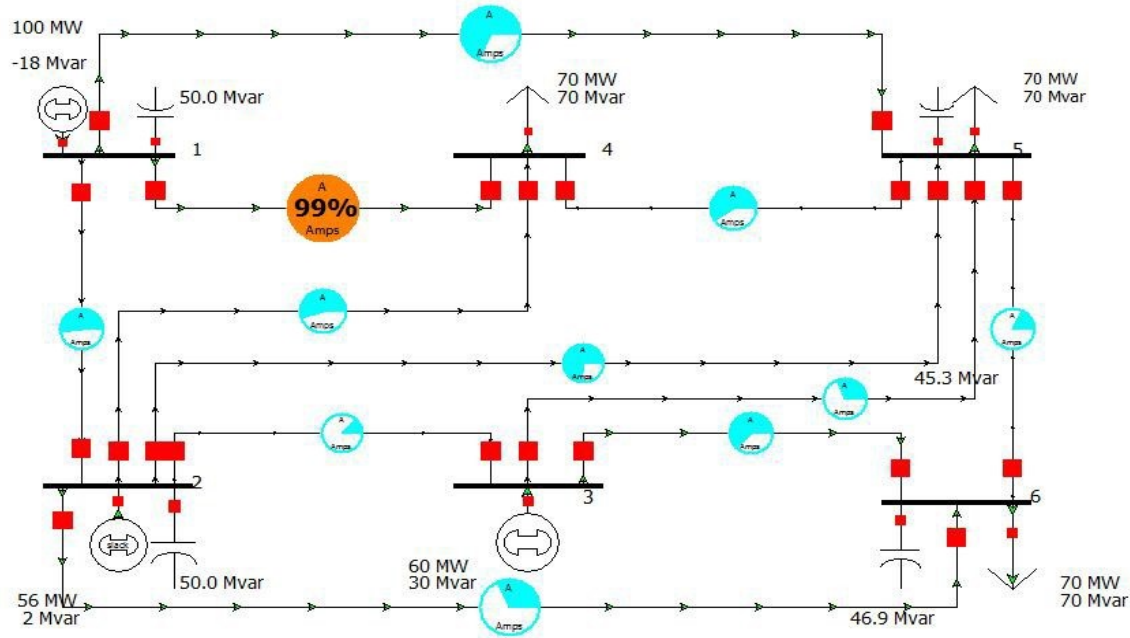


Figure 3. Simulink one line diagram of 6-bus system without D-Facts

Base Case Power Flow List

Table 4 shows the base case power flow values for IEEE-6 bus system without D-FACTS.

Table 4. Base case power flow list

| From bus | To bus | MW | Mvar | From bus | To bus | MW | Mvar |
|----------|--------|-------|--------|----------|--------|--------|--------|
| 1 | 2 | 18.27 | -9.61 | 2 | 1 | -17.86 | 8.43 |
| 1 | 4 | 48.53 | 34.76 | 4 | 1 | -46.71 | -29.32 |
| 1 | 5 | 33.28 | 7.31 | 5 | 1 | -32.33 | -6.61 |
| 2 | 3 | 4.40 | -2.35 | 3 | 2 | -4.39 | -0.60 |
| 2 | 4 | 21.88 | 31.36 | 4 | 2 | -21.70 | -30.20 |
| 2 | 5 | 19.97 | 8.95 | 5 | 2 | -19.47 | -9.36 |
| 2 | 6 | 27.88 | 5.17 | 6 | 2 | -27.31 | -5.96 |
| 3 | 5 | 19.61 | 8.66 | 5 | 3 | -19.03 | -9.79 |
| 3 | 6 | 44.78 | 22.37 | 6 | 3 | -44.27 | -20.81 |
| 4 | 5 | -2.18 | -10.48 | 5 | 4 | 2.38 | 7.43 |
| 5 | 6 | -1.55 | -6.39 | 6 | 5 | 1.58 | 3.72 |

No. of Overloads Occurred when Each Line is Opened

Table 5 shows the total no. of overloads that occurred in IEEE-6 bus system with single contingency. The total no. of overloads taken is 15 without D-FACTS in transmission line.

Table 5. Overload in each line

| FROM BUS | TO BUS | NO OF OVERLOAD |
|------------------------------|--------|----------------|
| 1 | 2 | 1 |
| 1 | 4 | 4 |
| 1 | 5 | 3 |
| 2 | 3 | 0 |
| 2 | 4 | 2 |
| 2 | 5 | 1 |
| 2 | 6 | 0 |
| 3 | 5 | 1 |
| 3 | 6 | 1 |
| 4 | 5 | 1 |
| 5 | 6 | 1 |
| Total no of overloads | | 15 |

Ranking of lines

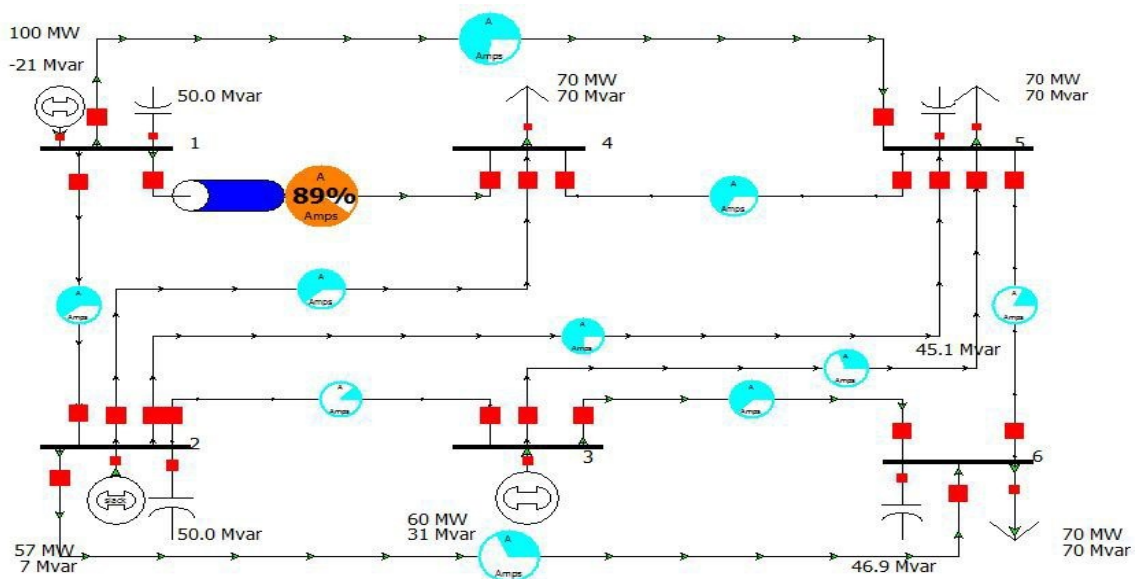
The transmission line 1-4 shows that it is ranked first due to maximum number of overloads.

Table 6. Ranking for 6 bus system without D-FACTS

| LINE | RANKING |
|------|------------|
| 1-4 | I (1009%) |
| 4-5 | II (295%) |
| 1-2 | III (229%) |
| 2-4 | IV (126%) |
| 2-5 | V (112%) |

IEEE 6 Bus System - Single Contingency (with D-FACTS)

The contingency analysis of 6-bus test system is shown in Figure 4.

**Figure 4.** Simulink one line diagram of 6-bus system with D-Facts

Base Case Power Flow List

Table 7 shows the base case power flow values for IEEE-6 bus system with D-FACTS.

Table 7. Base case power flow list

| From bus | To bus | MW | Mvar | From bus | To bus | MW | Mvar |
|----------|--------|-------|--------|----------|--------|--------|--------|
| 1 | 2 | 18.23 | -9.61 | 2 | 1 | -17.82 | 8.42 |
| 1 | 4 | 48.51 | 34.75 | 4 | 1 | -46.69 | -29.32 |
| 1 | 5 | 33.26 | 7.31 | 5 | 1 | -32.32 | -6.62 |
| 2 | 3 | 4.41 | -2.36 | 3 | 2 | -4.4 | -0.59 |
| 2 | 4 | 21.90 | 31.37 | 4 | 2 | -21.12 | -30.20 |
| 2 | 5 | 19.98 | 8.95 | 5 | 2 | -19.48 | -9.36 |
| 2 | 6 | 27.89 | 5.17 | 6 | 2 | -27.31 | -5.95 |
| 3 | 5 | 19.62 | 8.66 | 5 | 3 | -19.04 | -9.79 |
| 3 | 6 | 44.78 | 22.38 | 6 | 3 | -44.27 | -20.82 |
| 4 | 5 | -2.19 | -10.48 | 5 | 4 | 2.39 | 7.43 |
| 5 | 6 | -1.56 | -6.39 | 6 | 5 | 1.59 | 3.72 |

No. of Overloads Occurred when Each Line is Opened

Table 8 shows the total no. of overloads that occurred in IEEE-6 bus system with single contingency. The total no. of overloads taken is 10 with D-FACTS in transmission line.

Table 8. Overload occurred in each line

| From bus | To bus | No of overload |
|------------------------------|--------|----------------|
| 1 | 2 | 1 |
| 1 | 4 | 3 |
| 1 | 5 | 1 |
| 2 | 3 | 0 |
| 2 | 4 | 1 |
| 2 | 5 | 2 |
| 2 | 6 | 0 |
| 3 | 5 | 0 |
| 3 | 6 | 0 |
| 4 | 5 | 2 |
| 5 | 6 | 0 |
| Total no of overloads | | 10 |

Ranking of Lines

The transmission line 1-4 shows that it is ranked first due to maximum number of overloads (Table 9).

Table 9. Ranking of line

| LINE | RANKING |
|------|-----------|
| 1-4 | I (362%) |
| 2-5 | II(332%) |
| 1-2 | III(246%) |
| 2-5 | IV(218%) |
| 2-4 | V(126%) |

Comparison of IEEE 6 bus system

The comparison of IEEE-6 bus systems with D-FACTS and without D-FACTS between the connection of transmission lines is shown in Table 10 and Figure 5.

Table 10. Comparison of 6 bus system

| From bus | To bus | No. of overload without D-FACTS | No. of overload with D-FACTS |
|-------------------------------|--------|---------------------------------|------------------------------|
| 1 | 2 | 1 | 1 |
| 1 | 4 | 4 | 3 |
| 1 | 5 | 3 | 1 |
| 2 | 3 | 0 | 0 |
| 2 | 4 | 2 | 1 |
| 2 | 5 | 1 | 2 |
| 2 | 6 | 0 | 0 |
| 3 | 5 | 1 | 0 |
| 3 | 6 | 1 | 0 |
| 4 | 5 | 1 | 2 |
| 5 | 6 | 1 | 0 |
| Total no. of overloads | | 15 | 10 |

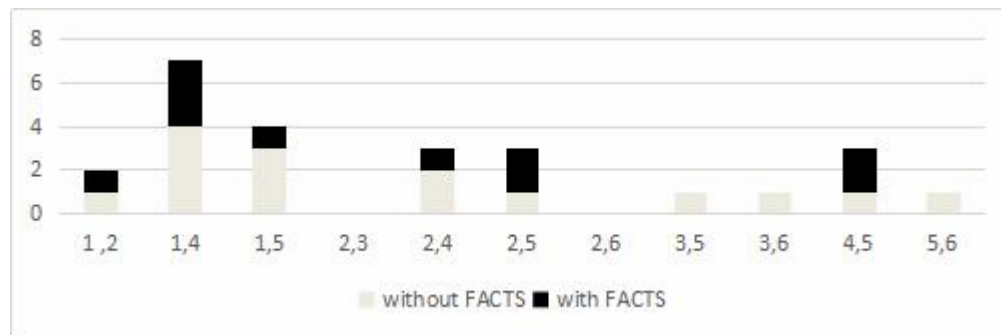


Figure 5. Bar chat for the IEEE 6 bus system comparison

CASE II

IEEE-6 Bus System - Multi Contingency (without D-FACTS)

Multiple contingency is that we calculate the number of overloaded lines in each case and ranking for line, when two or more lines are opened simultaneously

No. of Overloads when Double Contingency Take Place

Table 11. No. of overload for double contingency

| LINES OPENED | NO OF OVERLOADS |
|--------------|-----------------|
| (1-2,1-4) | 3 |
| (2-3,2-4) | 3 |

No. of Overloads Occurred in Each Line

Number of overloads in double contingency for each line is shown in Table 12, in which only two cases are taken.

Table 12. Overload occurred in each line (double contingency)

| From bus | To bus | No of overload |
|------------------------|--------|----------------|
| 1 | 2 | 0 |
| 1 | 4 | 1 |
| 1 | 5 | 1 |
| 2 | 3 | 0 |
| 2 | 4 | 1 |
| 2 | 5 | 1 |
| 2 | 6 | 0 |
| 3 | 5 | 0 |
| 3 | 6 | 0 |
| 4 | 5 | 2 |
| 5 | 6 | 0 |
| No of overloads | | 6 |

Ranking of Lines

The overall ranking is shown in Table 13. The line 4-5 is ranked first with the highest overload in two cases in double contingency.

Table 13. Ranking for double contingency

| Line | Ranking |
|------|---------|
| 4-5 | I |
| 1-5 | II |
| 1-4 | III |
| 2-4 | IV |
| 2-5 | V |

CASE III

IEEE-14 Bus System- Single Contingency (without D-FACTS)

The single line diagram for IEEE-14 bus system is shown in Figure 6 and the bus output data, generator data and load data values are given in Table 14.

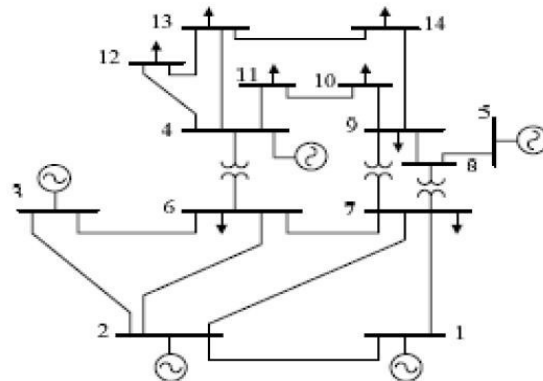


Figure 6. Single line diagram for IEEE-14 bus system

Table 14. Bus, generator and load value for IEEE-14 bus system

| Bus no | Bus code | Voltage Magnitude | Angle | Load | | Generator | | | | Injected Mvar |
|--------|----------|-------------------|-------|--------|-------|-----------|------|-------|-------|---------------|
| | | | | MW | Mvar | MW | Mvar | Q min | Q max | |
| 1 | 1 | 1.06 | 0 | 30.38 | 17.78 | 40 | -40 | 0 | 0 | 0 |
| 2 | 2 | 1.045 | 0 | 0 | 0 | 232 | 0 | -40 | 50 | 0 |
| 3 | 3 | 1.01 | 0 | 131.88 | 26.6 | 0 | 0 | 0 | 40 | 0 |
| 4 | 4 | 1 | 0 | 66.92 | 10 | 0 | 0 | 0 | 0 | 0 |
| 5 | 5 | 1 | 0 | 10.64 | 2.24 | 0 | 0 | 0 | 0 | 0 |
| 6 | 6 | 1.07 | 0 | 15.68 | 10.5 | 0 | 0 | -6 | 24 | 0 |
| 7 | 7 | 1 | 0 | 0 | 0 | 0 | 0 | 0 | 0 | 0 |
| 8 | 8 | 1.09 | 0 | 0 | 0 | 0 | 0 | -6 | 24 | 0 |
| 9 | 9 | 1 | 0 | 41.3 | 23.24 | 0 | 0 | 0 | 0 | 0 |
| 10 | 1 | 1 | 0 | 12.6 | 8.12 | 0 | 0 | 0 | 0 | 0 |
| 11 | 11 | 1 | 0 | 4.9 | 2.52 | 0 | 0 | 0 | 0 | 0 |
| 12 | 12 | 1 | 0 | 8.54 | 2.24 | 0 | 0 | 0 | 0 | 0 |
| 13 | 13 | 1 | 0 | 18.9 | 8.12 | 0 | 0 | 0 | 0 | 0 |
| 14 | 14 | 1 | 0 | 20.86 | 7 | 0 | 0 | 0 | 0 | 0 |

Line Data for IEEE-14 Bus System

The line data value for IEEE-14 bus system is given in Table 15 with resistance, reactance, susceptance and thermal value.

Table 15. Line data of IEEE-14 bus system

| From bus | To bus | R (p.u) | X (p.u) | B (p.u) | Thermal limit |
|----------|--------|---------|---------|---------|---------------|
| 1 | 2 | 0.01938 | 0.05917 | 0.0264 | 120 |
| 2 | 3 | 0.4699 | 0.19797 | 0.0219 | 65 |
| 2 | 4 | 0.05811 | 0.17632 | 0.0187 | 36 |
| 1 | 5 | 0.05403 | 0.22304 | 0.0246 | 65 |
| 2 | 5 | 0.05695 | 0.17388 | 0.017 | 50 |
| 3 | 4 | 0.06701 | 0.17103 | 0.0173 | 65 |
| 4 | 5 | 0.01335 | 0.04211 | 0.0064 | 45 |
| 5 | 6 | 0 | 0.25202 | 0 | 55 |
| 4 | 7 | 0 | 0.20912 | 0 | 32 |
| 7 | 8 | 0 | 0.17615 | 0 | 45 |
| 4 | 9 | 0 | 0.55618 | 0 | 18 |
| 7 | 9 | 0 | 0.11001 | 0 | 32 |
| 9 | 10 | 0.03181 | 0.0845 | 0 | 32 |
| 6 | 11 | 0.09498 | 0.1989 | 0 | 32 |
| 6 | 12 | 0.12291 | 0.25581 | 0 | 32 |
| 6 | 13 | 0.06615 | 0.13027 | 0 | 32 |
| 9 | 14 | 0.12711 | 0.27038 | 0 | 32 |
| 10 | 11 | 0.08205 | 0.19201 | 0 | 12 |
| 12 | 13 | 0.22092 | 0.19988 | 0 | 12 |
| 13 | 14 | 0.17093 | 0.34802 | 0 | 12 |

The contingency analysis of the 14-bus test system without D-FACTS contingency is shown in Figure 7 when the power flow is running on the power world simulator.

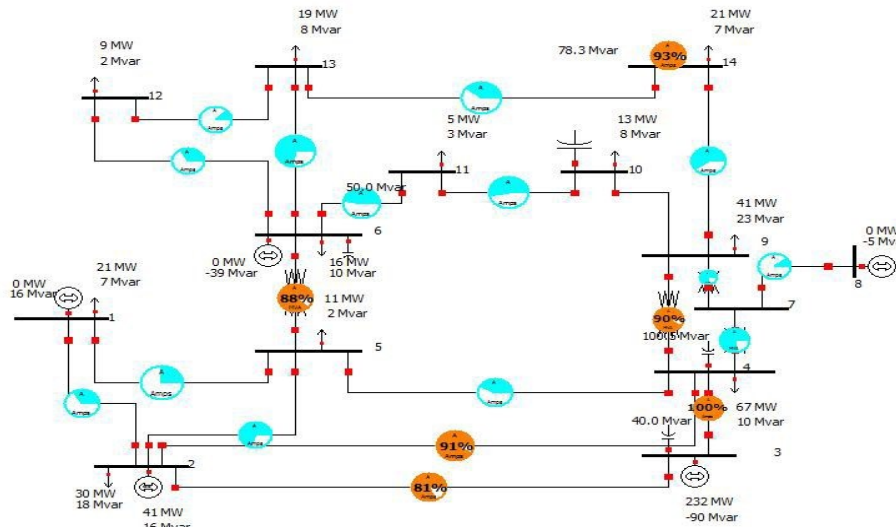


Figure 7. Simulink one line diagram of 14-bus system without D-Facts

Base Case Power Flow Analysis

Table 16 shows the base case power flow values for IEEE-14 bus system without D-FACTS.

Table 16. Base case power flow list

| Between bus | MW | Mvar | Between bus | MW | Mvar |
|-------------|--------|--------|-------------|---------|--------|
| 1-2 | -37.73 | 11.68 | 2-1 | 38.04 | -13.38 |
| 1-5 | 16.93 | -2.84 | 5-1 | -16.77 | 1.03 |
| 2-3 | -91.84 | 30.57 | 3-2 | 96.28 | -14.08 |
| 2-4 | 30.61 | -11.44 | 4-2 | -30.01 | 11.41 |
| 2-5 | 34.03 | -8.11 | 5-2 | -33.34 | 8.52 |
| 3-4 | 135.72 | -36.13 | 4-3 | -122.55 | 68.02 |
| 4-5 | 12.94 | 12.91 | 5-4 | -12.89 | -13.41 |
| 4-7 | 46.13 | -0.57 | 7-4 | -46.13 | 5.00 |
| 4-9 | 26.56 | -1.26 | 9-4 | -26.56 | 5.18 |
| 5-6 | 52.37 | 1.61 | 6-5 | -52.37 | 5.37 |
| 6-11 | 4.52 | -14.37 | 11-6 | -4.31 | 14.83 |
| 6-12 | 10.07 | 2.88 | 12-6 | -9.94 | -2.60 |
| 6-13 | 22.10 | 7.04 | 13-6 | -21.74 | -6.34 |
| 7-8 | 0 | 4.77 | 8-7 | 0 | -4.73 |
| 7-9 | 46.13 | -9.77 | 9-7 | -46.13 | 12.18 |
| 9-10 | 14.26 | -50.08 | 10-9 | -13.43 | 52.28 |
| 9-14 | 17.13 | 9.49 | 14-9 | -16.67 | -8.49 |
| 10-11 | 0.83 | 17.90 | 11-10 | -0.59 | -17.35 |
| 12-13 | 1.40 | 0.36 | 13-12 | -1.39 | -0.36 |
| 13-14 | 4.23 | -1.42 | 14-13 | -4.19 | 1.49 |

No. of Overload in Each Line

Table 17 shows the total no. of overloads that occurred in IEEE-14 bus system with single contingency. The total no. of overloads taken is 41 without D-FACTS in transmission line.

Table 17. Overload for each line

| Between line | overloads |
|------------------------------|-----------|
| 1-2 | 0 |
| 1-5 | 1 |
| 2-3 | 1 |
| 2-4 | 4 |
| 2-5 | 3 |
| 3-4 | 4 |
| 4-5 | 3 |
| 4-7 | 2 |
| 4-9 | 3 |
| 5-6 | 5 |
| 6-11 | 1 |
| 7-8 | 0 |
| 7-9 | 2 |
| 9-10 | 3 |
| 9-14 | 1 |
| 10-11 | 2 |
| 12-13 | 1 |
| 13-14 | 3 |
| Total no of overloads | 41 |

Ranking for Lines

From Table 18, the transmission line 5-6 is ranked first with the maximum number of overloads, when D-FACTS is not connected to any of lines.

Table 18. Ranking for IEEE-14 bus system (without D-FACTS)

| BETWEEN LINES | RANKING |
|---------------|---------|
| 5-6 | I |
| 3-4 | II |
| 2-4 | III |
| 9-10 | IV |
| 2-5 | V |

IEEE-14 Bus system - Single Contingency (with D-FACTS)

The contingency analysis of the 14-bus test system with D-FACTS is shown Figure 8, in which the power flow is running on the power world simulator.

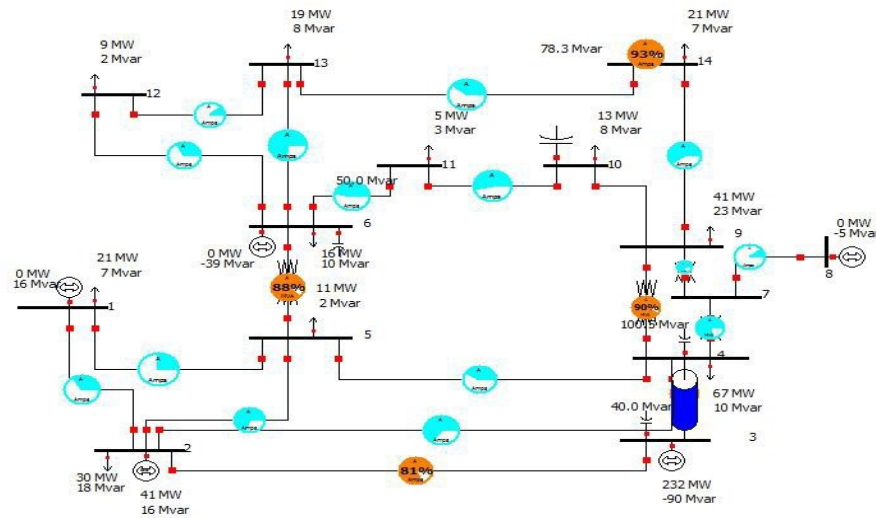


Figure 8. Simulink one line diagram of IEEE-14 bus system with D-FACTS

Base Case Power Flow List (with D-FACTS)

Table 19 shows the base case power flow values for IEEE-14 bus system with D-FACTS.

Table 19. Base case power flow list

| Between bus | MW | MVAR | Between bus | MW | MVAR |
|-------------|--------|--------|-------------|---------|--------|
| 1-2 | -38.45 | 11.82 | 2-1 | 38.77 | -13.48 |
| 1-5 | 17.59 | -3.56 | 5-1 | -16.76 | 1.05 |
| 2-3 | -95.44 | 32.33 | 3-2 | 96.28 | -14.08 |
| 2-4 | 32.06 | -12.96 | 4-2 | -30.01 | 11.41 |
| 2-5 | 35.07 | -9.09 | 5-2 | -33.35 | 8.52 |
| 3-4 | 135.72 | -36.12 | 4-3 | -122.55 | 68.92 |
| 4-5 | 12.94 | 12.92 | 5-4 | -12.90 | -13.42 |
| 4-7 | 46.13 | -0.58 | 7-4 | -46.13 | 5.01 |
| 4-9 | 26.56 | -1.26 | 9-4 | -26.56 | 5.18 |
| 5-6 | 52.37 | 1.61 | 6-5 | -52.37 | 5.38 |
| 6-11 | 4.52 | -14.37 | 11-6 | -4.31 | 14.83 |
| 6-12 | 10.07 | 2.88 | 12-6 | -9.94 | -2.60 |
| 6-13 | 22.10 | 7.04 | 13-6 | -21.74 | -6.34 |
| 7-8 | 0 | 4.77 | 8-7 | 0 | -4.73 |
| 7-9 | 46.13 | -9.77 | 9-7 | -46.26 | 12.13 |
| 9-10 | 14.26 | -50.08 | 10-9 | -13.43 | 52.28 |
| 9-14 | 17.13 | 9.49 | 14-9 | -16.67 | -8.49 |
| 10-11 | 0.83 | 17.90 | 11-10 | -0.59 | -17.35 |
| 12-13 | 1.40 | 0.36 | 13-12 | -1.39 | -0.36 |
| 13-14 | 4.23 | -1.42 | 14-13 | -4.19 | 1.49 |

No. of Overload in Each Line

Table 20 shows the total no. of overloads that occurred in the IEEE-14 bus system with single contingency. The total no. of overloads taken is 32 with D-FACTS in transmission line.

Table 20. Overload for each line

| Between line | Overloads |
|------------------------------|-----------|
| 1-2 | 0 |
| 1-5 | 0 |
| 2-3 | 1 |
| 2-4 | 1 |
| 2-5 | 3 |
| 3-4 | 1 |
| 4-5 | 2 |
| 4-7 | 2 |
| 4-9 | 2 |
| 5-6 | 5 |
| 6-11 | 1 |
| 6-12 | 1 |
| 6-13 | 2 |
| 7-8 | 0 |
| 7-9 | 0 |
| 9-10 | 3 |
| 9-14 | 1 |
| 10-11 | 2 |
| 12-13 | 1 |
| 13-14 | 4 |
| Total no of overloads | 32 |

Ranking

From Table 21, it is noted that the transmission line 5-6 is ranked first with the maximum number of overloads, when D-FACTS is connected.

Table 21. Ranking for IEEE-14 bus system with D-FACTS

| Between bus | Ranking |
|-------------|---------|
| 5-6 | I |
| 13-14 | II |
| 9-10 | III |
| 2-5 | IV |

Comparison of IEEE 14 Bus System

The comparison of IEEE-14 bus systems with D-Facts and without D-Facts between the connection of transmission lines is shown in Table 22 and Figure 9.

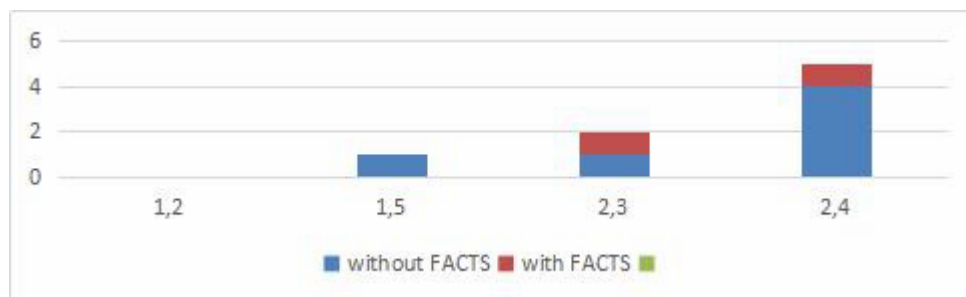
**Figure 9.** Bar chat for IEEE 14 bus system comparison

Table 22. Comparison of IEEE-14 bus systems with and without D-FACTS

| Between line | No. of overloads without D-FACTS | No. of overloads with D-FACTS |
|------------------------------|----------------------------------|-------------------------------|
| 1-2 | 0 | 0 |
| 1-5 | 1 | 0 |
| 2-3 | 1 | 1 |
| 2-4 | 4 | 1 |
| 2-5 | 3 | 3 |
| 3-4 | 4 | 1 |
| 4-5 | 3 | 2 |
| 4-7 | 2 | 2 |
| 4-9 | 3 | 2 |
| 5-6 | 5 | 5 |
| 6-11 | 1 | 1 |
| 6-12 | 0 | 1 |
| 6-13 | 2 | 2 |
| 7-8 | 0 | 0 |
| 7-9 | 2 | 0 |
| 9-10 | 3 | 3 |
| 9-14 | 1 | 1 |
| 10-11 | 2 | 2 |
| 12-13 | 1 | 1 |
| 13-14 | 3 | 4 |
| Total no of overloads | 41 | 32 |

CONCLUSIONS

Contingency analysis is used to foretell the results of outages that are caused in the transmission line. FACTS devices are used to bring down the flows within the limit in solidly loaded lines. The limit violations in the power system are effectively taken away after using the corrective actions. The security limits give an account from maximum violations of the element of test systems of both 6-bus and 14-bus system. In power world simulator, contingency analysis is not difficult to run the power system. Compared to other contingency analysis, it is more trustworthy.

CONFLICTS OF INTEREST

The authors declare that there is no conflict of interests regarding the publication of this paper.

REFERENCES

- [1] T. Guler, G. Gross, M. Liu, "Generalized Line Outage Distribution Factors", IEEE Trans. Power System, vol. 22, no.2, pp. 879-881, May 2007.
- [2] K.R. Rani, J. Amarnath, S.Kamakshaiah, "Contingency Analysis under Deregulated Power systems", Automatic Control and Systems Engineering Journal, vol. 11, no. 2, pp. 1-8, November 2011.
- [3] M. Ishimaru, R. Yokoyama, G. Shirai, K.Y. Lee, "Allocation and Design of Robust TCSC Controllers Based on Power System Stability Index", in Proceedings of 2002 IEEE Power Engineering Society Winter Meeting, vol.1, pp.573-578, November 2002. DOI: 10.1109/PESW.2002.985067
- [4] N.K. Sharma, S.P. Phulambrikar, M. Prajapati, A. Sharma, "Contingency Ranking and Analysis using Power System Analysis Toolbox (PSAT)", Innovative Systems Design and Engineering, vol. 4, no. 6, pp. 59-63, 2013.
- [5] EPRI, "Contingency Analysis-Baseline", IECSA vol. II, D38-1, 2010. <http://smartgrid.epri.com/UseCases/ContingencyAnalysis-Baseline.pdf> (accessed on 5/12/2018)
- [6] D.M. Chary, "Contingency Analysis in Power Systems, Transfer Capability Computation and Enhancement Using Facts Devices in Deregulated Power System", Ph.D. diss., Jawaharlal Nehru Technological University, 2011.
- [7] P. Preeedavichit, S.C. Srivtsava, "Optimal Reactive Power Dispatch considering FACTS devices," Electric Power System Res., vol. 46, pp. 251-257, Sep. 1998.
- [8] G.M. Huang, Y. Li, "Impact of Thyristor Controlled Series Capacitor on Bulk Power System Reliability", in Proceedings of IEEE Power Engineering Society Summer Meeting, vol.2, pp.975-980, November 2002. DOI: 10.1109/PESW.2002.1043518
- [9] D.S. Javan, H.R. Mashhadi, M. Rouhani, "Fast Voltage and Power Flow Contingencies Ranking using Enhanced Radial Basis Function Neural Network", Iranian Journal of Electrical & Electronic Engineering, vol. 7, no. 4, pp. 273-282, Dec. 2011.
- [10] A.J. Wood, B.F. Wallenberg, "Power Generation, Operation and Control". 2nd ed., New York, USA:John Wiley&Sons, pp. 410-432,1996.
- [11] S.R. Dahman, "N-1-1 Contingency Analysis using Power World Simulator", PowerWorld Corporation, 2012. <https://www.powerworld.com/files/SimulatorN-1-1.pdf> (accessed 5/12/2018)
- [12] Power World Corporation, "Simulator Version 16 user's guide", December 22, 2011. https://www.powerworld.com/files/Simulator16_Help_Printed.pdf (accessed on 5/12/2018).
- [13] J. Odom, "Transmission Planning Standards", 2012. https://www.nerc.com/pa/Stand/Project%20200602%20Assess%20Transmission%20Future%20Needs1/footnoteb_webinar_20121018_final_wjk.pdf (accessed on 5/12/2018)
- [14] Siemens PTI, "PSS®E Program Manual, Version 32", June 2009.

Article copyright: © 2018 B. Monisha and K. Balamurugan. This is an open access article distributed under the terms of the [Creative Commons Attribution 4.0 International License](https://creativecommons.org/licenses/by/4.0/), which permits unrestricted use and distribution provided the original author and source are credited.





CALL FOR PAPERS

Trends in Renewable Energy

ISSN Print: 2376-2136 ISSN online: 2376-2144

<http://futureenergysp.com/index.php/tre/>

Trends in Renewable Energy (TRE) is an open accessed, peer-reviewed semi-annual journal publishing reviews and research papers in the field of renewable energy technology and science. The aim of this journal is to provide a communication platform that is run exclusively by scientists. This journal publishes original papers including but not limited to the following fields:

- ✧ Renewable energy technologies
- ✧ Catalysis for energy generation, Green chemistry, Green energy
- ✧ Bioenergy: Biofuel, Biomass, Biorefinery, Bioprocessing, Feedstock utilization, Biological waste treatment,
- ✧ Energy issues: Energy conservation, Energy delivery, Energy resources, Energy storage, Energy transformation, Smart Grid
- ✧ Environmental issues: Environmental impacts, Pollution
- ✧ Bioproducts
- ✧ Policy, etc.

We publish the following article types: peer-reviewed reviews, mini-reviews, technical notes, short-form research papers, and original research papers.

The article processing charge (APC), also known as a publication fee, is fully waived for the Trends in Renewable Energy.

Call for Editorial Board Members

We are seeking scholars active in a field of renewable energy interested in serving as volunteer Editorial Board Members.

Qualifications

Ph.D. degree in related areas, or Master's degree with a minimum of 5 years of experience.

All members must have a strong record of publications or other proofs to show activities in the energy related field.

If you are interested in serving on the editorial board, please email CV to

editor@futureenergysp.com.